Mon. Not. R. Astron. Soc. **351,** 31–56 (2004) doi:10.1111/j.1365-2966.2004.07777.x

X-ray source populations in the Galactic plane

A. D. P. Hands,[1] R. S. Warwick,[1⋆] M. G. Watson[1] and D. J. Helfand[2]
[1]*Department of Physics and Astronomy, University of Leicester, University Road, Leicester, LE1 7RH*
[2]*Columbia Astrophysics Laboratory, Columbia University, 550 West 120th Street, New York, NY 10027, USA*

Accepted 2004 February 27. Received 2004 February 25; in original form 2003 November 21

ABSTRACT

We present the first results from the *XMM–Newton* Galactic Plane Survey (XGPS). In the first phase of the programme, 22 pointings were used to cover a region of approximately 3 deg^2 between 19° and 22° in Galactic longitude and ±0.6° in latitude. In total we have resolved over 400 point X-ray sources, at $\geqslant 5\sigma$ significance, down to a flux limit of $\sim 2 \times 10^{-14}$ erg s^{-1} cm^{-2} (2–10 keV). The sources exhibit a very wide range of spectral hardness, with interstellar absorption identified as a major influence. The source populations detected in the soft (0.4–2 keV) band and hard (2–6 keV) band show surprisingly little overlap. The majority of the soft sources appear to be associated with relatively nearby stars with active stellar coronae, judging from their high coincidence with bright stellar counterparts.

The combination of the XGPS measurements in the hard X-ray band with the results from earlier surveys carried out by *ASCA* and *Chandra* reveals the form of the low-latitude X-ray source counts over 4 decades of flux. It appears that extragalactic sources dominate below $\sim 10^{-13}$ erg s^{-1} cm^{-2} (2–10 keV), with a predominantly Galactic source population present above this flux threshold. The nature of the faint Galactic population observed by *XMM–Newton* remains uncertain, although cataclysmic variables and RS CVn systems may contribute substantially. *XMM–Newton* observes an enhanced surface brightness in the Galactic plane in the 2–6 keV band associated with Galactic ridge X-ray emission (GRXE). The integrated contribution of Galactic sources plus the breakthrough of extragalactic signal accounts for up to 20 per cent of the observed surface brightness. The XGPS results are consistent with the picture suggested from a deep *Chandra* observation in the Galactic plane, namely that the bulk of the GRXE is truly diffuse.

Key words: surveys – Galaxy: general – X-rays: general.

1 INTRODUCTION

With the current generation of X-ray astronomy missions, we are for the first time able to carry out high sensitivity, coherent surveys of selected regions of the Galactic plane. In particular, the *XMM–Newton* mirrors afford a large collecting area (∼4650 cm^{-2} total geometric area) with good spatial resolution (full width at half maximum, FWHM, ∼6 arcsec and half energy width, HEW, ∼15 arcsec on-axis) over a wide field of view (30-arcmin diameter). In combination with the EPIC CCD cameras, this provides an excellent facility for surveying sky regions subtending many square degrees down to relatively faint flux levels in both the hard (>2 keV) and soft (<2 keV) X-ray bands.

The goal of the *XMM–Newton* Galactic Plane Survey (XGPS) is two-fold. The first objective is to study the properties of the Galactic X-ray source population at intermediate flux levels (down to $\sim 2 \times 10^{-14}$ erg s^{-1} cm^{-2} in the 2–10 keV band, but an order of magnitude fainter in flux terms in the softer 0.4–2 keV band). The second is to search for extended, low X-ray surface brightness features including variations in the underlying diffuse Galactic ridge X-ray emission (GRXE; Worrall et al. 1982; Warwick et al. 1985; Koyama et al. 1986; Yamauchi & Koyama 1993; Kaneda et al. 1997; Valinia & Marshall 1998).

The nature of the X-ray source population at high X-ray fluxes was established by early all-sky surveys and subsequent identification programmes, which revealed that the brightest sources in our Galaxy are predominantly X-ray binaries and supernova remnants. More sensitive surveys of the Galactic plane have since been made, including those made by *ROSAT* (Motch et al. 1991) and *ASCA* (Sugizaki et al. 2001) complemented by the serendipitous surveys carried out with the *Einstein* observatory (Hertz & Grindlay 1984). Together, these surveys have provided some glimpses of the X-ray source population at lower X-ray fluxes, and hence effectively at lower X-ray luminosities for Galactic objects, although the picture is far from complete. At soft X-ray energies (< 2 keV) *ROSAT* studies in particular have shown that coronal emission from relatively

⋆E-mail: rsw@star.le.ac.uk

© 2004 RAS

Table 1. Observation log for the XGPS-I.

Field Name	Observation Date	Field Centre (J2000) R.A. ($^{h\,m\,s}$)	Dec. ($^{\circ}\,'\,''$)	MOS exposure[a]	pn exposure[b]	M OS fraction[c]	pn fraction[c]
Ridge 1	2000-10-08	18 26 00.4	−12 14 55.9	8393	5914	0.95	0.85
Ridge 2	2002-09-21	18 26 48.4	−11 52 48.7	13667	12046	1.00	1.00
Ridge 3	2000-10-11	18 27 36.4	−11 30 40.4	12044	9648	0.95	0.85
Ridge 4	2000-10-12	18 28 17.0	−11 07 53.0	9256	12998	0.94	0.42
Ridge 5	2002-09-17	18 29 06.0	−10 45 03.0	13667	12046	0.98	0.93
XGPS 1	2001-03-08	18 25 04.6	−11 50 00.4	7794	4797	1.00	1.00
XGPS 2	2001-03-10	18 27 34.0	−12 09 20.0	9144	–	1.00	–
XGPS 3	2001-03-10	18 25 49.0	−11 28 42.7	9144	–	1.00	–
XGPS 4	2001-03-10	18 28 19.4	−11 48 05.2	9144	–	1.00	–
XGPS 5	2001-03-22	18 26 35.7	−11 07 32.1	9994	7348	0.96	0.95
XGPS 6	2001-03-22	18 29 05.9	−11 26 57.4	8794	6148	0.44	0.23
XGPS 7	2001-03-24	18 27 21.2	−10 46 17.8	7637	4998	0.95	0.98
XGPS 8	2002-09-29	18 29 50.8	−11 05 41.2	13167	11546	1.00	1.00
XGPS 9	2001-03-26	18 28 06.4	−10 25 10.0	11894	9248	0.92	0.62
XGPS 10	2001-10-03	18 30 36.2	−10 44 29.3	9767	8146	0.97	0.83
XGPS 11	2002-09-19	18 29 43.9	−10 24 09.6	8409	6788	0.92	0.81
XGPS 12	2002-09-27	18 28 59.1	−10 06 50.9	7367	5746	1.00	1.00
XGPS 13	2003-04-10	18 31 25.5	−10 24 32.5	6666	5047	0.73	0.66
XGPS 14	2002-03-11	18 30 29.3	−10 02 47.1	7269	4998	1.00	1.00
XGPS 15	2002-03-27	18 29 36.6	−9 42 41.1	7274	4998	0.82	0.96
XGPS 16	2002-03-15	18 32 06.5	−10 01 51.8	7762	5486	1.00	1.00
XGPS 17	2002-03-29	18 31 13.9	−9 41 39.4	7274	4998	0.99	0.94

Notes. [a]Total exposure for the MOS 1 camera (s). [b]Total exposure for the pn camera (s). [c]Fraction of the exposure time used in producing images.

nearby active stars dominates (e.g. Motch et al. 1997). Above 2 keV the characteristics of the harder population are far less well-defined, although it is clear that accreting binary sources (both X-ray binaries and cataclysmic variables) make a significant contribution.

To date, the XGPS survey has been targeted at several locations in the Galactic segment between the Galactic Centre and the Scutum spiral arm. Here we report the results from the first phase of the XGPS (hereafter XGPS-I), which has entailed a total of 22 *XMM–Newton* pointings, covering a region of approximately 3 deg^2 between 19°–22° in Galactic longitude and ±0.°6 in latitude. Over 400 discrete point-like X-ray sources have been detected in XGPS-I and in this paper we focus on the properties of this source population and the contribution these discrete sources make to the GRXE. In a second paper (Hands et al., in preparation) we will present the results of a search for low-surface brightness, spatially extended X-ray sources in the XGPS-I fields and also report on the properties of the underlying diffuse GRXE.

2 OBSERVATIONS

The XGPS-I programme comprises 22 *XMM–Newton* pointings carried out during the period between 2000 October and 2003 April (see Table 1). Five of these observations formed part of the SSC Guaranteed Time programme (the Ridge 1–5 fields), whereas the remaining time was awarded to an AO1 programme (PI: RSW; the XGPS 1–17 fields). The allocated exposure times for these two sets of observation were 9 and 5 ks, respectively, although in most instances somewhat longer exposure times were actually scheduled (see Table 1). In all cases the EPIC cameras were operated in Full Window Mode with the medium filter selected. In the event, the completion of this survey proved problematic due to the impact of intervals of high instrumental background on the data quality, at least for a subset of the pointings.[1] Several of the pointings were in fact repeated so to mitigate the worst effects of this contamination (Table 1 refers to the observations actually used in the present work).

3 DATA ANALYSIS

3.1 Data screening and image extraction

We have analysed the X-ray data from the three EPIC cameras on *XMM–Newton*, two of which incorporate MOS CCDs (MOS 1 and MOS 2; Turner et al. 2001) and one based on pn technology (Strüder et al. 2001). As noted earlier, the instrument background in both the MOS and pn cameras is highly variable with the transition from quiescent conditions to a severe flaring episode often occurring on time-scales shorter than ∼1000 s and involving an increase in the background count rate by factors ranging from a few up to several orders of magnitude. In order to assess the background conditions in each of the XGPS-I observations, we have extracted the full-field light curve for events with energy in the range 0.2–12 keV. The results are illustrated in Fig. 1 for the MOS 1 camera.

Prior to constructing X-ray images, the X-ray events recorded in each EPIC camera for each observation must be filtered in various ways.[2] The first step was to use the full-field light curve to exclude time-intervals when the instrument background was unduly high.

[1] The background enhancements are attributed to a highly variable flux of soft protons which in orbit appear to be channelled by the X-ray mirrors on to the CCD detectors.

[2] We take as a starting point in our analysis the calibrated event list produced by the standard *XMM–Newton* pipeline, together with exposure maps and other pipeline products. We select X-ray events corresponding to patterns 0–12 for the MOS and 0–4 in the pn.

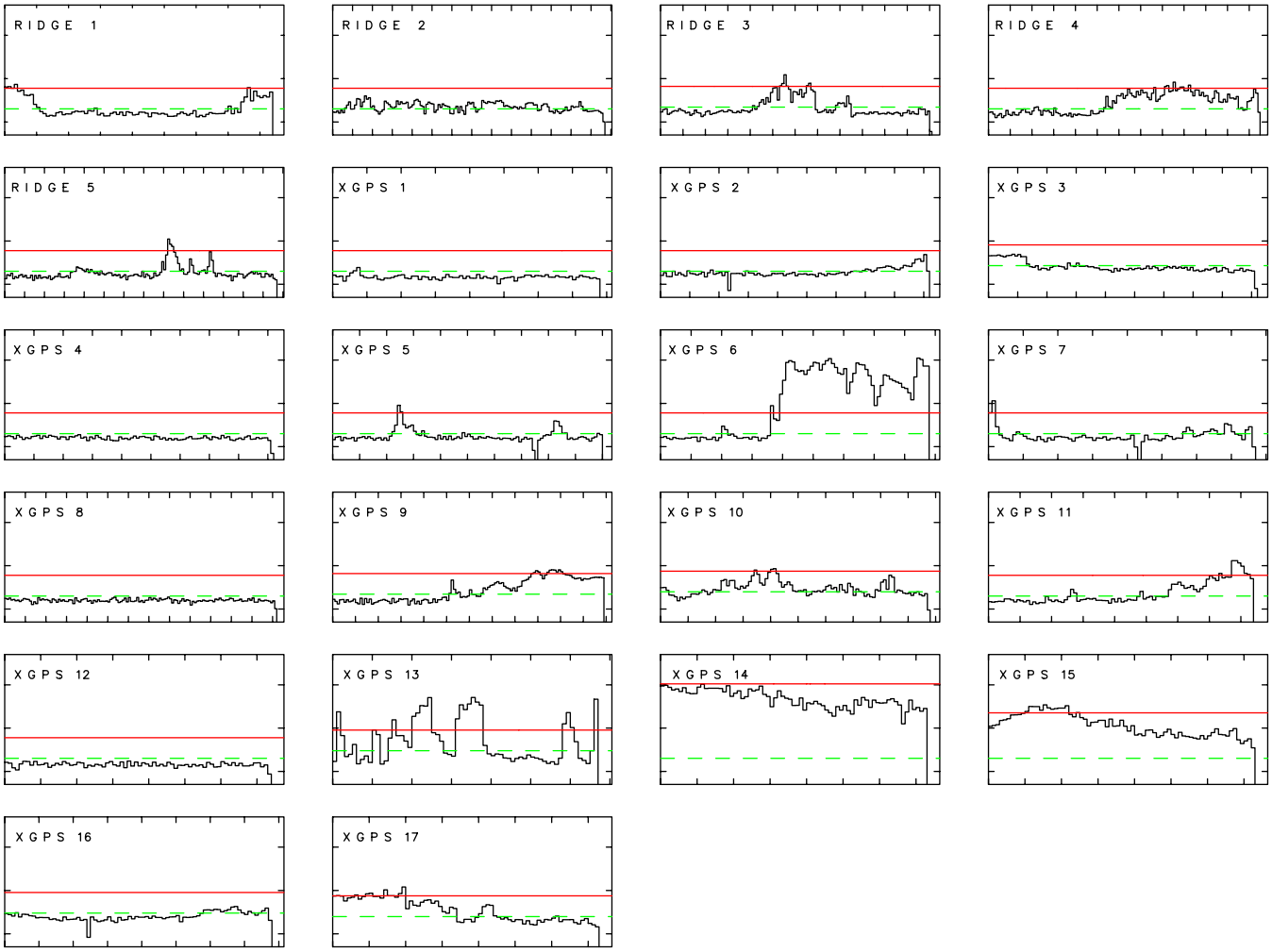

Figure 1. MOS 1 full-field light curves for all 22 XGPS-I observations. In each case the units of the vertical axis are counts per 100 s in the full 0.2–12 keV band. The scaling is logarithmic with the three tick marks corresponding to 100, 1000 and 10 000 counts per 100 s, respectively. The unit of the horizontal axis is time with tick marks every 1000 s. The thresholds used to exclude the most intense background flares are shown in each case (solid line). The more stringent thresholds used to extract data sets with 'near-quiescent' background conditions are also indicated (dashed line).

The fact that the XGPS-I observations are relatively short (i.e. 6–14 ks actual exposure time) and the background flaring episodes are rather common and have durations of several ks or longer, means that 'near-quiescent' background conditions are typically experienced only for a fraction of the total on-time (with this fraction approaching zero in some observations). As a compromise between selecting clean data on the one hand and having sufficient source counts to make source detection effective on the other, we set a threshold for data exclusion at a full-field count rate roughly three times higher than the 'lowest level' of the observation (see Fig. 1 and Table 1). For most of the observations this resulted in a cut at a rather similar count-rate setting. However, the XGPS 14 and XGPS 15 observations were subject to enhanced background levels throughout the exposure and for these a significantly higher threshold count-rate was required (implying a much reduced sensitivity to faint cosmic X-ray sources in these observations). For some purposes (e.g. searching for low-surface brightness X-ray features within a particular observation or looking for variations in the underlying GRXE across many fields) a much more stringent rejection of high background intervals is required. The thresholds used to identify near-quiescent background conditions are also shown in Fig. 1. All the data from the XGPS 14 and XGPS 15 observations were rejected for this analysis.

This empirical approach is broadly similar to that later adopted for the construction of the first *XMM–Newton* catalogue (Watson et al. 2003).

Once the temporal filter has been applied, the next step is to make images in specific energy bands for further analysis. Here we have used a soft (0.4–2.0 keV) band, a hard (2.0–6.0 keV) band and a broad-band representing the combination of the soft and hard channels (0.4–6 keV). Our choice of bands was made to optimize detection signal-to-noise ratio. Note that it differs somewhat from that used in the standard *XMM–Newton* data products. In the case of the MOS cameras we specifically excluded two narrow energy bands which are contaminated by fluorescent Al and Si lines originating within the detector (see Fig. 2).[3] Although the Si line is not a prominent feature in the pn background, for consistency we use the same energy band selection for the pn data.

[3] The energy ranges excluded were 1.4–1.575 keV and 1.675–1.8 keV corresponding to the K_α lines of neutral Al and Si respectively.

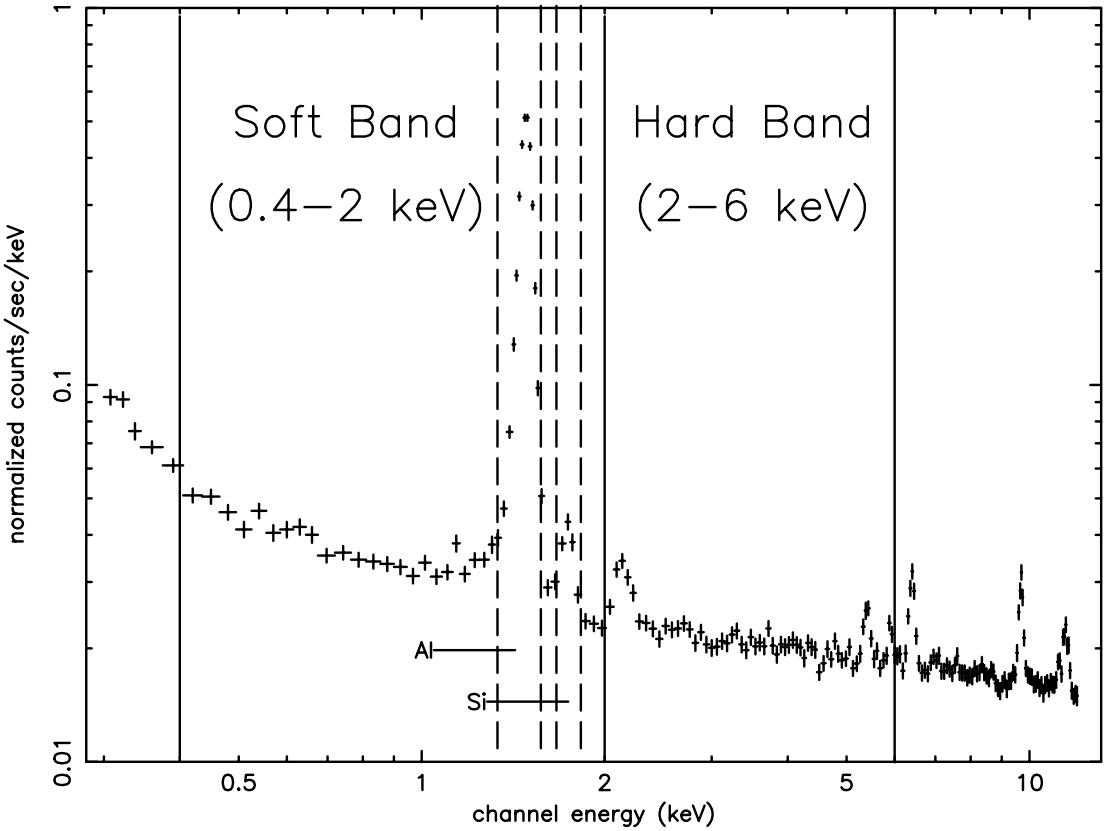

Figure 2. The spectra collected from edge regions of the MOS CCDs which lie underneath the filter wheel and hence are not exposed to the X-ray sky. The solid lines define the boundaries of the energy bands used in the analysis. The two regions identified by the dashed lines, which encompass the fluorescence lines of Al and Si produced within the MOS cameras, were specifically excluded from the soft band. Although other instrument fluorescence lines are present in the hard band, they are of relatively low intensity and have very little impact on the hard-band background count rates.

The final filter used to select the data is a spatial discriminator to distinguish between the areas of the CCDs which are exposed to the sky and those which are not. This is particularly important for the two MOS cameras for which a significant fraction of the area of the outer CCDs is shielded by the camera's filter wheel. The spatial mask used to perform this filtering was derived from a central band exposure map (2.0–4.5 keV), produced by the standard SAS pipeline procedure. In practice, we also applied additional masking so as to exclude the regions of the field of view where, due to the mirror vignetting, the effective exposure was less than 25 per cent of the on-axis value.

At this stage we were utilizing three energy bands (soft, hard and broad) per EPIC camera (MOS 1, MOS 2, pn), to give a total of nine separate X-ray images per observation, with each image consisting of a 600 × 600 array of 4-arcsec pixels. In order to improve the signal-to-noise ratio we subsequently co-added each pair of MOS images. In carrying out source detection we have treated the MOS and pn data as completely separate channels, which can be compared for quality control purposes.

Fig. 3 illustrates the sky coverage of the survey for both the MOS and pn cameras in the form of a mosaic of the exposure maps from the individual XGPS-I pointings. In effect the survey uses three rows of pointings in a close-packed hexagonal pattern (with a spacing between adjacent field centres of 24 arcmin), so as to give efficient (but not particularly uniform) coverage of a narrow strip of the Galactic plane.

3.2 Detecting sources

We have employed an iterative sliding-box algorithm to detect point sources in the individual XGPS-I fields.[4] Briefly, the process was as follows. The raw image was lightly smoothed and used to identify bright regions corresponding to individual point sources or groups of sources. These source regions were then excised and the remaining data heavily smoothed to produce a sky-background map.[5] After subtracting the derived background map from the raw image, the data were again lightly smoothed and then scanned for local peaks above a specified surface brightness threshold. At the position of each local peak, we use a cell of radius 16 arcsec to extract a source plus background counts value (C) from the original raw image and a corresponding background estimate (B) from the background map. The net count from the source (S) was then given simply as

[4] Our approach was developed before the standard SAS source detection chain was mature enough to be considered for this project. Although our procedures are simpler than those incorporated in the SAS chain used in standard *XMM–Newton* processing, we do not expect that a detailed comparison would reveal any major differences in results and in particular our approach to background estimation is better-matched to the specific background issues faced at low Galactic latitudes and in low exposures.

[5] The light smoothing was performed using a circular Gaussian mask with $\sigma = 8$ arcsec (1 pixel = 4 arcsec), whereas the mask used for heavy smoothing was a square top-hat function of dimension 160 arcsec.

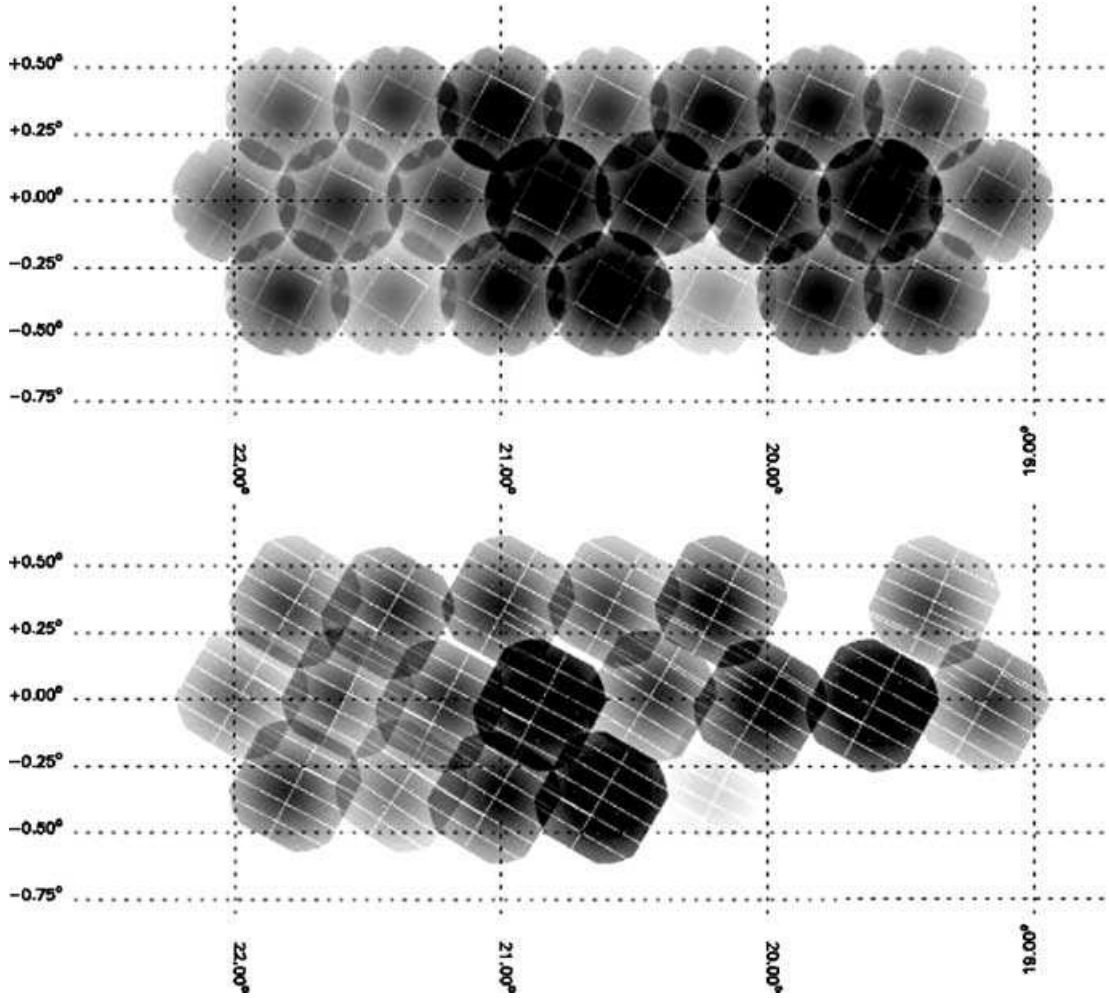

Figure 3. Top panel: a mosaicked (2–4.5 keV) exposure map showing the sky coverage provided by the MOS cameras over the full set of XGPS-I observations. The image is plotted in Galactic coordinates and employs a simple rectangular projection. The grey-scale (darker for longer exposures) corresponds to the accumulated (MOS 1 + MOS 2) exposure time at different points in the survey region, with the variation for each individual pointing largely reflecting the vignetting function of the *XMM–Newton* mirrors. Bottom panel: the same information for the pn camera. The gaps in the pn exposure map correspond to XGPS-I observations for which pipeline-processed pn data are not available. The maximum exposure is 18 and 6.5 ks in the MOS and pn images, respectively.

$S = C - B$. In order for a peak to qualify as a source detection, two criteria were applied, namely S $\geqslant$ 10 and S $\geqslant 5\sqrt{B}$, implying a detection significance of $\geqslant 5\sigma$. The list of sources detected by this method were subsequently used to define a new source mask and a revised background map. A further iteration of the source detection procedure then resulted in a final source list for the observation in question. Because the sensitivity to point sources depends on both the exposure time and the particle background rate, the sensitivity map of the full survey shows a somewhat different spatial variation to that of the corresponding exposure map (Fig. 4, top panel).

The process described above produces six separate source lists per XGPS-I observation (two detector channels and three spectral bandpasses). These source lists were merged by correlating all sources lying within 20 arcsec of each other. The position offsets for detections of the same source in two detector channels or in different bandpasses of the same detector were found to be distributed such that 68 per cent (90 per cent) were contained within a radius of $\approx$2.8 arcsec ($\approx$4 arcsec), which is consistent with the estimated statistical errors on the positions for sources at the faint end of the brightness distribution. However, a much broader correlation region was chosen so that sources would not be identified as distinct if the separation between them was less than or comparable to the half energy width of the EPIC point spread function. Fig. 5 shows a comparison of the MOS and pn broad-band detections in a central part of the Ridge 3 observation. In total four sources are detected in this subregion but interestingly only one of them is classed as a detection in *both* the MOS and pn cameras (see Section 4.1).

With the merging process for each observation completed, the next step was to select the best position information for each individual source and use this position to determine its flux. Here we used a *quality* parameter from the source detection process, representing the fraction of 'good pixels' in the source cell. This parameter is particularly useful in flagging sources near CCD chip gaps or distorted by bad columns in the CCD. The source position was taken from the (detector/spectral) channel with the highest *quality* value. Where more than one channel had *quality* = 1 we arbitrarily used the priority sequence pn/broad, MOS/broad, pn/hard, MOS/hard, pn/soft, MOS/soft. At the assigned 'best position' we then extracted counts estimates (S = C-B) using both a 16 arcsec and a 24 arcsec radius cell. The measured counts were subsequently corrected for the

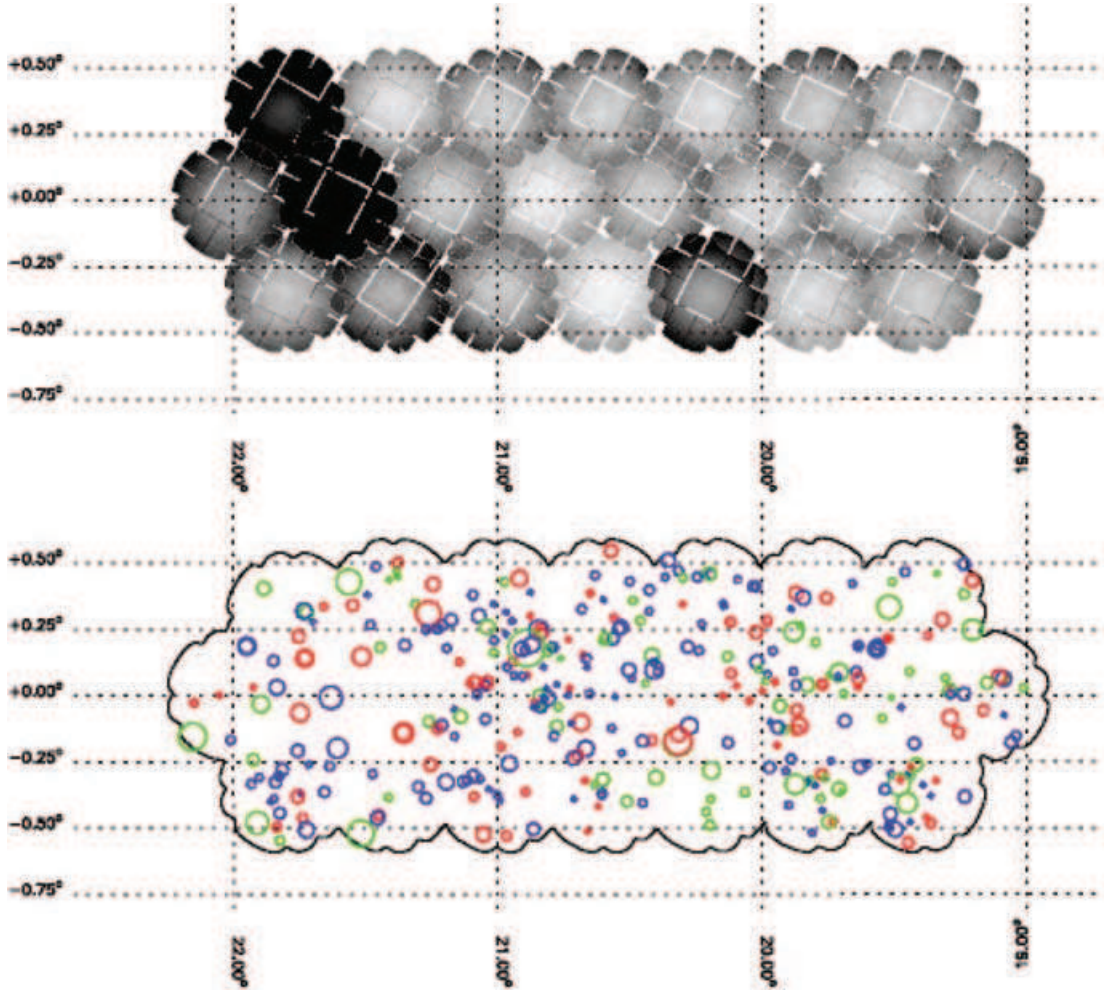

Figure 4. Top panel: mosaic showing the variation in source detection sensitivity across the 22 XGPS-I fields. The broad-band (0.4–6 keV) source count rate required to give a 5σ detection varies from 0.5 count ks^{-1} (white) to 3 count ks^{-1} (black) across the survey region dependent on the exposure time and particle background rate. Bottom panel: schematic image showing the sources detected by the MOS cameras in the soft (0.4–2 keV), hard (2–6 keV) and broad (0.4–6 keV) energy bands. Blue circles represent sources detected in the hard band but not the soft band; red circles represent sources detected in the soft band but not the hard band; green circles represent the remaining sources which are either detected in the soft and hard bands or in the broad-band alone. The radius of each circle is a logarithmic measure of the count rate of source.

signal loss outside the source cell and converted to on-axis count rates using appropriate exposure map information.[6] We use the counts derived from the smaller cells in the source counts analysis, as these are matched to the source detection process and the derived sensitivity curves (see Section 4.3). For all other purposes we use the counts based on the 24-arcsec radius cells.

The final step was to combine the source lists from the individual XGPS-I observations into one source catalogue. This involved the removal of a small number of duplicate entries where sources had been detected in more than one observation in regions where there was overlapping coverage; in practice preference was always given to the highest sensitivity detection.

[6] A source cell of radius 16 arcsec (4 pixel) encompasses ∼70 per cent of the counts from a point source (averaged over the field of view), whereas the corresponding value for a 24 arcsec (6 pixel) radius cell is 80 per cent. Unless otherwise stated, all the X-ray count rates quoted here are corrected for the signal loss due to the limited size of the source cell.

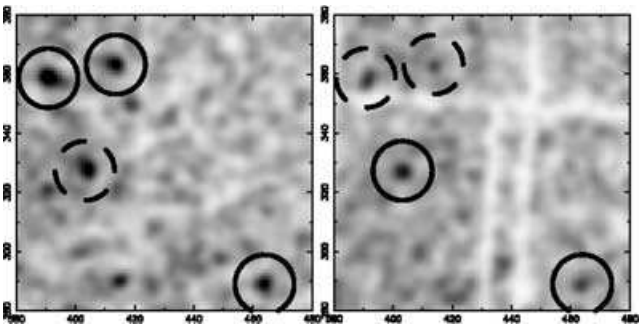

Figure 5. Lightly smoothed MOS (left) and pn (right) images of a part of the Ridge 3 field in the broad (0.4–6 keV) band. The circles drawn with solid lines indicate local peaks (above a specified threshold) which meet the two source-detection criteria, whereas the circles drawn with dashed lines indicate peaks which failed this test. A total of four sources are detected in this subfield, but only one source is classed as a significant detection in *both* the MOS and pn cameras.

3.3 Extracting source spectra

An algorithm was also developed to extract the net spectra of a defined set of sources in any particular field. In this case a more stringent version of the background rejection filtering was employed with the result that the two XGPS-I observations badly affected by background flaring were excluded (see Fig. 1). The source plus background events were accumulated from within circular regions of radius 24 arcsec centred on the identified source positions, with a similarly positioned array of annuli of radius 24–96 arcsec used to extract corresponding background events. Where two sources occur close to each other, the region of the annulus contaminated by the other source was excised. Background subtraction was carried out on a source-by-source basis and the resulting net-spectra summed over the defined set of sources prior to division by the effective exposure time. In effect this procedure provides the count-weighted average spectrum of the set of sources under consideration.

4 RESULTS

One of the main aims of the present survey is to study the X-ray source population of the Galaxy at relatively faint fluxes. In this section we consider the X-ray source catalogue derived from the XGPS-I programme, the X-ray spectral properties of the sources and the source count statistics. We also give brief details of possible optical counterparts based on available wide-field optical data and other published catalogue information.

4.1 The XGPS-I source catalogue

A total of 424 discrete X-ray sources satisfied the detection criteria. Fig. 4 (bottom panel) illustrates the spatial distribution of the XGPS-I sources across the survey region. The full source catalogue, including the source positions and the measured count rates in both the MOS and pn cameras, is presented in Appendix A. The X-ray spectral hardness ratio (HR) quoted for each source is defined as:

$$HR = \frac{H - S}{H + S} \quad (1)$$

where H is the number of counts measured in the hard band and S is the corresponding number of soft counts. For sources detected in both camera systems we summed the MOS and pn counts in the two energy bands before calculating HR. A correction for the differential vignetting was not applied to the HR value because this was generally small compared to the statistical error.

The numbers of sources detected in each camera system and in each energy band are given in Table 2. Of the 424 sources in the catalogue, 132 are detected in both the pn and MOS cameras, which represents 59 per cent of the pn sample but only 38 per cent of the MOS sources. The fact that there are more source detections in the MOS channel than in the pn camera reflects both the lack of pn data for some of the fields and also the longer exposures times typically achieved for the MOS detectors (the set-up time for the pn camera is a significant overhead for these rather short observations). For both the MOS and pn instruments, considerably more sources were detected in the hard energy band than in the soft band. It is surprising that the overlap between the spectral channels, i.e. the number of sources independently detected in both the hard and soft spectral bands, is so small (only ∼10–15 per cent of the sample). This spectral characteristic presumably also explains why the broad-band channel is only marginally more sensitive than its component bands, as demonstrated by the fact that only ∼11 per cent of the sources were detected solely in the broad-band. Ebisawa et al. (2001) have noted a similar lack of overlap between the soft and hard source populations detected in deep *Chandra* observations of the Galactic plane.

Table 2. Summary of source detections in each camera and energy band.

	Energy band					
Camera	Soft	Hard	Broad	H&S[a]	B-only[b]	Total
pn	90	128	171	22	26	222
MOS	135	215	266	43	38	345

Notes. [a]Number of sources detected in both the hard and soft bands. [b]Number of sources detected only in the broad-band.

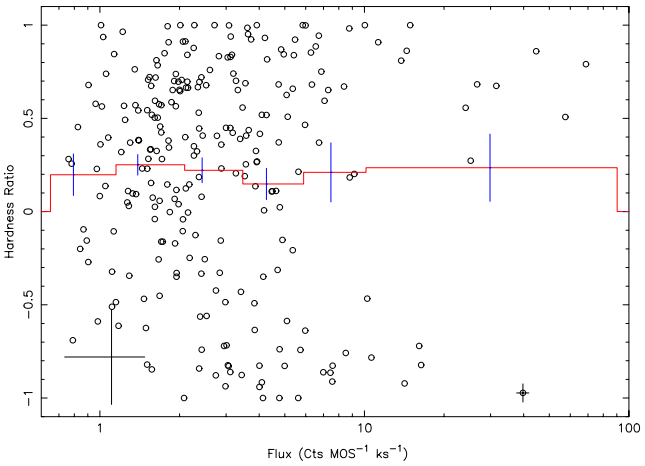

Figure 6. The relationship between spectral hardness and source count rate for sources detected in the MOS cameras. Error bars are shown for representative high and low count-rate points. The histogram charts the variation in the average HR with count rate.

4.2 The spectral properties of the XGPS-I sources

The range of spectral hardness exhibited by the XGPS-I sources is illustrated in Fig. 6 which shows HR versus MOS count rate for sources detected in the MOS cameras. There is clearly a huge spread encompassing the full range of the HR parameter (i.e. HR $= -1$ to $+1$). Given this scatter, it is not surprising that there is little evidence for a variation of the average HR with decreasing count rate (as might be predicted, for example, if fainter sources are on average more distant and as a consequence are more strongly absorbed).

We have investigated the typical spectral form of the XGPS-I source population by considering the integrated spectra of different subsets of sources. In fact, we split the population into three groups depending on the HR parameter as follows: (i) soft sources with HR < -0.5; (ii) mid-range sources with $-0.5 \leqslant$ HR $\leqslant 0.5$ and (iii) hard sources with HR > 0.5. We use the procedure described in Section 3.3 to extract the integrated spectra for the individual fields and then sum over the set of observations to obtain the average spectrum for each source group. To avoid undue bias, an extremely bright source detected in XGPS 9 (XGPS-I J182833-103659 – see Section 4.5), which contains a comparable number of counts to all the other sources put together, was excluded from this process.

The integrated MOS spectra obtained as above were analysed using the XSPEC software package. Following standard practice, the spectra were binned prior to analysis to give a minimum of 20 counts

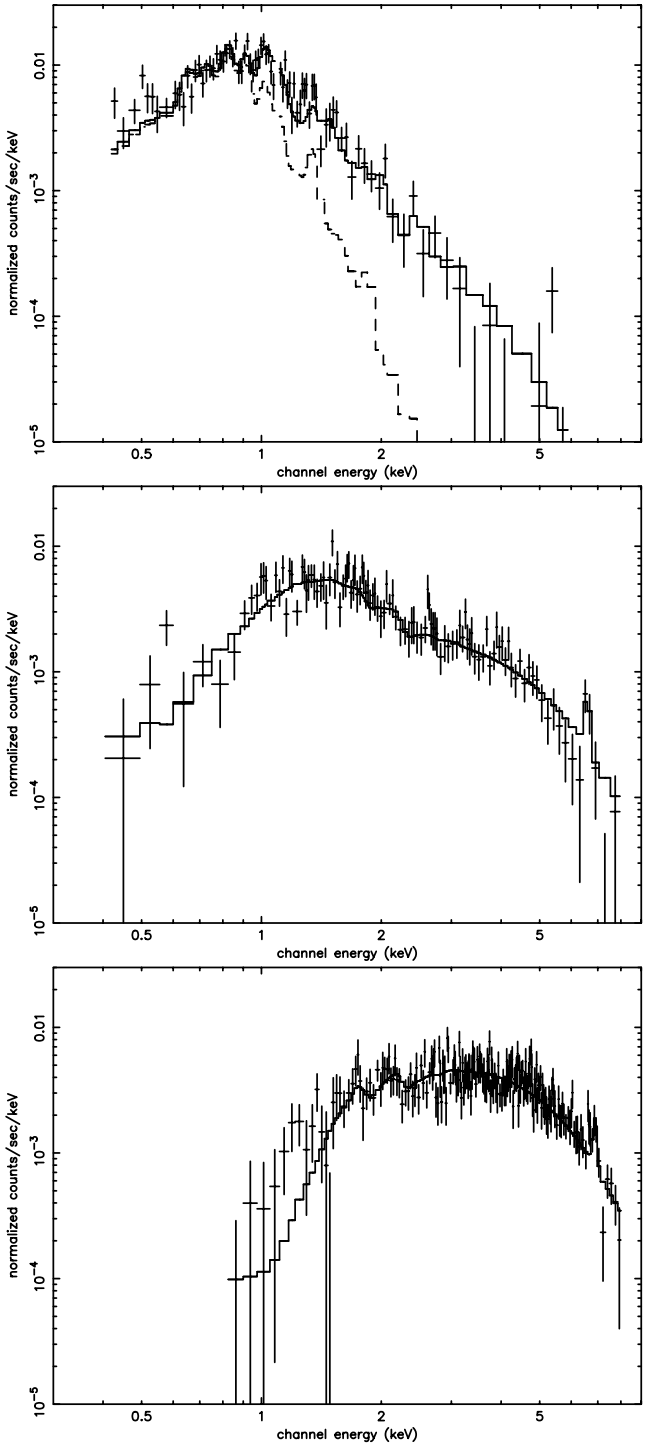

Figure 7. Top panel: the integrated EPIC MOS spectrum of the soft XGPS-I sources with HR < -0.5. Middle panel: the integrated EPIC MOS spectrum of the XGPS-I sources with mid-range hardness ratios i.e. $-0.5 \leqslant$ HR $\leqslant 0.5$. Bottom panel: the integrated EPIC MOS spectrum of the hard XGPS-I sources with HR > 0.5. In each case the histogram represents the best-fitting spectral model described in the text. In the top panel we also show the contribution of the lower temperature MEKAL component to the measured spectrum.

per spectral channel. From Fig. 7 it is immediately evident that the spectra of the three groups of sources are very different.

Initially we fitted the soft-source spectrum in the 0.4–6.0 keV range with three different models: a power-law, bremsstrahlung and MEKAL thermal plasma model, including absorption in each case. The pure continuum models provided the best fits (albeit with modest reduced χ^2), with the power-law model requiring a very steep spectral index and the bremsstrahlung model requiring a relatively low temperature (see Table 3). In contrast, a single-temperature solar-abundance MEKAL model provided a poor fit to the spectrum. However, because the pure continuum models are probably not physically realistic characterizations of this soft spectrum, we also investigated a two-component solar-abundance MEKAL model (plus absorption). The result, with the two-temperature parameters fixed at representative values (here we use kT=0.25 and 1.5 keV, respectively), was a slight improvement in terms of χ^2 to those obtained for the power-law and bremsstrahlung models. Table 3 provides details of the fit and Fig. 7 compares the best-fitting two-temperature model with the data.

Table 3. Modelling of the soft-source spectral data.

Model	$N_{\rm H}^a$	Γ	kT_1^b	$kT^b{}_2$	χ^2 (dof)
Power-law	$0.65^{+0.08}_{-0.05}$	$5.8^{+0.06}_{-0.03}$	–	–	164 (107)
Brems.	$0.32^{+0.13}_{-0.04}$	–	$0.38^{+0.03}_{-0.02}$	–	173 (106)
1-MEKAL	$\sim$0.60	–	$\sim$0.5	–	299 (107)
2-MEKAL	$0.44^{+0.03}_{-0.03}$	–	0.25^c	1.5^c	160 (107)

Notes. ^{a}In units of 10^{22} cm^{-2}. ^{b}In keV. ^{c}Fixed parameter.

An initial investigation of both the mid-range and hard-source spectra (over the spectral range 0.4–8 keV) demonstrated that a simple power-law continuum plus absorption model provided a good description of both data sets with a fairly similar value for the spectral index ($\Gamma \approx 1.6$) but with the absorption column density for the mid-range sample significantly lower than for the hard-spectrum sources. On this basis, we fitted the two spectra *simultaneously* with the absorbed power-law model, but with the spectral index as the only tied parameter. The result was a good fit ($\chi^2 = 440$ for 421 dof) with $\Gamma = 1.60^{+0.10}_{-0.13}$ and $N_{\rm H}$ values of $0.5^{+0.08}_{-0.08} \times 10^{22}$ and $3.7^{+0.3}_{-0.4} \times 10^{22}$ cm^{-2} for the mid-range and hard-source spectra, respectively. With Γ fixed at 1.7 the respective $N_{\rm H}$ values became $0.6^{+0.06}_{-0.05} \times 10^{22}$ and $3.9^{+0.2}_{-0.3} \times 10^{22}$ cm^{-2}. A comparison of the best-fitting models with the data are again shown in Fig. 7.

Both the mid-range and hard source spectra contain a line emission feature in the 6–7 keV band, consistent with Fe K$_\alpha$ emission. Although the data are of limited quality, we determine the line centroid values to be 6.59 ± 0.07 and 6.88 ± 0.06 keV for the medium and hard sources, respectively; the equivalent widths are measured to be 370 ± 250 and 240 ± 110 eV.

The fact that the soft-source spectrum is well fitted by a canonical two-temperature model with a relatively low absorption column is consistent with the bulk of the soft population being relatively nearby active stars. The spectra of the mid-range and hard-source samples are less easy to characterize. Certainly many of the faint hard sources may be active galactic nuclei (AGN; see Section 5.1) but the relatively hard continuum spectrum and iron-line properties also match the spectral properties of cataclysmic variables (CVs) and RS CVns. For example, CVs often exhibit a two-temperature thermal spectrum with $kT \sim 0.5$–1 keV and $\sim$5–10 keV (e.g. Baskill, Wheatley & Osborne 2004). With significant line of sight absorption the latter component dominates and readily mimics the hard power-law form inferred above.

4.3 The XGPS-I source counts

In order to study the number density of discrete X-ray sources as a function of count rate it is necessary to correct for the variation in

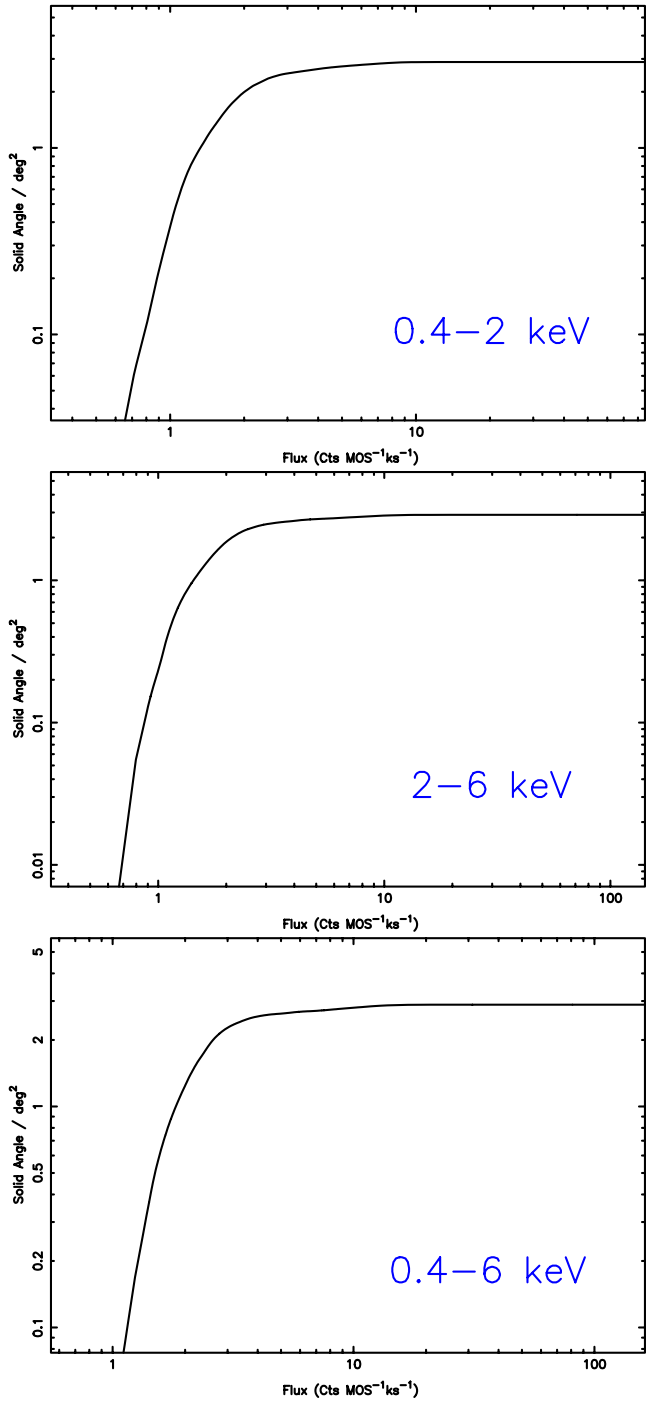

Figure 8. Sensitivity curves for the source count analysis based on detections with the MOS cameras in three energy bands. The total solid angle coverage of the survey (for very bright sources) is $\sim$3 deg^2.

the source detection sensitivity across the set of XMM fields which comprise the survey. Here we concentrate solely on the sources detected in the MOS cameras.

The first step in the correction process was to calculate a sensitivity map for source detection (in 'on-axis' count-rate units) for each XGPS-I observation based on the exposure map (which accounts for vignetting and other relevant factors such as chip gaps) and the derived MOS background map. The total survey area over which a source of a given count rate was detectable was then readily calculated by summing over the set of sensitivity maps comprising the XGPS-I survey. The derived effective area curves are shown in Fig. 8 for the three energy bands of the survey.

The X-ray source counts are then constructed by summing the contributions of individual sources after correction for the survey sensitivity. For example, consider a source detected at some particular offset angle in one of the XGPS-I observations. Its on-axis count rate is obtained by simply dividing the corrected net counts by the value of the exposure map at the source position. We then use the derived sensitivity curves to determine the solid angle (Ω) over which a source of that count rate was detectable. This source then contributes $1/\Omega$ to the source counts at its measured count-rate value. The final source count is obtained by summing the contributions of all the detected sources.[7]

In order to obtain an estimate of the magnitude of the error that should be assigned to the derived source counts at a given flux we have carried out a Monte Carlo simulation of the *post-detection* process used to construct the source counts (NB bearing in mind that with integral counts the measurements are not independent from point to point). This simulation also demonstrated that the changing gradient of the sensitivity curves at low fluxes introduces a significant bias in the source counts; in effect the Poissonian variation in the measured flux of a source has an asymmetric effect on the value of Ω that is derived. We correct for this bias by simulating the source counts both with and without such flux errors, noting the differences and adjusting the measured data accordingly. In practice, this procedure resulted in a reduction in the inferred number density of sources at the survey limit by up to 40 per cent.

Fig. 9 shows the corrected integral source counts in the three bands. It is evident that XGPS-I survey detects discrete X-ray sources in the Galactic plane down to surface density of roughly 200 deg^{-2}.

By linearly fitting the data in binned, differential form, we determined the slope of the integral counts to be -1.5 ± 0.2 for both the soft and hard sources and -1.3 ± 0.2 for the broad-band sources. (These values represent the slopes of the source counts after excluding, in each case, a handful sources at the bright end of the flux range.)

4.4 Optical/X-ray source correlations

Although the X-ray positions typically have statistical errors of $\leqslant$4 arcsec (see Section 3.2), we have searched for optical counterparts within a nominal 6-arcsec error circle. Specifically we have used optical data from the SuperCOSMOS digitization of the sky survey plates from the UK Schmidt telescope (UKST). Appendix A identifies the brightest optical source (if any) on the red (R) plate within the error circle of each XGPS-I source and quotes the corresponding optical R magnitude. Cross-references to the optical source in the USNO-A2.0 catalogue and/or the SIMBAD data base are also noted. Of the 424 X-ray point sources, 188 have possible optical counterparts identified by this procedure.

The correlation of optical magnitude versus X-ray count rate (here we focus on detections with *quality* > 0.8 in the MOS cameras) is a scatter diagram. Similarly a plot of X-ray hardness ratio versus optical R magnitude also shows significant scatter (Fig. 10), although there is hint of X-ray spectral hardening as one goes to optically fainter sources in the range $R = 12$–18.

[7] Sources with *quality* < 0.8, such as those located at a CCD chip edge or strongly affected by bad pixels were excluded.

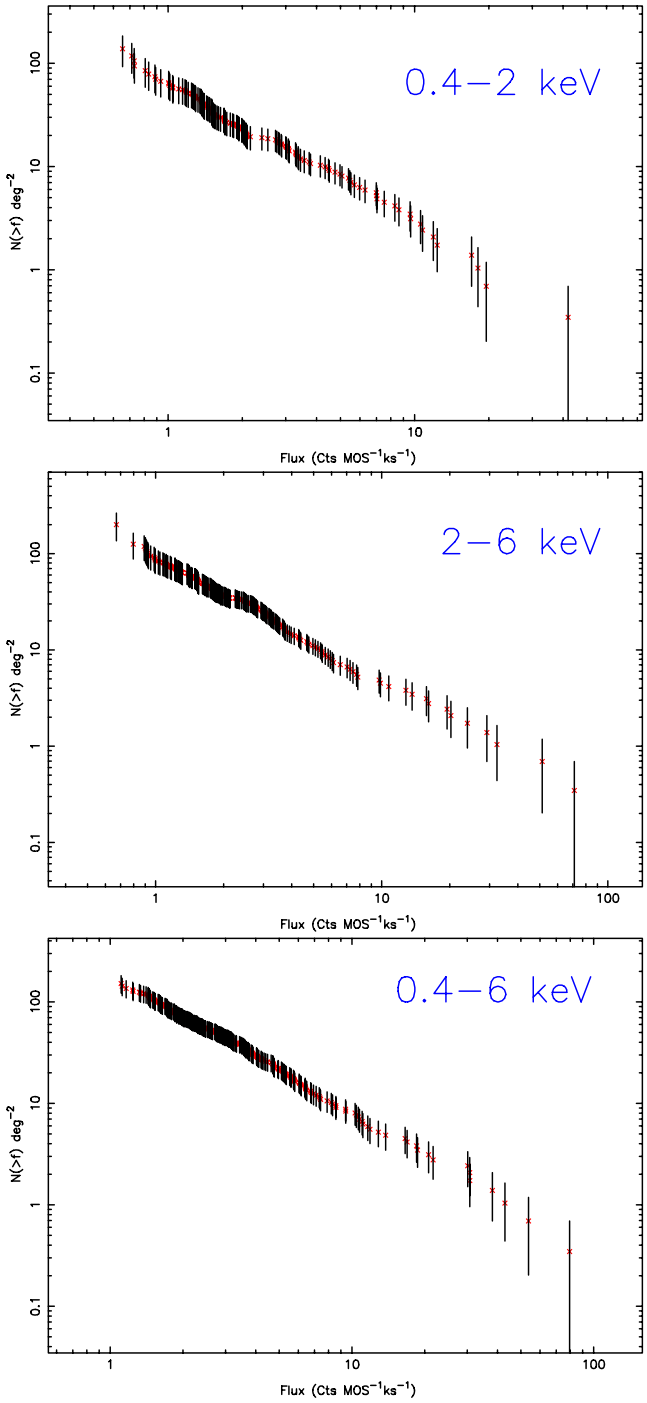

Figure 9. The derived X-ray source counts plotted in three energy bands and corrected at faint fluxes for the bias in the coverage correction induced by flux errors (see text).

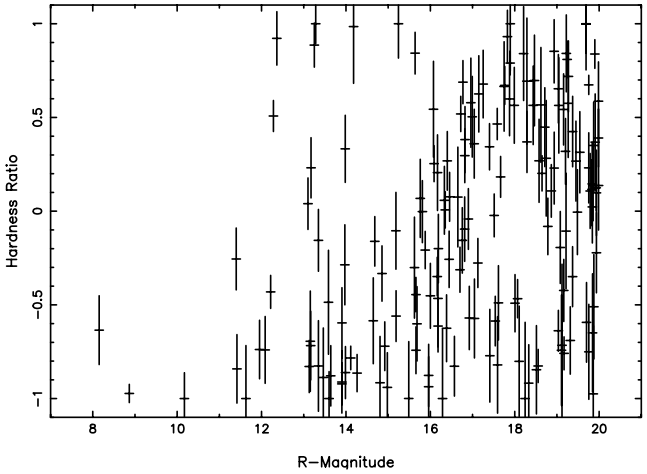

Figure 10. X-ray spectral hardness ratio versus optical *R*-magnitude. This refers to the brightest optical object in the X-ray error circle of each XGPS-I source. The probability that the optical source is the true optical counterpart of the X-ray source decreases both with increasing *R* and hardness ratio – see the discussion in the text.

We have investigated how the number of optical/X-ray correlations varies with optical magnitude for three subsets of sources divided according to the X-ray hardness ratio (i.e. the soft-, mid-range and hard-spectrum samples defined earlier). Fig. 11 shows how the fraction of X-ray sources with an associated optical source rises with increasing *R*. For the hard X-ray source sample, the rate of optical correlation is essentially the same as the chance rate. However, both the soft and mid-range samples have significantly higher rates of optical/X-ray associations than expected by chance. For these, we can compare the observed and chance rates to estimate the fraction of genuine optical identifications within the full list of optical associations (see Fig. 11, lower panel).

The X-ray sources with soft spectra (HR < -0.5) have a particularly high rate of association with bright optical objects. For example, ∼45 per cent of such sources have an optical object brighter than $R = 18$ within *6* arcsec of the X-ray position and of these roughly 75 per cent are likely to be the correct counterpart. At $R = 20$ the two factors become ∼65 and ∼55 per cent respectively. On the basis of the inferred X-ray/optical ratio and the X-ray spectral characteristics discussed earlier, it is likely that many of these soft X-ray sources are nearby late-type stars with active coronae.

Having identified a subset of the optical/X-ray associations which have a relatively high probability of being the correct identification, we can use the measured optical to X-ray positional offsets to check the astrometry of the X-ray positions, including any component relating to an overall shift (and rotation) of the *XMM–Newton* reference frame. Fig. 12 shows the radial distribution of the optical/X-ray offsets for the soft sources with associated optical objects brighter than $R = 20$. Allowing for a uniform distribution of chance coincidences we find the radius encompassing 68 per cent (90 per cent) of the 'real' identifications is 3.3 arcsec (4.7 arcsec) which is comparable to our earlier estimate of the statistical errors associated with the X-ray positions. This analysis demonstrates that any systematic astrometric shift of the *XMM–Newton* reference frame (for each field) to the true celestial frame must be small (of the order 1–2 arcsec at most), a result that is in accord with other studies (e.g. Barcons et al. 2002; Watson et al. 2003). Of the 22 XGPS fields, 17 have at least one soft source with an optical counterpart brighter than $R = 20$ within 4.7 arcsec. Conversely, we calculate that an incidence of five fields with zero correlations is not a particularly unlikely event. Unfortunately this does mean that for the latter fields we have no independent check of the *XMM–Newton* aspect solution (the fields in question are Ridge 4 and XGPS 2, 4, 6 and 14), but we have no reason to believe the astrometric accuracy of any of these fields is anomalous.

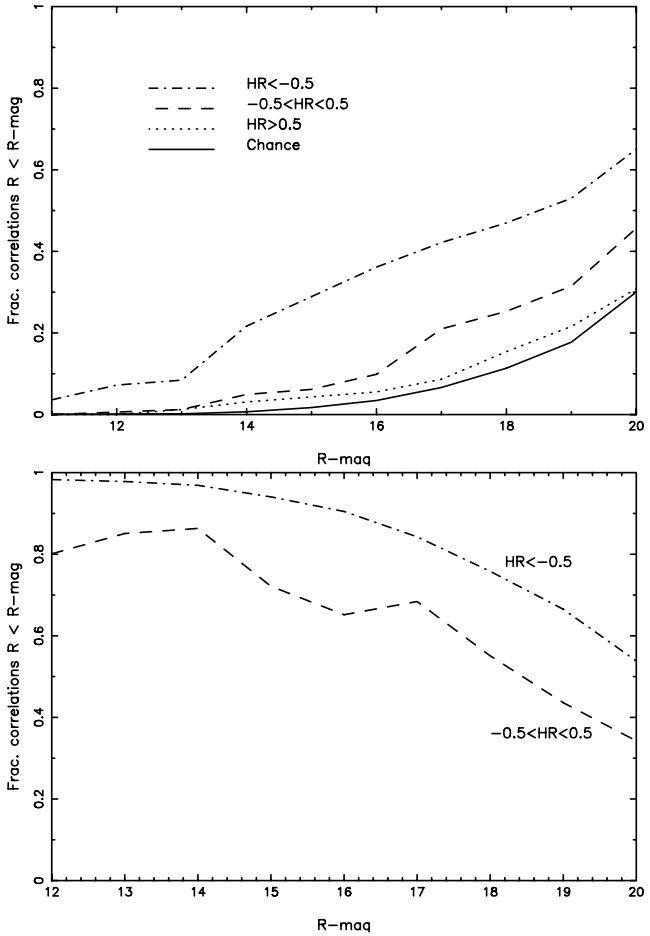

Figure 11. Top panel: the fraction of X-ray sources with an associated optical source plotted versus the limiting R magnitude of the optical sample. The three upper curves correspond to X-ray sources with spectral hardness in three ranges, namely soft sources with HR < -0.5, mid-range sources with $-0.5 \leqslant$ HR $\leqslant 0.5$ and hard sources with HR > 0.5. The lower curve shows the chance coincidence rate for finding an optical source in a 6-arcsec error circle in this region of the sky. Bottom panel: the fraction of the optical/X-ray associations that are likely to represent real identifications. The two curves correspond to the soft (upper) and mid-range (lower) spectral samples.

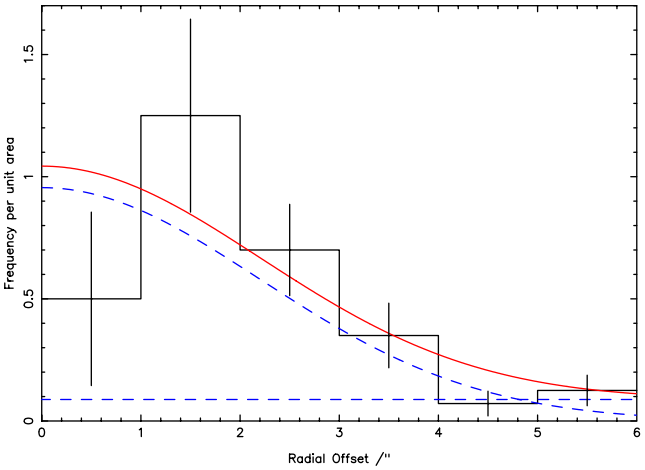

Figure 12. The distribution of the optical/X-ray offsets measured for the soft source sample in radial bins of 1-arcsec width. The error bars correspond to $\pm 1\sigma$. The solid-line represents the sum of the uniform distribution of the chance coincidences and the assumed Gaussian distribution of the real identifications. The latter has $\sigma = 2.2$ arcsec corresponding to a 68 per cent (90 per cent) probability error circle radius of 3.3 arcsec (4.7 arcsec).

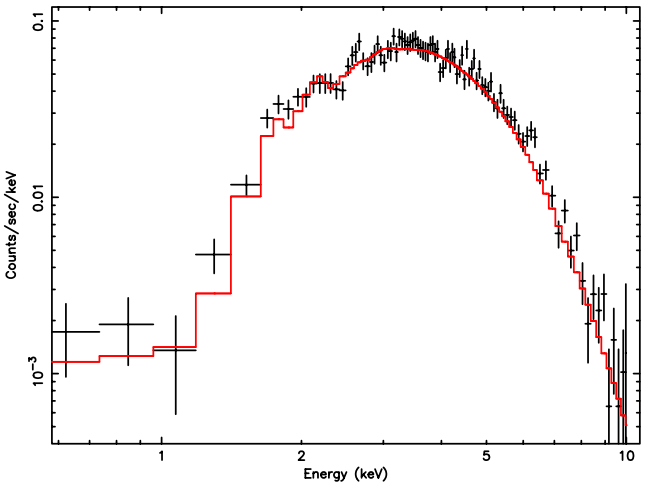

Figure 13. The measured count-rate spectrum of a bright transient source. The histogram corresponds to the best-fitting model detailed in the text.

4.5 A bright transient source

Only one source in the XGPS-I catalogue is bright enough to merit individual spectral extraction. The source, designated XGPS-I J182833-103659, is located at RA $18^{\rm h}28^{\rm m}34\overset{\rm s}{.}0$, Dec. (J2000) $-10^\circ 36' 59''$ (Galactic coordinates $l = 20\overset{\circ}{.}9, b = 0\overset{\circ}{.}2$). Fitting an absorbed thermal bremsstrahlung model to the measured spectrum yields a temperature of $\sim$7 keV and an absorption column of $\sim 5 \times 10^{22}$ cm^{-2} (see Fig. 13). This column density is consistent with either an extragalactic or a distant Galactic origin. In the latter case (assuming a distance of $\sim$15 kpc) the observed flux is equivalent to an X-ray luminosity of $\sim 10^{35}$ erg s^{-1}.

Cornelisse et al. (2002) discovered six type I X-ray bursters in *BeppoSAX* Wide Field Camera (WFC) observations, one of which is positionally coincident with this bright XGPS-I source, although the WFC 99 per cent confidence error circle of 2.8 arcmin is relatively large. The peak flux measured by *BeppoSAX* for this source (during a burst) was $(1.1 \pm 0.4) \times 10^{-8}$ erg s^{-1} cm^{-2} (2–10 keV) with a burst duration of $\sim$30 s. In the same energy band we measure $\sim 7.5 \times 10^{-12}$ erg s^{-1}cm^{-2} (after correcting for absorption). This is more than three orders of magnitude fainter than the burst peak, but may be only a factor $\sim$10 fainter than the high-state persistent flux of this source for which Cornelisse et al. (2002) quote only an upper limit of $< 1.9 \times 10^{-10}$ erg s^{-1} cm^{-2}. XGPS-I J182833-103659 shows no variation in its light curve over the short *XMM–Newton* observation, indicating that we are detecting persistent emission. The source position was in fact covered by two XGPS-I observations, XGPS 9 and Ridge 5, but the source was detected only in the former. This places an upper flux limit on the low state of the source of approximately 2×10^{-14} erg s^{-1} cm^{-2} in the 2–10 keV band. This source thus clearly shows significant variability: by a factor $\sim$300 between *XMM–Newton* observations and quite possibly by a much larger factor overall, making it very likely to be a previously unrecognised X-ray transient source. X-ray bursts are of course commonly associated with X-ray transient systems. The observed low state is also consistent with the absence of the source

Table 4. Correlation of XGPS-I sources with the *ASCA* catalogue.

XMM ID	*ASCA* name
XGPS-I J182534-121454	AX J182538-1214
XGPS-I J182846-111711	AX J182846-1116
XGPS-I J182525-114525	AX J182530-1144
XGPS-I J183038-100249	AX J183039-1002
XGPS-I J183117-100921	AX J183116-1008
XGPS-I J183209-093906	AX J183206-0938/AX J183206-0940
–	AX J183114-0943
–	AX J182651-1206

from the catalogue derived from the *ASCA* Galactic Plane Survey (Sugizaki et al. 2001).

4.6 Comparison with *ASCA*

The region surveyed by XGPS-I is entirely covered by the *ASCA* Galactic Plane Survey (Sugizaki et al. 2001) which resolved 163 sources in the Galactic plane within a longitude span of 90° centred on $l = 0°$. Of these 163 sources nine fall within the nominal region covered by the XGPS-I observations. We have detected seven of these sources as summarized in Table 4. Note that, two of the *ASCA* sources are linked to the same XGPS-I source as a consequence of the relatively poor spatial resolution and large positional errors of the former.

5 DISCUSSION

5.1 Source populations and the log *N*–log *S* relation

The source number versus flux (log *N*–log *S*) relation can provide important information on the spatial distribution and the luminosity functions of the various Galactic source populations. Here we combine our present measurements with those from other missions to examine how various categories of source may contribute to the observed hard band source counts. An investigation of the soft band log *N*–log *S*, including a comparison with earlier *ROSAT* measurements, will be the subject of a future paper.

In order to relate the *XMM–Newton* measurements to observations from other satellites it is necessary to convert the measured source counts from count-rate to flux units. Table 5 lists the conversion factors from MOS count rate in the 2–6 keV band to the corresponding flux (in erg $s^{-1}\,cm^{-2}$) in the 2–10 keV band for a variety of spectral forms calculated using PIMMS (Mukai 1993).

In the present analysis we adopt a factor 2.6×10^{-14} erg $s^{-1}cm^{-2}$/MOS count ks^{-1} corresponding to a power-law source spectrum with spectral index $\Gamma = 1.7$ absorbed by a column density $N_H = 1 \times 10^{22}$ cm^{-2}. This is clearly a compromise given the range of spectral form established earlier (see Section 4.2); we estimate

Table 5. Factors[a] to convert from the MOS count rate in the 2–6 keV band to the observed flux in the 2–10 keV band for different power-law spectra with a range of interstellar absorptions.

$\Gamma \backslash N_H$ [b]	0.0	1.0	3.0	5.0	7.0
1.4	2.7	3.0	3.4	3.9	4.4
1.7	2.4	2.6	3.0	3.4	3.9
2.0	2.1	2.3	2.7	3.1	3.4

Notes. [a]In units of 10^{-14} erg $s^{-1}cm^{-2}$/(MOS count ks^{-1}). [b]In units of 10^{22} cm^{-2}.

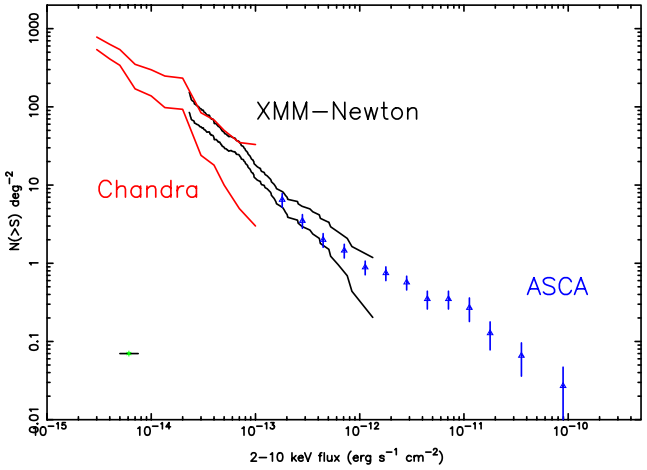

Figure 14. The 2–10 keV log *N*– log *S* relation measured in the Galactic plane based on *ASCA*, *XMM–Newton* and *Chandra* observations (see the text for references). In the case of both the *XMM–Newton* and *Chandra* measurements we show the upper and lower bounds of the derived source counts rather than individual data points. The magnitude of the relative flux scaling uncertainty applicable to the three data sets is indicated by the horizontal error bar.

that the effective uncertainty in the flux scaling may be as large as ±30 per cent.

Fig. 14 shows the measured log *N*–log *S* relation in the 2–10 keV band based on the XGPS-I measurements. Here we have clipped one high flux point with large error bars and two low-flux points requiring very large coverage correction, from the equivalent representation in Fig. 9. For comparison the source counts derived from the extensive survey of the Galactic plane between $l = \pm 45°$ carried out by *ASCA* (Sugizaki et al. 2001) and from recent deep *Chandra* observations in the Galactic plane at $l = 28°$ (Ebisawa et al. 2001) are also shown.

As can be seen from Fig. 14, the flux range probed by the XGPS-I measurements is intermediate between that sampled by the *ASCA* and *Chandra* programmes. The agreement between the XGPS-I and *ASCA* surveys is rather good given the very different coverage of the Galactic plane inherent in the two programmes. The agreement between the XGPS-I and *Chandra* source counts is also good bearing in mind the different pointing directions and the fact that at $\sim 3 \times 10^{-14}$ erg $s^{-1}cm^{-2}$ there are only ∼6 sources in the latter survey. Based on this compilation, the log *N*–log *S* relation appears to first flatten, then steepen, then flatten again as one moves from bright sources at $\sim 10^{-10}$ erg $s^{-1}cm^{-2}$ to faint sources at a limiting flux of $\sim 3 \times 10^{-15}$ erg $s^{-1}cm^{-2}$ in the 2–10 keV band.

The first step in modelling the measured composite log *N*–log *S* relation in terms of various underlying source populations is to quantify the contribution of extragalactic sources. It has in fact been recently demonstrated that even in heavily obscured regions of the Galactic plane the X-ray source counts measured at faint fluxes in the hard band are dominated by this component (Ebisawa et al. 2001). The extragalactic log *N*–log *S* relation in the 2–10 keV band has been determined over a wide range of X-ray flux from HEAO-1 A2 observations at the bright end (Piccinotti et al. 1982) through to recent ultradeep *Chandra* observations which probe below $\sim 10^{-15}$ erg $s^{-1}cm^{-2}$ (Rosati et al. 2002; Cowie et al. 2002; Alexander et al. 2003; Moretti et al. 2003; Harrison et al. 2003). Here we use the empirical form for the extragalactic 2–10 keV log *N*–log *S* specified by Campana et al. (2001) based on a comparison of deep *Chandra* observations with *ASCA*, *BeppoSAX* and

other data sets. The integral form of the extragalactic source counts flatten from a power-law slope of -1.67 at intermediate fluxes to a value of -0.58 at faint fluxes with the break occurring near $\sim 2 \times 10^{-14}$ erg s^{-1}cm^{-2}.

A very important factor in modelling the extragalactic contribution to the Galactic plane log N–log S is the signal loss due to absorption in the line-of-sight column density through Galaxy. Our spectra analysis of the sources with the hardest spectra (see Section 4.2) sets a *lower limit* of $N_{\rm H} = 3.9 \times 10^{22}$ cm^{-2} for an assumed power-law source spectrum with $\Gamma = 1.7$, whereas the bright transient source discussed earlier (Section 4.5) required $N_{\rm H} = 5.0 \times 10^{22}$ cm^{-2}. By way of comparison, Ebisawa et al. (2001) argue that $N_{\rm H} = 4$–6×10^{22} cm^{-2} at l=28° when one accounts for both neutral and molecular hydrogen along the line of sight. Based on the H I measurements of Dickey & Lockman (1990) and molecular hydrogen measurements of Dame, Hartmann & Thaddeus (2001), one might infer a similar value for the XGPS-I region. On the other hand, Nevalainen et al. (2001) measure a foreground Galactic column density of $7.9 \pm 0.5 \times 10^{22}$ cm^{-2} for a cluster of galaxies at (l, b) = (21.3, -0.7). Here we adopted a hard band transmission factor of 0.68 corresponding to a line-of-sight column density of 5×10^{22} cm^{-2} (for a power-law $\Gamma = 1.7$ source spectrum) which, in broad terms, aligns the extragalactic prediction with the observed *Chandra* source counts at faint fluxes (see Fig. 15). Clearly variation in the Galactic $N_{\rm H}$ from field to field in the Galactic plane will introduce a significant variance in the extragalactic contamination of the log N–log S relation; of necessity here we present only an approximate description of a very complicated situation.

We have investigated the possible contribution of various Galactic source populations to the measured composite log N–log S relation through the use of relatively simple prescriptions for the source luminosity function, the source distribution in the Galaxy and the effects of absorption. In brief, the predicted source counts are calculated by a numerical integration along a line of sight at (l, b) = (20, 0). We assume the maximum diameter of the Galaxy is 20 kpc and the Galactocentric radius of the Sun is 8.5 kpc. We model the absorption in the plane in terms of a local hydrogen density of 0.55 cm^{-3}. We assume the source and particle densities decline exponentially with respect to Galactocentric radius ($R_{\rm G}$) and height above the plane (z) (the assumed scale factors were 8500 kpc and 200 pc in $R_{\rm G}$ and z for the sources and 8500 kpc and 100 pc for the particle density).

We first consider relatively luminous Galactic X-ray binary sources containing either a neutron star or (in a few cases) a stellar mass black-hole. Low-mass X-ray binaries (LMXBs) are found preferentially in the Galactic Bulge and Galactic Centre regions whereas high-mass X-ray binaries (HMXRB) tend to avoid the inner 3–4 kpc of the Galaxy but are widely distributed in the Galactic disc (Grimm, Gilfanov & Sunyaev 2002). The composite log N–log S measured at $l = 20°$ might therefore include contributions from both populations. In order to model the combined LMXB/HMXRB contribution we assume a power-law form for luminosity function with a slope of -1.3 in the differential form (cf. Grimm et al. 2002). In practice, a luminosity function restricted to the range 10^{34}–10^{36} erg s^{-1} proved sufficient to account for the observed form of the log N–log S relation at the bright source end (see Fig. 15). The normalization of the binary luminosity function needed to match the log N–log S relation translates via the source distribution model to a Galactic population of $\sim$200 such X-ray binaries with an integrated Galactic X-ray luminosity of $\sim 1.6 \times 10^{37}$ erg s^{-1}.

With the bright and faint ends of the measured log N–log S relation represented respectively by Galactic X-ray binaries and the breakthrough of extragalactic sources, an excess number of sources (relatively to the prediction) is most apparent in the flux range 10^{-13} to 10^{-12} erg s^{-1} cm^{-2}. The requirement on any source population invoked to fill this gap is that its source count must be relatively steep at the top end of this range but should gradually turn over below 10^{-13} erg s^{-1}cm^{-2}, so as not to overpredict the total source density in the flux range sampled by the *Chandra* observations.

For illustrative purposes we consider a source population with an X-ray luminosity function described by a log-normal function centred on $L_{\rm X} = 10^{31}$ erg s^{-1} with $\sigma = 1.0$ and a local spatial density of $\sim 10^{-6}$ pc^{-3}. A source with $L_{\rm X} = 10^{31}$ erg s^{-1}, at a distance of 1 kpc has an X-ray flux of 10^{-13} erg s^{-1}cm^{-2}. At larger distances (and hence lower fluxes), the effects of increasing absorption will serve to flatten the counts of such sources. In addition by $\sim 10^{-14}$ erg s^{-1}cm^{-2} the most luminous sources in the population are detectable out to the edge of the Galaxy with the result that the overall log N–log S relation flattens further. Fig. 15 shows the predicted source count relation for the low-luminosity source population considered above. In combination the two Galactic source populations plus the extragalactic component provide an excellent match to the observed composite log N–log S curve.

What class of X-ray source might comprise the low-luminosity population considered above? The most likely candidate population is cataclysmic variables (CVs), close binary systems in which a white dwarf accretes material from a Roche-lobe filling late-type companion. CVs are often relatively bright hard X-ray sources with $L_{\rm X} = 10^{30-32}$ erg s^{-1} (e.g. Verbunt et al. 1997). In an earlier analysis, Watson (1999) suggested that X-ray faint CVs might show up in large numbers in deep Galactic surveys carried out in the hard X-ray band if their typical X-ray luminosity is $L_{\rm X} = 10^{31}$ erg s^{-1} (2–10 keV) and space density is $\sim 10^{-5}$ pc^{-3}. The latter value is compatible with the CV space density derived empirically by Patterson (1984) and is not out of line with at least some theoretical estimates (e.g. Kolb 1993). In this context, the space density assumed in our modelling of the low-luminosity population becomes a rather conservative requirement, particularly because other categories of source, such as RS CVn binaries (e.g. Makarov 2003, and references therein) and Be-star X-ray binaries in quiescence (e.g. Terman, Taam & Savage 1998), might also contribute to the low-luminosity population. The overall requirement is for a Galactic population of 1.2×10^5 objects which produce a Galactic X-ray luminosity of 1.3×10^{37} erg s^{-1} in the 2–10 keV band, comparable to the integrated X-ray luminosity inferred earlier for the X-ray binary population.

5.2 Contribution of discrete sources to the GRXE

Using all XGPS-I observations except the two most contaminated by flaring (XGPS 14, XGPS 15) and the one containing the bright transient source (XGPS 9), we have measured the total full-field MOS count rate (including the resolved sources) in the hard *XMM–Newton* band (2–6 keV). After correcting for the underlying instrumental background (e.g. see Willingale et al. 2003) and for mirror vignetting of the sky background signal, we obtain 3.7 ± 0.1 MOS count s^{-1}deg^{-2}. This signal is substantially larger than that measured at high Galactic latitude in the MOS cameras consistent with the presence of the GRXE in the field of view for all the XGPS-I pointings.

Applying the same count-rate to flux conversion factor as used in Section 5.1, the *total* surface brightness of the GRXE corresponds to 9.6×10^{-11} erg s^{-1} cm^{-2} deg^{-2} in the 2–10 keV band. Earlier estimates put the value variously at 11×10^{-11} erg s^{-1} cm^{-2} deg^{-2}

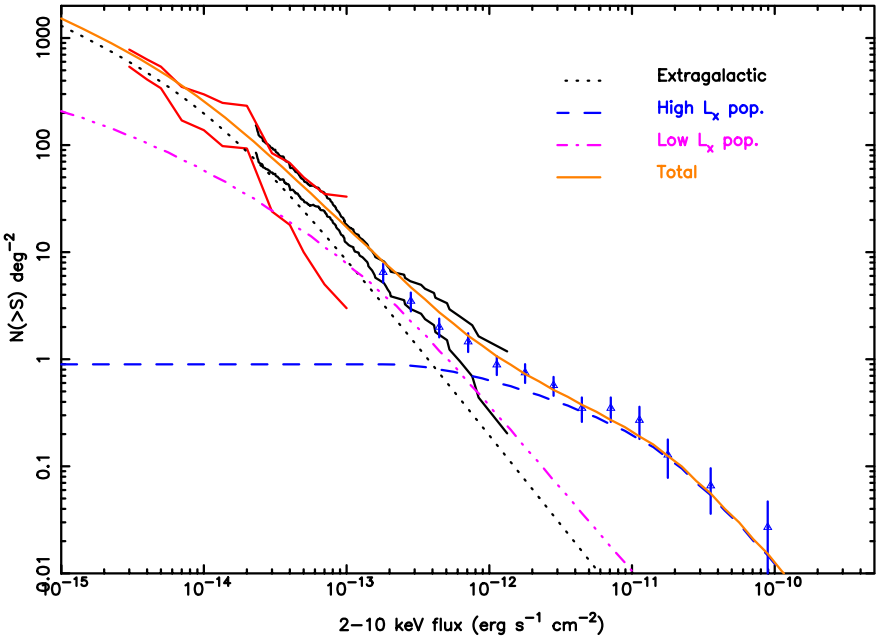

Figure 15. The measured 2–10 keV log N–log S relation compared with with the predicted contributions of various X-ray source populations (see the text).

(*Chandra*; Ebisawa et al. 2001), 5.2×10^{-11} erg s^{-1} cm^{-2} deg^{-2} (*ASCA*; Sugizaki et al. 2001), and 2.5×10^{-11} erg s^{-1} cm^{-2} deg^{-2} (*RXTE*; Valinia & Marshall 1998), depending on the region of sky surveyed.

By integrating the *observed* hard band X-ray source counts we find that the resolved sources with count rates in the range 0.7 to 70 MOS count ks^{-1} (2–6 keV) (on-axis) contribute 0.34 count s^{-1} deg^{-2}, corresponding to 9 per cent of the observed surface brightness. In addition, we estimate that the contribution of the residual extragalactic background after transmission through Galactic $N_{\rm H}$ of 5×10^{22} cm^{-2} amounts to a further 10 per cent of the measured surface brightness. Because the extrapolation of the log N–log S curves for the high-luminosity and low-luminosity Galactic source populations below the XGPS-I detection threshold adds little to the integrated signal, the implication is that ∼80 per cent of the measured GRXE surface brightness remains unaccounted for.

The deep *Chandra* observations show that extragalactic sources dominate down to fluxes of $\sim 3 \times 10^{-15}$ erg s^{-1} cm^{-2} (2–10 keV) (Ebisawa et al. 2001). A new Galactic population, contributing significantly to the GRXE, might emerge at fainter fluxes but the requirement (deduced by scaling the properties of the low-luminosity population considered earlier) of, say, $L_{\rm X} = 10^{28}$ erg s^{-1} combined with a space density of 10^{-2} pc^{-3}, does not fit any known population of sources. It would appear therefore that the bulk of the GRXE is truly diffuse in origin although the origin is still uncertain. Possible mechanisms include the interaction of low-energy cosmic-ray electrons or ions with interstellar matter (Valinia et al. 2000; Tanaka 2002), in situ electron acceleration (Dogiel et al. 2002; Masai et al. 2002) and magnetic reconnection (Tanuma et al. 2001). This issue will be addressed in a later paper on diffuse emission from the XGPS survey region.

6 CONCLUSION

The XGPS-I survey, which covers approximately 3 deg^2 of the Galactic plane near $l = 20^\circ$, has resulted in a catalogue containing over 400 discrete X-ray sources. The measured X-ray source counts trace the source population down to a limiting flux of $\sim 2 \times 10^{-14}$ erg s^{-1} cm^{-2} in the 2–10 keV band at which point the source density is between 100–200 sources per square degree. Consistent with an earlier *Chandra* study, the source counts at this flux are predominately due to extragalactic sources, despite the fact that the fluxes of extragalactic objects are significantly suppressed by absorption in the Galactic plane. However, the conclusion of the present work is that at fluxes above 10^{-13} erg s^{-1} cm^{-2} (2–10 keV) Galactic source populations do come to the fore.

The Galactic source population observed between 10^{-13} and 10^{-12} erg s^{-1} cm^{-2} could comprise largely CVs and RS CVn systems with X-ray luminosities in the range 10^{30-32} erg s^{-1} but the details remain uncertain on the basis of the X-ray information alone. Extensive programmes to identify and characterize optical/infrared counterparts are required, although this will be taxing given the high obscuration and high object density in the Galactic plane.

The present work demonstrates that the strategy of the XGPS programme, namely the use of shallow observations to give relatively wide angle coverage is close to optimum in terms of maximizing the number of Galactic source detections.

ACKNOWLEDGMENTS

ADPH acknowledges support from PPARC in the form of a research studentship and DJH acknowledges support from NASA grant NAG5-9870. We are also very happy to acknowledge the underpinning contributions made by the ESA Science Operations (SOC) team and the *XMM–Newton* EPIC and SSC consortia to the research programme reported here.

REFERENCES

Alexander D. M. et al., 2003, AJ, 126, 539
Barcons X. et al., 2002, A&A, 382, 522
Baskill D. S., Wheatley P. J., Osborne J. P., 2004, MNRAS, submitted
Campana S., Moretti A., Lazzati D., Tagliaferri G., 2001, ApJ, 560, L19

Cornelisse R. et al., 2002, A&A, 392, 885
Cowie L. L., Garmire G. P., Bautz M. W., Barger A. J., Brandt W. N., Hornschemeier A. E., 2002, ApJ, 566, L5
Dame T. M., Hartmann D., Thaddeus P., 2001, ApJ, 547, 792
Dickey J. M., Lockman F. J., 1990, ARA&A, 28, 215
Dogiel V. A., Inoue H., Masai K., Schönfelder V., Strong A. W., 2002, ApJ, 581, 1061
Ebisawa K., Maeda Y., Kaneda H., Yamauchi S., 2001, Sci, 293, 1633
Grimm H.-J., Gilfanov M., Sunyaev R., 2002, A&A, 391, 923
Harrison F. A., Eckart M. E., Mao P. H., Helfand D. J., Stern D., 2003, ApJ, 596, 944
Hertz P., Grindlay J. E., 1984, ApJ, 278, 137
Kaneda H., Makishima K., Yamauchi S., Koyama K., Matsuzaki K., Yamasaki N. Y., 1997, ApJ, 491, 638
Kolb U., 1993, A&A, 271, 149
Koyama K., Makishima K., Tanaka Y., Tsunemi H., 1986, PASJ, 38, 121
Makarov V. V., 2003, AJ, 126, 1996
Masai K., Dogiel V. A., Inoue H., Schönfelder V., Strong A. W., 2002, ApJ, 581, 1071
Moretti A., Campana S., Lazzati D., Tagliaferri G., 2003, ApJ, 588, 696
Motch C. et al., 1991, A&A, 246, L24
Motch C., Guillout P., Haberl F., Pakull M., Pietsch W., Reinsch K., 1997, A&A, 318, 111
Mukai K., 1993, Legacy, 3, 21
Nevalainen J., Lumb D., dos Santos S., Siddiqui H., Stewart G., Parmar A. N., 2001, A&A, 374, 66
Patterson J., 1984, ApJS, 54, 443
Piccinotti G., Mushotzky R. F., Boldt E. A., Holt S. S., Marshall F. E., Serlemitsos P. J., Shafer R. A., 1982, ApJ, 253, 485
Rosati P. et al., 2002, ApJ, 566, 667
Strüder L. et al., 2001, A&A, 365, L18
Sugizaki M., Mitsuda K., Kaneda H., Matsuzaki K., Yamauchi S., Koyama K., 2001, ApJ, 134, 77
Tanaka Y., 2002, A&A, 382, 1052
Tanuma S., Yokoyama T., Kudoh T., Shibata K., 2001, ApJ, 551, 312
Terman J. L., Taam R. E., Savage C. O., 1998, MNRAS, 293, 113
Turner M. J. L. et al., 2001, A&A, 365, L18
Valinia A., Marshall F., 1998, ApJ, 505, 134
Valinia A., Tatischeff V., Arnaud K., Ebisawa K., Ramaty R., 2000, ApJ, 543, 733
Verbunt F., Bunk W. H., Ritter H., Pfeffermann E., 1997, A&A, 327, 602
Warwick R. S., Turner M. J. L., Watson M. G., Willingale R., 1985, Nat, 317, 218
Watson M. G., 1999, in Hellier C., Mukai K., ASP Conf. Ser. Vol. 157, Annapolis Workshop on Magnetic Cataclysmic Variables. Astron. Soc. Pac., San Francisco, p. 291
Watson M. G. et al., Astron. Nachr., 324, 89
Willingale R., Hands A. D. P., Warwick R. W., Snowden S. L., Burrow D. N., 2003, MNRAS, 343, 995
Worrall D., Marshall F., Boldt E., Swank J., 1982, ApJ, 255, 111
Yamauchi S., Koyama K., 1993, ApJ, 404, 620

APPENDIX A: THE XGPS-I SOURCE CATALOGUE

This paper has been typeset from a TEX/LATEX file prepared by the author.

Table A1. The XGPS-I source catalogue.

XGPS-I		Equinox J2000		MOS count ks^{-1}				pn count ks^{-1}						Optical
Designation	Obs	RA	DEC	s	h	b	q	s	h	b	q	HR	*R*	Identification
J182416-115554	X1	18 24 16.63	−11 55 54.5	0.7 ± 0.7	2.8 ± 1.1	**3.4 ± 1.3**	0.51	0.0 ± 2.1	3.7 ± 2.2	1.7 ± 2.6	1.00	0.72	19.4	GPSR 19.236+0.495
J182426-115918	X1	18 24 26.61	−11 59 18.8	**3.9 ± 1.1**	0.0 ± 0.7	**4.0 ± 1.3**	1.00	**18.7 ± 3.7**	0.9 ± 1.7	**19.9 ± 4.1**	1.00	−0.94	14.9	U0750_13092026
J182436-115127	X1	18 24 36.20	−11 51 27.5	0.3 ± 0.4	0.5 ± 0.5	**0.8 ± 0.6**	1.00	0.0 ± 1.2	0.5 ± 1.0	0.0 ± 1.5	0.63	0.45	–	
J182441-115903	X1	18 24 41.19	−11 59 3.5	1.1 ± 0.6	1.4 ± 0.6	**2.4 ± 0.9**	1.00	1.3 ± 1.5	1.4 ± 1.5	2.6 ± 2.1	0.41	0.08	–	
J182446-120429	X1	18 24 46.45	−12 4 29.5	0.0 ± 0.7	0.0 ± 0.6	0.0 ± 0.9	0.02	**11.2 ± 3.3**	2.1 ± 2.3	**13.5 ± 4.0**	0.98	−0.69	9.8	U0750_13103886 BD-12 5039
J182448-114454	X1	18 24 48.58	−11 44 54.2	0.0 ± 0.4	**2.1 ± 0.7**	**2.1 ± 0.7**	1.00	0.6 ± 1.2	2.4 ± 1.4	**3.1 ± 1.8**	1.00	0.84	18.2	–
J182502-114320	X1	18 25 2.29	−11 43 20.8	0.7 ± 0.4	0.9 ± 0.5	**1.6 ± 0.7**	1.00	0.0 ± 1.1	0.2 ± 2.5	0.0 ± 1.6	0.18	0.08	16.6	U0750_13113393
J182506-114819	X1	18 25 6.78	−11 48 19.1	0.4 ± 0.3	0.5 ± 0.3	0.8 ± 0.5	1.00	0.9 ± 0.9	2.0 ± 1.0	**2.9 ± 1.4**	1.00	0.22	–	
J182506-120433	X1	18 25 6.85	−12 4 33.6	**7.0 ± 1.2**	**10.7 ± 1.6**	**17.6 ± 2.0**	0.78	62.4 ± 20.4	**65.6 ± 22.1**	**128 ± 30**	0.27	0.15	13.8	U0750_13116348
J182511-115726	X1	18 25 11.68	−11 57 26.3	**4.0 ± 0.9**	0.7 ± 0.7	**4.8 ± 1.2**	1.00	**8.4 ± 1.9**	1.2 ± 1.2	**9.7 ± 2.2**	1.00	−0.74	11.9	U0750_13119237
J182514-121859	R1	18 25 14.46	−12 18 59.4	0.9 ± 0.6	0.3 ± 0.6	1.1 ± 0.8	1.00	**6.4 ± 2.4**	0.0 ± 1.4	4.2 ± 2.7	1.00	−0.78	–	
J182517-114350	X1	18 25 17.24	−11 43 50.1	0.1 ± 0.4	1.1 ± 0.5	1.2 ± 0.7	1.00	0.2 ± 1.0	**4.4 ± 1.6**	**4.5 ± 1.9**	1.00	0.86	–	
J182521-113533	X3	18 25 21.10	−11 35 33.9	0.0 ± 0.4	**1.7 ± 0.7**	1.5 ± 0.8	1.00	–	–	–	–	1.00	–	
J182524-114525	X1	18 25 24.48	−11 45 25.1	**4.4 ± 0.7**	**27.4 ± 1.7**	**31.5 ± 1.8**	1.00	**13.5 ± 2.2**	**55.0 ± 4.3**	**67.9 ± 4.9**	1.00	0.67	19.7	–
J182530-115610	X1	18 25 30.97	−11 56 10.0	**1.4 ± 0.5**	0.1 ± 0.4	**1.5 ± 0.6**	0.92	2.4 ± 1.4	0.5 ± 1.1	**2.9 ± 1.7**	1.00	−0.82	17.5	U0750_13130699
J182531-114340	X1	18 25 31.58	−11 43 40.3	0.8 ± 0.5	0.7 ± 0.5	1.5 ± 0.7	1.00	2.6 ± 1.5	3.1 ± 1.6	**5.6 ± 2.2**	1.00	0.02	19.8	–
J182532-122055	R1	18 25 32.66	−12 20 55.0	0.4 ± 0.4	1.4 ± 0.6	**1.7 ± 0.7**	1.00	0.0 ± 1.3	0.0 ± 1.2	0.0 ± 1.9	0.73	0.58	19.2	–
J182533-121649	R1	18 25 33.33	−12 16 49.3	0.9 ± 0.6	0.7 ± 0.5	**1.4 ± 0.8**	0.86	2.0 ± 1.3	**5.2 ± 1.5**	**7.1 ± 2.0**	1.00	0.23	13.1	U0750_13132239
J182533-121556	R1	18 25 33.52	−12 15 56.5	1.0 ± 1.4	**5.9 ± 1.9**	6.3 ± 2.4	0.39	1.0 ± 1.1	**4.4 ± 1.4**	**5.5 ± 1.8**	0.73	0.67	19.2	–
J182534-121453	R1	18 25 34.00	−12 14 53.5	**5.14 ± 0.7**	0.38 ± 0.4	**5.36 ± 0.8**	0.80	**41.87 ± 3.4**	2.05 ± 1.2	**44.02 ± 3.7**	1.00	−0.89	13.2	U0750_13132439
J182535-121558	R1	18 25 35.40	−12 15 58.2	0.2 ± 0.3	0.1 ± 0.3	0.2 ± 0.5	1.00	2.3 ± 1.2	2.1 ± 1.2	**4.3 ± 1.7**	1.00	−0.10	–	
J182537-120645	R1	18 25 37.97	−12 6 45.2	0.3 ± 0.4	0.2 ± 0.4	0.5 ± 0.6	1.00	**2.5 ± 1.5**	0.1 ± 1.1	2.4 ± 1.9	1.00	−0.62	–	
J182544-113153	X3	18 25 44.08	−11 31 53.4	**2.8 ± 0.5**	0.3 ± 0.3	**3.0 ± 0.6**	1.00	–	–	–	–	−0.82	–	
J182544-121303	R1	18 25 44.20	−12 13 3.0	**1.4 ± 0.4**	**2.2 ± 0.5**	**3.5 ± 0.7**	1.00	1.1 ± 0.9	1.1 ± 0.9	1.8 ± 1.4	0.31	0.19	–	
J182549-121823	R1	18 25 49.81	−12 18 23.4	0.1 ± 0.3	0.0 ± 0.3	0.0 ± 0.5	1.00	2.7 ± 1.3	0.6 ± 1.0	**3.3 ± 1.6**	1.00	−0.65	19.8	–
J182550-114837	R2	18 25 50.51	−11 48 37.6	**0.9 ± 0.5**	0.0 ± 0.5	0.9 ± 0.7	1.00	0.0 ± 0.0	0.0 ± 0.0	0.0 ± 0.0	0.00	−1.00	–	
J182553-112519	X3	18 25 53.33	−11 25 19.4	**4.1 ± 0.6**	1.1 ± 0.4	**5.1 ± 0.8**	1.00	–	–	–	–	−0.59	17.5	U0750_13144978
J182553-112713	X3	18 25 53.86	−11 27 13.0	0.2 ± 0.3	**5.3 ± 0.7**	**5.5 ± 0.7**	1.00	–	–	–	–	0.92	12.3	U0750_13145056
J182558-120414	R1	18 25 58.37	−12 4 14.2	0.8 ± 0.5	0.9 ± 0.6	**1.6 ± 0.8**	1.00	0.5 ± 1.5	3.3 ± 1.7	3.8 ± 2.2	1.00	0.32	–	
J182559-114710	R2	18 25 59.88	−11 47 10.5	0.0 ± 0.4	**2.6 ± 0.6**	**2.3 ± 0.7**	1.00	0.0 ± 1.3	**9.5 ± 2.0**	**9.1 ± 2.4**	1.00	1.00	–	
J182601-110904	X5	18 26 1.19	−11 9 4.2	0.0 ± 0.3	0.0 ± 0.4	0.0 ± 0.5	0.94	0.5 ± 1.1	**2.7 ± 1.4**	**3.3 ± 1.8**	1.00	0.69	–	
J182601-122031	R1	18 26 1.64	−12 20 31.7	0.5 ± 0.4	0.4 ± 0.5	0.7 ± 0.6	1.00	2.0 ± 1.4	0.6 ± 1.3	**2.3 ± 1.9**	1.00	−0.34	–	
J182603-121952	R1	18 26 3.04	−12 19 52.8	0.0 ± 0.4	**1.2 ± 0.5**	0.7 ± 0.6	1.00	0.1 ± 1.1	0.0 ± 1.1	0.0 ± 1.6	1.00	0.97	18.4	U0750_13151482

Column 1: the X-ray source designation. **Column 2**: the XGPS-I survey field in which the source was detected. **Column 3**: the X-ray position. **Column 4**: the derived MOS count rates in the soft (s), hard (h) and broad-bands (b) with $\geqslant 5\sigma$ detections shown in bold and negative fluxes set to zero. **Column 5**: the MOS *quality* flag. **Column 6**: the derived pn count rates in the soft (s), hard (h) and broad-bands (b) with $\geqslant 5\sigma$ detections shown in bold and negative fluxes set to zero. **Column 7**: the pn *quality* flag. **Column 8**: the X-ray hardness ratio HR (see text). **Column 9**: the *R* magnitude of the brightest optical source within a 6 arcsec error circle based on the SuperCOSMOS digitisation of the *R* plate from the UK Schmidt Survey. **Column 10**: the designation of the optical source, if any, within a 6 arcsec X-ray error circle. Here, U = USNO, with all the other references taken from the SIMBAD data base. **Footnote**: the count rates quoted in this table are measured count rates and have not been corrected for the signal loss due to the limited size of the source cell (see Section 3.2).

Table A1 – *continued*

XGPS-I		Equinox J2000		MOS count ks^{-1}				pn count ks^{-1}						Optical
Designation	Obs	RA	DEC	s	h	b	q	s	h	b	q	HR	*R*	Identification
J182603-120933	R1	18 26 3.23	−12 9 33.7	0.0 ± 0.3	**4.1 ± 0.7**	**3.9 ± 0.8**	1.00	0.0 ± 1.0	0.0 ± 0.0	0.0 ± 0.0	0.14	1.00	15.2	U0750_13151668
J182603-120640	R1	18 26 3.74	−12 6 40.3	**1.3 ± 0.5**	0.3 ± 0.5	1.5 ± 0.7	1.00	1.3 ± 1.2	0.0 ± 1.1	0.1 ± 1.6	0.35	−0.69	13.1	U0750_13152275
J182604-114719	R2	18 26 4.00	−11 47 19.1	0.1 ± 0.4	**8.8 ± 0.9**	**8.8 ± 1.0**	1.00	0.0 ± 1.2	**14.2 ± 2.1**	**13.7 ± 2.4**	1.00	0.98	–	
J182605-111626	X5	18 26 5.18	−11 16 26.8	0.8 ± 0.6	**1.5 ± 0.7**	2.4 ± 0.9	1.00	0.7 ± 1.3	0.5 ± 1.5	1.2 ± 2.0	1.00	0.19	–	
J182606-111553	X5	18 26 6.36	−11 15 53.3	0.7 ± 0.5	**1.6 ± 0.7**	**2.3 ± 0.9**	1.00	0.5 ± 1.3	0.5 ± 1.4	0.9 ± 1.9	1.00	0.35	19.8	–
J182607-111204	X5	18 26 7.10	−11 12 4.8	0.2 ± 0.4	**1.3 ± 0.6**	1.4 ± 0.7	1.00	1.2 ± 1.1	1.0 ± 1.3	2.3 ± 1.7	1.00	0.42	–	
J182607-120627	R1	18 26 7.17	−12 6 27.0	**3.1 ± 0.7**	**1.7 ± 0.6**	**4.7 ± 0.9**	1.00	**6.1 ± 1.8**	3.1 ± 1.5	**8.9 ± 2.4**	1.00	−0.31	16.7	U0750_13154481
J182608-114317	X3	18 26 8.06	−11 43 17.8	0.0 ± 0.5	**1.5 ± 0.8**	1.2 ± 1.0	0.98	–	–	–	–	1.00	–	
J182608-121514	R1	18 26 8.21	−12 15 14.7	**2.5 ± 0.5**	0.3 ± 0.4	**2.7 ± 0.7**	1.00	**6.8 ± 1.5**	0.0 ± 0.9	**5.6 ± 1.7**	1.00	−0.88	13.6	U0750_13155125
J182608-112553	X3	18 26 8.31	−11 25 53.0	0.0 ± 0.3	**0.6±0.4**	0.3 ± 0.5	1.00	–	–	–	–	1.00	–	
J182608-115614	R2	18 26 8.56	−11 56 14.6	0.4 ± 0.3	1.3 ± 0.5	**1.6 ± 0.6**	1.00	0.6 ± 1.1	1.2 ± 1.3	1.7 ± 1.7	1.00	0.50	–	
J182609-120659	R1	18 26 9.36	−12 6 59.8	0.5 ± 0.4	**1.5 ± 0.6**	1.8 ± 0.7	1.00	0.4 ± 1.2	1.3 ± 1.3	1.5 ± 1.8	1.00	0.49	–	
J182609-114319	R2	18 26 9.38	−11 43 19.3	0.9 ± 0.4	**1.4 ± 0.5**	**2.3 ± 0.7**	1.00	1.3 ± 1.3	3.1 ± 1.7	4.3 ± 2.2	1.00	0.30	–	
J182614-110616	X5	18 26 14.55	−11 6 16.3	0.7 ± 0.4	**1.8 ± 0.5**	**2.4 ± 0.7**	1.00	0.0 ± 1.0	0.0 ± 1.1	0.0 ± 1.5	0.59	0.45	–	
J182614-110549	X5	18 26 14.69	−11 5 49.6	**1.9 ± 0.5**	**2.6 ± 0.6**	**4.5 ± 0.8**	1.00	**4.7 ± 1.3**	**5.9 ± 1.5**	**10.6 ± 2.0**	0.73	0.11	–	
J182615-122429	R1	18 26 15.03	−12 24 29.9	0.6 ± 0.7	**1.8 ± 0.8**	2.1 ± 1.1	1.00	0.0 ± 1.8	3.7 ± 2.0	2.4 ± 2.7	1.00	0.69	–	
J182617-112930	X3	18 26 17.74	−11 29 30.0	0.6 ± 0.4	0.7 ± 0.4	**1.3 ± 0.6**	1.00	–	–	–	–	0.10	19.9	–
J182621-105608	X5	18 26 21.66	−10 56 8.3	0.9 ± 0.7	**4.2 ± 1.0**	**5.1 ± 1.2**	1.00	0.0 ± 0.0	0.0 ± 0.0	0.0 ± 0.0	0.00	0.63	17.1	–
J182622-122409	R1	18 26 22.23	−12 24 9.9	0.6 ± 0.7	**2.9 ± 1.0**	**3.3 ± 1.2**	1.0	0.7 ± 1.9	**6.6 ± 2.5**	**6.7 ± 3.2**	0.98	0.70	–	
J182622-110344	X5	18 26 22.71	−11 3 44.2	0.0 ± 0.3	**2.2 ± 0.5**	**2.1 ± 0.6**	1.00	0.5 ± 1.0	**4.6 ± 1.4**	**5.1 ± 1.7**	1.00	0.91	–	
J182625-113422	X3	18 26 25.05	−11 34 22.7	0.8 ± 0.4	1.0 ± 0.5	**1.8 ± 0.7**	1.00	–	–	–	–	0.15	19.8	–
J182625-105918	X5	18 26 25.68	−10 59 18.5	0.4 ± 0.5	**1.8 ± 0.6**	**2.1 ± 0.8**	1.00	0.0 ± 1.2	1.5 ± 1.3	0.7 ± 1.7	1.00	0.70	18.4	–
J182625-112854	X3	18 26 25.73	−11 28 54.0	**1.3 ± 0.5**	**12.6 ± 1.1**	**13.8 ±1.2**	1.00	–	–	–	–	0.81	19.2	–
J182628-112224	X3	18 26 28.22	−11 22 24.8	**1.1 ± 0.6**	1.1 ± 0.6	**2.2 ± 0.8**	1.00	–	–	–	–	0.00	19.4	–
J182628-120922	R1	18 26 28.66	−12 9 22.5	**6.6 ± 1.1**	0.5 ± 0.6	**6.9 ± 1.2**	1.00	**11.4 ± 2.4**	1.0 ± 1.3	**12.3 ± 2.7**	1.00	−0.86	13.9	U0750_13170745
J182628-105754	X5	18 26 28.85	−10 57 54.8	0.9 ± 0.5	0.0 ± 0.5	0.4 ± 0.7	1.00	**5.2 ± 1.7**	0.0 ± 1.3	3.5 ± 2.1	0.67	−1.00	11.6	U0750_13170977
J182629-110057	X5	18 26 29.47	−11 0 57.5	**0.9 ± 0.4**	**0.9 ± 0.5**	**1.7 ± 0.7**	1.00	**5.5 ± 1.5**	**3.4 ± 1.3**	**8.9 ± 2.0**	1.00	−0.16	14.6	U0750_13171480
J182629-114541	R2	18 26 29.70	−11 45 41.3	0.6 ± 0.3	0.3 ± 0.3	0.9 ± 0.5	1.00	**2.8 ± 1.1**	0.5 ± 1.1	3.4 ± 1.5	1.00	−0.57	16.9	U0750_13171638
J182631-114537	R2	18 26 31.49	−11 45 37.4	1.0 ± 0.3	**1.5 ± 0.4**	**2.5 ± 0.5**	1.00	0.5 ± 0.9	**3.4 ± 1.2**	**4.1 ± 1.5**	0.86	0.41	–	
J182633-111142	X5	18 26 33.10	−11 11 42.6	0.7 ± 0.3	**0.5 ± 0.3**	**1.2 ± 0.4**	1.00	0.0 ± 0.7	**2.5 ± 1.0**	1.8 ± 1.2	0.9	0.32	19.2	–
J182634-111208	X5	18 26 34.71	−11 12 8.3	0.0 ± 0.2	**1.2 ± 0.4**	**1.2 ± 0.5**	1.00	0.0 ± 0.8	**3.7 ± 1.2**	**3.4 ± 1.4**	1.00	0.96	–	
J182635-115606	R2	18 26 35.71	−11 56 6.4	0.4 ± 0.3	0.5 ± 0.3	0.8 ± 0.4	1.00	**3.3 ± 1.0**	1.3 ± 0.9	**4.7 ± 1.4**	1.00	−0.28	17.1	U0750_13175953
J182636-114648	R2	18 26 36.32	−11 46 48.6	**2.4 ± 0.4**	0.9 ± 0.3	**3.4 ± 0.5**	1.00	**5.6 ± 1.1**	**2.3 ± 1.0**	**7.9 ± 1.5**	1.00	−0.43	12.2	U0750_13176371
J182636-105714	X5	18 26 36.60	−10 57 14.4	0.2 ± 0.4	**1.3 ± 0.6**	1.6 ± 0.8	1.00	0.0 ± 1.3	2.3 ± 1.8	1.6 ± 2.2	1.00	0.80	–	
J182637-121234	R1	18 26 37.20	−12 12 34.9	**3.6 ± 0.9**	0.0 ± 0.7	**3.1 ± 1.1**	1.00	0.0 ± 1.8	0.7 ± 1.5	0.3 ± 2.1	0.41	−0.86	–	
J182637-115522	R2	18 26 37.31	−11 55 22.9	0.3 ± 0.3	0.6 ± 0.3	**0.9 ± 0.4**	1.00	1.1 ± 0.8	0.1 ± 0.9	1.3 ± 1.2	1.00	−0.16	16.7	U0750_13177676
J182638-104341	X7	18 26 38.36	−10 43 41.6	**3.5 ± 1.0**	0.5 ± 0.7	**4.0 ± 1.3**	1.00	4.0 ± 2.0	0.0 ± 2.3	3.3 ± 2.8	1.00	−0.83	13.3	U0750_13179391
J182638-110030	X5	18 26 38.46	−11 0 30.2	0.0 ± 0.3	0.6 ± 0.4	0.6 ± 0.6	1.00	0.0 ± 1.2	**3.7 ± 1.4**	**2.8 ± 1.8**	1.00	0.99	–	
J182639-114216	R2	18 26 39.76	−11 42 16.4	**9.0 ± 0.9**	**1.6 ± 0.5**	**10.6 ± 1.0**	1.00	**34.6 ± 2.5**	3.25 ± 1.5	**38.3 ± 3.0**	1.00	−0.78	14.1	U0750_13179120
J182641-115827	R2	18 26 41.29	−11 58 27.0	0.2 ± 0.3	**1.0 ± 0.4**	**1.1 ± 0.5**	1.00	0.1 ± 0.9	3.6 ± 1.3	3.7 ± 1.6	1.00	0.84	–	

© 2004 RAS, MNRAS **351,** 31–56

Table A1 – *continued*

XGPS-I Designation	Obs	Equinox J2000 RA	DEC	MOS count ks^{-1} s	h	b	q	pn count ks^{-1} s	h	b	q	HR	*R*	Optical Identification
J182642-112122	X5	18 26 42.42	−11 21 22.7	**3.1 ± 0.8**	0.7 ± 0.6	**3.8 ± 1.0**	1.00	3.6 ± 1.9	0.8 ± 1.6	4.3 ± 2.5	1.00	−0.63	8.1	U0750_13181513 HD 169754
J182643-114230	R2	18 26 43.32	−11 42 30.1	0.0 ± 0.4	**1.7 ± 0.5**	1.2 ± 0.6	1.00	0.2 ± 1.1	**3.2 ± 1.5**	**3.4 ± 1.8**	1.00	0.94	18.9	IRAS 18239-1144
J182643-114735	R2	18 26 43.70	−11 47 35.0	**0.6 ± 0.3**	0.3 ± 0.3	**0.9 ± 0.4**	1.00	0.5 ± 0.8	0.7 ± 0.9	1.3 ± 1.2	1.00	−0.10	16.8	U0750_13182208
J182645-111507	X5	18 26 45.05	−11 15 7.7	**1.2 ± 0.4**	1.0 ± 0.4	**2.2 ± 0.6**	1.00	**3.0±1.2**	1.0 ± 1.1	**3.9 ± 1.6**	1.00	−0.25	–	
J182646-114034	R2	18 26 46.16	−11 40 34.1	0.3 ± 0.4	0.5 ± 0.5	**0.8 ± 0.7**	1.00	2.4 ± 1.3	1.2 ± 1.5	3.6 ± 2.0	1.00	−0.20	16.1	U0750_13184310
J182649-114903	R2	18 26 49.68	−11 49 3.8	0.2 ± 0.2	0.3 ± 0.3	0.6 ± 0.4	1.00	2.1 ± 0.8	2.8 ± 0.9	**5.1 ± 1.2**	1.00	0.16	–	
J182650-112640	R3	18 26 50.51	−11 26 40.6	0.3 ± 0.5	**1.5 ± 0.7**	**1.7 ± 0.8**	1.00	1.7 ± 1.5	2.5 ± 1.6	4.2 ± 2.2	1.00	0.42	19.3	–
J182651-110339	X5	18 26 51.29	−11 3 39.6	**0.5 ± 0.3**	0.1 ± 0.3	0.5 ± 0.5	0.98	0.0 ± 0.8	0.0 ± 0.8	0.0 ± 1.2	0.73	−0.72	19.1	–
J182653-110352	X5	18 26 53.35	−11 3 52.1	0.6 ± 0.3	0.7 ± 0.4	1.2 ± 0.5	1.00	**1.4 ± 1.0**	1.1 ± 1.0	2.3 ± 1.4	1.00	0.01	–	
J182653-105529	X5	18 26 53.88	−10 55 29.4	0.4 ± 0.5	**2.2 ± 0.8**	2.4 ± 1.0	1.00	0.0 ± 0.0	0.0 ± 0.0	0.0 ± 0.0	0.00	0.70	–	
J182655-114524	R2	18 26 55.10	−11 45 24.4	0.7 ± 0.4	0.9 ± 0.4	**1.6 ± 0.5**	1.00	0.2 ± 0.8	0.5 ± 0.9	0.8 ± 1.2	1.00	0.15	–	
J182655-105038	X7	18 26 55.39	−10 50 38.2	0.3 ± 0.5	**1.6 ± 0.7**	**1.9 ± 0.8**	1.00	1.2 ± 1.4	3.8 ± 1.8	4.8 ± 2.3	1.00	0.59	19.9	–
J182655-114244	R2	18 26 55.80	−11 42 44.2	0.0 ± 0.3	0.2 ± 0.4	0.1 ± 0.5	1.00	**3.9 ± 1.2**	0.3 ± 1.2	4.0 ± 1.7	1.00	−0.71	–	
J182656-114011	R2	18 26 56.54	−11 40 11.8	**1.8 ± 0.6**	0.8 ± 0.6	**2.5 ± 0.8**	1.00	**6.6 ± 1.6**	1.4 ± 1.5	**8.2 ± 2.2**	1.00	−0.56	15.1	U0750_13192255
J182658-113300	R3	18 26 58.42	−11 33 0.7	0.5 ± 0.5	**1.1 ± 0.6**	**1.6 ± 0.8**	1.00	1.3 ± 1.4	2.2 ± 1.5	**3.7 ± 2.0**	1.00	0.33	13.9	U0750_13193578
J182658-115544	R2	18 26 58.53	−11 55 44.0	0.8 ± 0.3	0.9 ± 0.4	**1.7 ± 0.5**	1.00	1.4 ± 0.9	0.0 ± 1.0	0.0 ± 1.3	1.00	−0.26	16.4	U0750_13193888
J182659-110936	X5	18 26 59.18	−11 9 36.0	0.2 ± 0.3	**1.3 ± 0.4**	**1.5 ± 0.5**	1.00	0.0 ± 0.8	0.0 ± 0.8	0.0 ± 1.2	0.27	0.71	–	
J182659-115312	R2	18 26 59.20	−11 53 12.0	0.3 ± 0.3	0.0 ± 0.3	0.3 ± 0.4	1.00	1.2 ± 0.8	**2.7 ± 1.0**	**4.0 ± 1.3**	1.00	0.16	–	
J182701-114628	R2	18 27 1.62	−11 46 28.0	0.7 ± 0.4	0.4 ± 0.4	1.2 ± 0.5	1.00	**3.0 ± 1.1**	**3.7 ± 1.2**	**6.7 ± 1.6**	1.00	−0.02	17.5	–
J182703-113714	R3	18 27 3.66	−11 37 14.1	**3.17 ± 0.8**	**2.07 ± 0.7**	**5.36 ± 1.0**	1.00	**7.58 ± 2.0**	**5.35 ± 1.8**	**12.97 ± 2.7**	0.88	−0.21	15.8	U0750_13196685
J182705-104302	X7	18 27 5.23	−10 43 2.6	0.5 ± 0.4	**1.5 ± 0.6**	**1.9 ± 0.7**	1.00	0.5 ± 1.2	2.7 ± 1.5	3.2 ± 1.9	1.00	0.56	18.4	U0750_13198612
J182705-120453	X2	18 27 5.38	−12 4 53.4	0.6 ± 0.5	**2.7 ± 0.8**	**3.3 ± 0.9**	0.59	–	–	–	–	0.62	–	
J182706-112437	R3	18 27 6.40	−11 24 37.4	0.2 ± 0.4	**3.9 ± 0.7**	**4.2 ± 0.8**	1.00	0.0 ± 1.2	**7.7 ± 1.7**	**6.4 ± 2.0**	1.00	0.93	17.8	U0750_13199496 GPSR5 20.021+0.124
J182708-113459	R3	18 27 8.66	−11 34 59.9	0.2 ± 0.4	**2.0 ± 0.6**	2.2 ± 0.7	1.00	0.0 ± 1.3	0.0 ± 1.3	0.0 ± 1.9	0.41	0.85	–	
J182709-105318	X7	18 27 9.48	−10 53 18.5	0.7 ± 0.4	1.0 ± 0.5	**1.7 ± 0.7**	1.00	0.0 ± 1.3	1.0 ± 1.4	0.0 ± 1.8	1.00	0.28	–	
J182711-105743	X7	18 27 11.10	−10 57 43.2	0.0 ± 0.5	**1.8 ± 0.8**	1.5 ± 0.9	1.00	4.4 ± 2.0	5.4 ± 2.3	**9.8 ± 3.0**	1.00	0.39	–	
J182711-112550	R3	18 27 11.36	−11 25 50.0	0.7 ± 0.4	0.8 ± 0.4	**1.5 ± 0.6**	1.00	0.0 ± 1.1	0.8 ±1.1	0.5 ± 1.5	1.00	0.23	18.9	–
J182712-102832	X9	18 27 12.07	−10 28 32.9	0.0 ± 0.0	0.0 ± 0.0	0.0 ± 0.0	0.00	**9.3 ± 3.0**	2.7 ± 2.6	**12.1 ± 3.9**	1.00	−0.57	13.9	U0750_13204067
J182712-112803	R3	18 27 12.12	−11 28 3.6	0.2 ± 0.3	**1.2 ± 0.4**	**1.4 ± 0.5**	1.00	0.7 ± 1.0	1.1 ± 1.1	1.7 ± 1.5	1.00	0.54	19.1	U0750_13204022
J182714-111814	R3	18 27 14.47	−11 18 14.9	1.1 ± 0.6	1.3 ± 0.7	**2.4 ± 0.9**	1.00	2.4 ± 1.7	**4.3 ± 2.1**	**6.7 ± 2.7**	1.00	0.19	–	
J182714-113027	R3	18 27 14.96	−11 30 27.2	**0.9 ± 0.4**	0.4 ± 0.4	1.2 ± 0.5	1.00	**1.7 ± 1.0**	0.0 ± 1.0	**1.7 ± 1.4**	1.00	−0.60	15.6	U0750_13206027
J182716-114832	R2	18 27 16.88	−11 48 32.2	0.6 ± 0.4	**3.0 ± 0.6**	**3.5 ± 0.7**	1.00	1.2 ± 1.1	**7.4 ± 1.5**	**8.0 ± 1.9**	1.00	0.69	16.7	U0750_13207576
J182718-112821	R3	18 27 18.33	−11 28 21.9	**0.6 ± 0.3**	**0.8 ± 0.4**	**1.4 ± 0.5**	1.00	0.0 ± 0.9	1.3 ± 1.0	1.1 ± 1.3	0.88	0.38	16.8	U0750_13208642
J182721-104715	X7	18 27 21.45	−10 47 15.1	0.0 ± 0.3	**0.6 ± 0.3**	0.4 ± 0.4	1.00	0.0 ± 1.0	0.0 ± 1.0	0.0 ± 1.4	1.00	1.00	–	
J182721-120730	X2	18 27 21.71	−12 7 30.2	**2.9 ± 0.6**	**1.0 ± 0.4**	**3.8 ± 0.7**	1.00	–	–	–	–	−0.49	18.0	–
J182721-104355	X7	18 27 21.94	−10 43 55.5	**0.9 ± 0.4**	0.4 ± 0.4	1.2 ± 0.6	1.00	0.6 ± 1.1	0.0 ± 1.1	0.0 ± 1.5	1.00	−0.47	16.1	U0750_13211445
J182722-111149	X5	18 27 22.07	−11 11 49.7	0.6 ± 0.5	**1.2 ± 0.6**	**1.8 ± 0.7**	1.00	3.5 ± 1.7	1.7 ± 1.6	5.2 ± 2.3	1.00	0.00	15.8	U0750_13211722

Table A1 – *continued*

XGPS-I Designation	Obs	Equinox J2000 RA	DEC	MOS count ks^{-1} s	h	b	q	pn count ks^{-1} s	h	b	q	HR	R	Optical Identification
J182722-105656	X7	18 27 22.85	−10 56 56.2	0.5 ± 0.5	1.6 ± 0.7	**1.9 ± 0.8**	1.00	2.6 ± 1.8	0.0 ± 1.6	1.1 ± 2.3	1.00	0.07	15.7	–
J182723-110910	R4	18 27 23.88	−11 9 10.4	0.8 ± 0.6	**2.8 ± 0.9**	**3.5 ± 1.1**	1.00	0.0 ± 0.0	0.0 ± 0.0	0.0 ± 0.0	0.00	0.56	–	
J182726-121304	X2	18 27 26.28	−12 13 4.8	**0.9 ± 0.4**	0.0 ± 0.3	0.9 ± 0.5	1.00	–	–	–	–	−0.97	19.8	–
J182726-120641	X2	18 27 26.35	−12 6 41.1	**0.8 ± 0.4**	0.0 ± 0.3	0.7 ± 0.5	1.00	–	–	–	–	−1.00	–	
J182726-101550	X9	18 27 26.88	−10 15 50.5	0.0 ± 0.0	0.0 ± 0.0	0.0 ± 0.0	0.00	**24.5 ± 4.2**	0.0 ± 2.3	**24.9 ± 4.9**	0.59	−1.00	–	
J182726-112041	R3	18 27 26.89	−11 20 41.4	**1.5 ± 0.5**	0.9 ± 0.5	**2.4 ± 0.7**	1.00	**2.9 ± 1.4**	1.2 ± 1.4	**4.1 ± 1.4**	0.88	−0.33	14.8	U0750_13215286
J182727-122036	X2	18 27 27.10	−12 20 36.5	1.3 ± 0.6	**2.6 ± 0.7**	**3.9 ± 0.9**	1.00	–	–	–	–	0.32	–	
J182727-112851	R3	18 27 27.66	−11 28 51.0	**0.8 ± 0.3**	0.1 ± 0.3	0.9 ± 0.4	1.00	0.0 ± 0.8	0.0 ± 0.8	0.0 ± 1.2	0.65	−0.80	18.1	U0750_13216023
J182728-113742	R3	18 27 28.76	−11 37 42.6	**2.9 ± 0.6**	0.2 ± 0.4	**3.1 ± 0.7**	1.00	**8.2 ± 1.7**	1.1 ± 1.4	**9.3 ± 2.2**	1.00	−0.83	13.1	U0750_13216684
J182730-113514	R3	18 27 30.76	−11 35 14.3	0.3 ± 0.3	0.6 ± 0.4	0.9 ± 0.5	0.82	**2.6 ± 1.2**	2.3 ± 1.2	**5.1 ± 1.7**	1.00	0.05	–	
J182731-105123	X7	18 27 31.86	−10 51 23.1	**1.1 ± 0.4**	0.5 ± 0.4	**1.5 ± 0.6**	1.00	**5.1 ± 1.5**	0.6 ± 1.1	**5.6 ± 1.9**	1.00	−0.62	16.3	U0750_13219420
J182732-113358	R3	18 27 32.46	−11 33 58.5	**1.0 ± 0.4**	**3.1 ± 0.5**	**4.1 ± 0.6**	1.00	2.3 ± 1.1	**7.8 ± 1.4**	**10.0 ± 1.8**	1.00	0.52	16.7	U0750_13220110
J182733-120734	X2	18 27 33.35	−12 7 34.5	**0.9 ± 0.4**	**0.8 ± 0.4**	**1.6 ± 0.6**	1.00	–	–	–	–	−0.04	–	
J182734-120645	X2	18 27 34.25	−12 6 45.7	0.0 ± 0.3	**0.7 ± 0.4**	0.7 ± 0.5	1.00	–	–	–	–	1.00	19.6	–
J182734-112305	R3	18 27 34.47	−11 23 5.7	**1.0 ± 0.4**	0.0 ± 0.3	**0.8 ± 0.5**	1.00	**3.5 ± 1.2**	1.2 ± 1.1	**4.8 ± 1.7**	1.00	−0.69	19.3	–
J182735-121059	X2	18 27 35.62	−12 10 59.9	0.0 ± 0.3	**0.9 ± 0.3**	0.8 ± 0.4	1.00	–	–	–	–	1.00	–	
J182736-105340	X7	18 27 36.57	−10 53 40.3	1.4 ± 0.5	**3.8 ± 0.7**	**5.1 ± 0.9**	1.00	0.8 ± 1.4	**4.5 ± 1.8**	**5.2 ± 2.2**	0.59	0.51	–	
J182737-111338	R4	18 27 37.25	−11 13 38.6	0.6 ± 0.6	1.5 ± 0.7	2.0 ± 1.0	1.00	0.3 ± 1.8	**7.1 ± 2.5**	**7.2 ± 3.0**	1.00	0.64	–	
J182738-105328	X7	18 27 38.52	−10 53 28.8	1.4 ± 0.5	**2.3 ± 0.6**	**3.6 ± 0.8**	1.00	1.1 ± 1.4	**5.8 ± 1.9**	**6.8 ± 2.3**	1.00	0.41	–	
J182738-104359	X7	18 27 38.64	−10 43 59.0	0.5 ± 0.4	**1.5 ± 0.5**	**2.0 ± 0.6**	1.00	0.3 ± 1.0	**4.3 ± 1.4**	**4.3 ± 1.8**	1.00	0.65	19.0	U0750_13225258
J182740-102812	X9	18 27 40.08	−10 28 12.4	**6.8 ± 0.8**	0.6 ± 0.5	**7.4 ± 1.0**	1.00	**21.0 ± 2.7**	1.1 ± 1.5	**22.3 ± 3.1**	1.00	−0.86	14.2	U0750_13226146 1RXS J182742.4-102813
J182740-113955	R3	18 27 40.40	−11 39 55.3	**7.1 ± 0.9**	0.4 ± 0.5	**7.6 ± 1.0**	1.00	**28.9 ± 3.0**	3.8 ± 1.8	**33.3 ± 3.5**	1.00	−0.83	18.5	U0750_13226450
J182740-120327	X2	18 27 40.66	−12 3 27.3	0.1 ± 0.4	**1.3 ± 0.5**	1.3 ± 0.6	1.00	–	–	–	–	0.87	19.3	–
J182740-120553	X2	18 27 40.97	−12 5 53.4	**0.8 ± 0.4**	0.3 ± 0.4	**1.1 ± 0.5**	1.00	–	–	–	–	−0.51	19.8	–
J182741-121344	X2	18 27 41.04	−12 13 44.7	0.0 ± 0.3	**1.0 ± 0.4**	0.9 ± 0.5	1.00	–	–	–	–	0.92	–	
J182741-112715	R3	18 27 41.26	−11 27 15.9	**1.2 ± 0.3**	0.0 ± 0.3	**1.2 ± 0.4**	1.00	**4.3 ± 1.1**	1.8 ± 1.0	**6.2 ± 1.5**	0.98	−0.61	16.1	U0750_13227020
J182742-115731	X4	18 27 42.57	−11 57 31.1	0.4 ± 0.6	**1.7 ± 0.9**	1.9 ± 1.1	1.00	–	–	–	–	0.65	–	
J182744-113955	R3	18 27 44.80	−11 39 55.4	**2.0 ± 0.6**	0.4 ± 0.5	**2.4 ± 0.8**	1.00	**6.5 ± 1.9**	0.0 ± 1.4	**6.0 ± 2.3**	0.86	−0.84	11.4	U0750_13229697
J182745-120606	X2	18 27 45.55	−12 6 6.8	**5.3 ± 0.7**	**18.9 ± 1.2**	**24.1 ± 1.4**	1.00	–	–	–	–	0.56	–	
J182746-110255	R4	18 27 46.33	−11 2 55.1	**2.2 ± 0.5**	**3.5 ± 0.7**	**5.6 ± 0.9**	1.00	4.0 ± 1.6	**5.9 ± 1.9**	**9.9 ± 2.5**	1.00	0.21	–	
J182746-103150	X9	18 27 46.74	−10 31 50.1	0.0 ± 0.5	**1.7 ± 0.7**	0.7 ± 0.8	0.59	0.0 ± 1.2	1.9 ± 1.7	1.9 ± 2.1	1.00	0.99	16.2	U0750_13231392
J182748-115625	X4	18 27 48.02	−11 56 25.2	1.7 ± 0.7	**2.3 ± 0.8**	**3.9 ± 1.0**	1.00	–	–	–	–	0.14	19.8	U0750_13232314
J182748-112130	R3	18 27 48.98	−11 21 30.2	**1.1 ± 0.4**	0.1 ± 0.4	1.2 ± 0.6	1.00	**3.5 ± 1.5**	0.0 ± 1.3	3.4 ± 2.0	1.00	−0.96	–	
J182749-105322	X7	18 27 49.17	−10 53 22.4	0.4 ± 0.4	**2.9 ± 0.7**	**3.2 ± 0.8**	1.00	0.8 ± 1.5	**4.4 ± 1.9**	5.2 ± 2.4	1.00	0.74	–	
J182749-102532	X9	18 27 49.42	−10 25 32.8	**0.83 ± 0.4**	**1.15 ± 0.5**	**1.98 ± 0.6**	0.88	2.56 ± 1.2	1.97 ± 1.4	**4.49 ± 1.9**	1.00	0.04	13.1	U0750_13233572
J182749-113725	R3	18 27 49.60	−11 37 25.4	1.1 ± 0.5	0.9 ± 0.5	**2.1 ± 0.7**	1.00	3.2 ± 1.5	**5.7 ± 1.7**	**8.9 ± 2.3**	1.00	0.12	19.9	–
J182749-113341	R3	18 27 49.99	−11 33 41.8	0.0 ± 0.3	**0.3 ± 0.3**	0.1 ± 0.4	1.00	0.5 ± 1.0	0.1 ± 1.1	0.5 ± 1.5	1.00	0.38	19.0	–
J182750-110408	R4	18 27 50.74	−11 4 8.2	0.3 ± 0.4	**1.5 ± 0.5**	**1.6 ± 0.6**	1.00	0.3 ± 1.2	2.8 ± 1.6	2.8 ± 2.0	1.00	0.72	19.2	–
J182750-113547	R3	18 27 50.99	−11 35 47.5	0.9 ± 0.4	**3.1 ± 0.6**	**4.0 ± 0.7**	1.00	**3.2 ± 1.3**	**5.6 ± 1.6**	**8.7 ± 2.1**	1.00	0.42	–	
J182752-105149	X7	18 27 52.54	−10 51 49.6	**1.2 ± 0.5**	**2.1 ± 0.6**	**3.4 ± 0.8**	1.00	0.9 ± 1.5	**4.3 ± 1.9**	**5.2 ± 2.4**	0.73	0.39	19.9	–

© 2004 RAS, MNRAS **351,** 31–56

Table A1 – *continued*

XGPS-I Designation	Obs	Equinox J2000 RA	DEC	MOS count ks^{-1} s	h	b	q	pn count ks^{-1} s	h	b	q	HR	*R*	Optical Identification
J182755-114958	X4	18 27 55.70	−11 49 58.9	0.3 ± 0.4	**1.0 ± 0.5**	**1.2 ± 0.6**	1.00	–	–	–	–	0.57	18.6	–
J182755-120346	X2	18 27 55.75	−12 3 46.3	0.3 ± 0.4	**2.3 ± 0.6**	**2.6 ± 0.7**	1.00	–	–	–	–	0.76	–	
J182756-105124	X7	18 27 56.14	−10 51 24.4	0.6 ± 0.4	0.5 ± 0.5	**1.1 ± 0.6**	1.00	0.1 ± 1.3	0.0 ± 1.5	0.1 ± 2.0	1.00	−0.11	19.2	U0750_13238574
J182756-110450	R4	18 27 56.84	−11 4 50.9	0.5 ± 0.4	**11.0 ± 0.8**	**11.3 ± 0.9**	1.00	1.2 ± 1.1	**22.9 ± 2.5**	**23.3 ± 2.8**	1.00	0.91	–	
J182757-110542	R4	18 27 57.24	−11 5 42.7	0.2 ± 0.3	**1.6 ± 0.5**	**1.6 ± 0.6**	1.00	0.0 ± 1.0	0.0 ± 1.2	0.0 ± 1.7	0.27	0.79	–	
J182757-120941	X2	18 27 57.24	−12 9 41.6	**13.9 ± 1.0**	**2.3 ± 0.5**	**16.1 ± 1.1**	1.00	–	–	–	–	−0.72	–	
J182800-121501	X2	18 28 0.47	−12 15 1.1	**0.9 ± 0.4**	0.0 ± 0.3	0.7 ± 0.5	1.00	–	–	–	–	−1.00	18.2	–
J182803-121638	X2	18 28 3.83	−12 16 38.4	**1.2 ± 0.5**	0.9 ± 0.5	**2.1 ± 0.7**	1.00	–	–	–	–	−0.10	15.1	U0750_13244399
J182804-113337	R3	18 28 4.91	−11 33 37.1	0.2 ± 0.3	0.1 ± 0.4	0.4 ± 0.6	1.00	0.0 ± 1.2	**3.3 ± 1.6**	2.6 ± 2.0	1.00	0.66	–	
J182805-113830	R3	18 28 5.26	−11 38 30.4	0.9 ± 0.5	0.6 ± 0.6	1.5 ± 0.8	1.00	4.2 ± 1.9	4.2 ± 2.0	**8.0 ± 2.8**	1.00	−0.08	18.7	U0750_13245254
J182806-113735	R3	18 28 6.01	−11 37 35.5	**0.9 ± 0.5**	0.1 ± 0.5	**1.2 ± 0.7**	1.00	0.4 ± 1.5	0.8 ± 1.8	0.5 ± 2.4	1.00	−0.49	13.5	U0750_13246006
J182806-103419	X9	18 28 6.07	−10 34 19.6	**1.2 ± 0.5**	0.0 ± 0.4	1.1 ± 0.7	1.00	0.0 ± 1.1	0.6 ± 1.6	0.0 ± 1.9	1.00	−0.74	19.1	–
J182808-105946	R4	18 28 8.10	−10 59 46.7	0.7 ± 0.4	**4.1 ± 0.6**	**4.7 ± 0.8**	1.00	0.0 ± 0.0	0.0 ± 0.0	0.0 ± 1.9	0.14	0.68	–	
J182808-112711	R3	18 28 8.49	−11 27 11.2	0.0 ± 0.4	0.1 ± 0.4	0.0 ± 0.5	1.00	**2.5 ± 1.4**	0.0 ± 1.3	1.4 ± 1.9	0.76	−0.84	–	
J182809-104423	R5	18 28 9.16	−10 44 23.6	**1.3 ± 0.5**	0.0 ± 0.4	0.9 ± 0.7	0.98	0.0 ± 0.0	0.0 ± 0.0	0.0 ± 0.0	0.00	−1.00	16.2	U0750_13248381
J182810-114933	X4	18 28 10.50	−11 49 33.8	**1.9 ± 0.5**	0.8 ± 0.3	**2.8 ± 0.6**	1.00	–	–	–	–	−0.42	19.1	–
J182811-114147	X4	18 28 11.38	−11 41 47.6	0.0 ± 0.4	**2.4 ± 0.6**	2.1 ± 0.7	1.00	–	–	–	–	1.00	17.7	U0750_13249762
J182811-121220	X2	18 28 11.58	−12 12 20.5	0.0 ± 0.3	**0.9 ± 0.4**	0.6 ± 0.5	1.00	–	–	–	–	1.00	18.2	U0750_13249956
J182811-110435	R4	18 28 11.63	−11 4 35.1	**0.7 ± 0.3**	**0.8 ± 0.4**	**1.4 ± 0.5**	1.00	0.7 ± 1.1	**4.6 ± 1.4**	**5.1 ± 1.8**	1.00	0.38	–	
J182811-102540	X9	18 28 11.92	−10 25 40.9	0.0 ± 0.2	**1.1 ± 0.4**	1.0 ± 0.5	1.00	1.3 ± 1.0	2.0 ± 1.2	3.5 ± 1.6	1.00	0.65	13.8	U0750_13250193 IRAS 18254-1027
J182812-115031	X4	18 28 12.51	−11 50 31.0	0.6 ± 0.3	0.7 ± 0.3	**1.4 ± 0.5**	1.00	–	–	–	–	0.09	–	
J182813-102859	X9	18 28 13.49	−10 28 59.7	0.1 ± 0.3	**0.5 ± 0.4**	0.7 ± 0.4	1.00	0.0 ± 0.9	0.0 ± 1.0	0.0 ± 1.4	0.73	0.64	–	
J182813-102035	X9	18 28 13.57	−10 20 35.4	0.2 ± 0.3	**1.9 ± 0.5**	**2.1 ± 0.6**	0.73	0.8 ± 1.1	**4.4 ± 1.6**	5.1 ± 2.0	1.00	0.76	–	
J182813-120730	X2	18 28 13.59	−12 7 30.1	0.4 ± 0.4	**3.9 ± 0.7**	**4.3 ± 0.8**	1.00	–	–	–	–	0.82	–	
J182813-110117	R4	18 28 13.76	−11 1 17.4	0.1 ± 0.3	**1.4 ± 0.4**	**1.4 ± 0.5**	1.00	1.5 ± 1.2	1.8 ± 1.4	3.2 ± 1.9	1.00	0.57	–	
J182813-103808	X9	18 28 13.84	−10 38 8.7	**4.3 ± 0.8**	0.6 ± 0.7	**5.0 ± 1.1**	1.00	**7.5 ± 2.5**	0.0 ± 2.4	6.3 ± 3.4	0.71	−0.83	16.5	U0750_13251657
J182814-103728	X9	18 28 14.23	−10 37 28.9	0.8 ± 0.6	**13.8 ± 1.4**	**14.4 ± 1.5**	1.00	1.6 ± 1.9	**15.3 ± 3.3**	**16.6 ± 3.7**	0.88	0.86	–	
J182814-104859	R5	18 28 14.82	−10 48 59.3	**1.0 ± 0.4**	0.1 ± 0.4	0.9 ± 0.6	1.00	0.0 ± 0.0	0.0 ± 0.0	0.0 ± 0.0	0.00	−0.82	–	
J182815-115432	X4	18 28 15.05	−11 54 32.8	**2.3 ± 0.5**	**2.5 ± 0.5**	**4.8 ± 0.7**	1.00	–	–	–	–	0.02	–	
J182816-103823	X9	18 28 16.15	−10 38 23.8	**1.7 ± 0.7**	1.2 ± 0.8	**2.9 ± 1.0**	1.00	**6.9 ± 2.5**	0.0 ± 2.5	2.5 ± 3.3	1.00	−0.49	–	
J182816-111132	R4	18 28 16.28	−11 11 32.9	**0.7 ± 0.4**	0.1 ± 0.4	0.7 ± 0.5	0.98	2.0 ± 1.3	0.2 ± 1.3	1.9 ± 1.9	1.00	−0.75	19.7	–
J182816-115518	X4	18 28 16.36	−11 55 18.4	0.4 ± 0.3	0.6 ± 0.4	**1.0 ± 0.5**	1.00	–	–	–	–	0.23	–	
J182816-105007	R5	18 28 16.93	−10 50 7.4	0.3 ± 0.4	**1.8 ± 0.6**	**2.0 ± 0.7**	1.00	0.0 ± 0.0	0.0 ± 0.0	0.0 ± 0.0	0.00	0.70	–	
J182817-103109	X9	18 28 17.98	−10 31 9.9	0.3 ± 0.3	**0.9 ± 0.4**	**1.3 ± 0.5**	1.00	1.3 ± 1.2	3.7 ± 1.6	5.1 ± 2.0	1.00	0.49	–	
J182819-100205	X12	18 28 19.27	−10 2 5.8	**1.4 ± 0.5**	1.3 ± 0.5	**2.5 ± 0.7**	1.00	**3.9 ± 1.5**	1.3 ± 1.3	**5.2 ± 2.0**	1.00	−0.25	11.4	U0750_13255545
J182820-114752	X4	18 28 20.65	−11 47 52.9	**1.1 ± 0.4**	**0.8 ± 0.3**	**1.9 ± 0.5**	1.00	–	–	–	–	−0.17	–	
J182821-104245	R5	18 28 21.07	−10 42 45.3	0.0 ± 0.3	**1.0 ± 0.4**	0.6 ± 0.5	1.00	1.1 ± 1.1	2.0 ± 1.3	2.6 ± 1.7	1.00	0.63	–	
J182821-101125	X12	18 28 21.84	−10 11 25.9	**5.0 ± 0.9**	0.0 ± 0.4	**4.8 ± 0.9**	1.00	**23.2 ± 3.0**	0.0 ± 1.1	**22.4 ± 3.2**	1.00	−1.00	10.1	U0750_13257479
J182821-104202	R5	18 28 21.86	−10 42 2.5	0.9 ± 0.4	**1.5 ± 0.5**	**2.4 ± 0.6**	1.00	0.0 ± 1.0	4.0 ± 1.4	3.0 ± 1.7	1.00	0.53	–	

Table A1 – *continued*

XGPS-I Designation	Obs	Equinox J2000 RA	DEC	MOS count ks^{-1} s	h	b	q	pn count ks^{-1} s	h	b	q	HR	R	Optical Identification
J182822-114927	X4	18 28 22.59	−11 49 27.6	0.3 ± 0.3	**0.7 ± 0.3**	**1.0 ± 0.4**	1.00	–	–	–	–	0.36	–	
J182822-114724	X4	18 28 22.78	−11 47 24.0	0.3 ± 0.3	**0.7 ± 0.3**	**1.1 ± 0.4**	1.00	–	–	–	–	0.40	–	
J182823-114157	X4	18 28 23.43	−11 41 57.4	0.4 ± 0.4	**0.9 ± 0.4**	**1.3 ± 0.6**	1.00	–	–	–	–	0.37	–	
J182823-105107	R5	18 28 23.71	−10 51 7.7	0.0 ± 0.4	**1.2 ± 0.5**	**0.9 ± 0.6**	1.00	1.1 ± 1.2	2.6 ± 1.5	3.8 ± 1.9	1.00	0.68	–	
J182824-121006	X2	18 28 24.17	−12 10 6.5	0.5 ± 0.5	**6.0 ± 0.9**	**6.3 ± 1.0**	1.00	–	–	–	–	0.85	18.9	–
J182824-120833	X2	18 28 24.47	−12 8 33.0	0.3 ± 0.4	**1.7 ± 0.6**	**1.9 ± 0.8**	1.00	–	–	–	–	0.70	–	
J182825-112721	R3	18 28 25.05	−11 27 21.3	0.0 ± 0.4	**2.5 ± 0.7**	**2.5 ± 0.8**	1.00	2.3 ± 1.9	4.4 ± 2.2	6.6 ± 2.9	0.98	0.68	17.2	U0750_13259803
J182827-104131	R5	18 28 27.07	−10 41 31.6	**1.1 ± 0.4**	**1.8 ± 0.5**	**2.8 ± 0.6**	1.00	1.2 ± 1.1	**4.9 ± 1.4**	**5.8 ± 1.7**	1.00	0.41	–	
J182827-113818	X4	18 28 27.44	−11 38 18.0	0.8 ± 0.5	**2.3 ± 0.6**	**3.1 ± 0.8**	1.00	–	–	–	–	0.45	18.7	U0750_13261369
J182827-100245	X12	18 28 27.44	−10 2 45.5	0.9 ± 0.4	0.5 ± 0.4	**1.3 ± 0.5**	1.00	0.3 ± 0.9	0.1 ± 0.9	0.3 ± 1.3	0.59	−0.34	–	
J182827-104454	R5	18 28 27.73	−10 44 54.0	0.5 ± 0.3	0.6 ± 0.4	**1.1 ± 0.5**	1.00	0.0 ± 0.8	0.0 ± 0.8	0.0 ± 1.1	1.00	0.14	19.9	–
J182827-111751	R4	18 28 27.77	−11 17 51.8	1.3 ± 0.6	**7.3 ± 1.0**	**8.4 ± 1.2**	1.00	4.3 ± 2.3	**19.7 ± 3.6**	**23.4 ± 4.2**	1.00	0.67	17.7	U0750_13261547
J182828-102357	X9	18 28 28.14	−10 23 57.3	0.6 ± 0.3	**4.4 ± 0.6**	**4.9 ± 0.7**	1.00	0.0 ± 1.0	**9.8 ± 1.9**	**8.7 ± 2.1**	1.00	0.84	15.6	U0750_13261865
J182828-103741	X9	18 28 28.77	−10 37 41.5	0.3 ± 0.5	**6.5 ± 1.2**	**6.7 ± 1.3**	1.00	0.0 ± 1.8	**16.6 ± 4.0**	15.6 ± 4.3	0.59	0.94	–	
J182829-121406	X2	18 28 29.49	−12 14 6.4	**1.8 ± 0.6**	0.9 ± 0.6	**2.8 ± 0.9**	1.00	–	–	–	–	−0.33	–	
J182830-114516	X4	18 28 30.05	−11 45 16.8	**14.9 ± 1.0**	**1.5 ± 0.4**	**16.4 ± 1.1**	1.00	–	–	–	–	−0.82	–	
J182830-115147	X4	18 28 30.69	−11 51 47.7	**1.0 ± 0.4**	**0.7 ± 0.3**	**1.7 ± 0.5**	1.00	–	–	–	–	−0.16	–	
J182831-100332	X12	18 28 31.01	−10 3 32.8	0.3 ± 0.3	0.5 ± 0.4	**0.7 ± 0.5**	1.00	0.1 ± 0.7	0.5 ± 0.9	0.5 ± 1.2	1.00	0.28	18.7	–
J182831-103123	X9	18 28 31.46	−10 31 23.4	0.0 ± 0.4	**1.1 ± 0.5**	1.1 ± 0.6	0.98	0.2 ± 1.2	1.3 ± 1.7	1.3 ± 2.1	1.00	0.93	–	
J182831-104108	R5	18 28 31.71	−10 41 8.1	0.1 ± 0.3	0.4 ± 0.4	0.4 ± 0.4	1.00	0.0 ± 0.8	**2.0 ± 1.1**	1.7 ± 1.4	1.00	0.90	–	
J182831-095805	X12	18 28 31.91	−9 58 5.9	0.0 ± 0.3	**2.2 ± 0.6**	**1.9 ± 0.7**	1.00	1.6 ± 1.1	**5.2 ± 1.6**	**6.8 ± 1.9**	0.90	0.74	–	
J182833-103823	X9	18 28 33.60	−10 38 23.0	0.0 ± 0.0	0.0 ± 0.0	0.0 ± 0.0	0.00	0.9 ± 1.9	**16.3 ± 4.0**	15.5 ± 4.5	1.00	0.89	–	
J182833-102652	X9	18 28 33.60	−10 26 52.0	**1.8 ± 0.4**	**4.0 ± 0.6**	**5.9 ± 0.7**	1.00	**2.8 ± 1.4**	**12.6 ± 2.2**	**15.5 ± 2.6**	0.73	0.47	17.5	–
J182833-103659	X9	18 28 33.96	−10 36 59.5	**18.7 ± 1.4**	**414 ± 6.6**	**427 ± 6.6**	0.43	**62.5 ± 5.4**	**1249 ± 23.2**	**1285 ± 23.5**	1.00	0.91	15.6	U0750_13265703 SAX J1828.5-1037 1RXS J1828.5-1037
J182835-105951	R4	18 28 35.80	−10 59 51.3	0.0 ± 0.4	**0.8 ± 0.5**	0.7 ± 0.6	1.00	0.0 ± 0.0	0.0 ± 1.5	0.0 ± 2.1	0.3	0.84	–	
J182836-103653	R5	18 28 36.23	−10 36 53.3	0.9 ± 0.4	**1.2 ± 0.5**	**2.1 ± 0.6**	1.00	1.8 ± 1.4	0.3 ± 1.3	1.4 ± 1.9	0.41	−0.04	16.9	U0750_13267401
J182836-100207	X12	18 28 36.92	−10 2 7.1	0.8 ± 0.4	0.2 ± 0.3	**1.0 ± 0.5**	1.00	1.3 ± 0.9	0.4 ± 0.9	1.6 ± 1.2	1.00	−0.59	–	
J182836-103603	X9	18 28 36.97	−10 36 3.8	0.0 ± 0.5	**6.5 ± 1.1**	**5.8 ± 1.2**	1.00	0.0 ± 1.8	**15.1 ± 3.6**	13.9 ± 4.0	1.00	1.00	–	
J182839-111630	R4	18 28 39.26	−11 16 30.0	**4.3 ± 0.9**	1.6 ± 0.7	**6.0 ± 1.1**	1.00	**21.2 ± 3.7**	1.9 ± 2.3	**22.8 ± 4.5**	0.86	−0.64	19.0	U0750_13269349
J182839-115324	X4	18 28 39.70	−11 53 24.2	0.0 ± 0.3	**0.9 ± 0.4**	0.7 ± 0.5	1.00	–	–	–	–	1.00	–	
J182841-102931	X9	18 28 41.50	−10 29 31.7	0.4 ± 0.4	**1.3 ± 0.5**	**1.7 ± 0.6**	1.00	0.8 ± 1.3	1.6 ± 1.7	2.4 ± 2.1	1.00	0.46	–	
J182842-104219	R5	18 28 42.26	−10 42 19.3	0.0 ± 0.2	**1.1 ± 0.3**	**1.0 ± 0.4**	1.00	0.0 ± 0.7	**2.3 ± 0.9**	1.5 ± 1.1	1.00	1.00	–	
J182843-101849	X12	18 28 43.54	−10 18 49.9	1.5 ± 0.7	**2.7 ± 0.9**	**3.9 ± 1.1**	1.00	0.0 ± 0.0	0.0 ± 0.0	0.0 ± 0.0	0.00	0.27	18.5	U0750_13272302
J182844-105428	R5	18 28 44.38	−10 54 28.1	0.3 ± 0.3	**1.4 ± 0.5**	**1.6 ± 0.6**	1.00	0.0 ± 0.9	4.0 ± 1.3	3.7 ± 1.6	1.00	0.81	–	
J182844-115653	X4	18 28 44.47	−11 56 53.7	**1.1 ± 0.5**	0.4 ± 0.4	**1.5 ± 0.6**	1.00	–	–	–	–	−0.47	–	
J182845-101000	X12	18 28 45.86	−10 10 0.9	1.4 ± 0.4	0.7 ± 0.4	**1.9 ± 0.6**	1.00	0.0 ± 0.6	0.0 ± 0.7	0.0 ± 1.0	0.14	−0.33	–	
J182845-111711	R4	18 28 45.94	−11 17 11.0	**71.4 ± 4.0**	**5.6 ± 1.7**	**78.5 ± 4.4**	0.00	**218 ± 10.7**	**17.8 ± 3.9**	**238 ± 11.6**	1.00	−0.86	11.8	U0750_13273777

© 2004 RAS, MNRAS **351,** 31–56

Table A1 – *continued*

XGPS-I Designation	Obs	Equinox J2000 RA	DEC	MOS count ks^{-1} s	h	b	q	pn count ks^{-1} s	h	b	q	HR	*R*	Optical Identification
J182846-115552	X4	18 28 46.86	−11 55 52.3	**2.0 ± 0.5**	**2.5 ± 0.6**	**4.5 ± 0.8**	1.00	–	–	–	–	0.11	18.8	U0750_13274575
J182847-100616	X12	18 28 47.10	−10 6 16.3	0.0 ± 0.2	0.3 ± 0.3	0.2 ± 0.4	1.00	1.1 ± 0.8	1.2 ± 0.8	**2.4 ± 1.1**	0.98	0.28	–	
J182847-101334	X12	18 28 47.76	−10 13 34.6	38.7 ± 2.1	0.8 ± 0.5	**39.7 ± 2.2**	1.00	**136 ± 6.4**	1.1 ± 1.1	**138 ± 6.5**	0.88	−0.97	8.8	U0750_13275198 HD 170248 1RXS J182846.4-101336
J182848-104942	R5	18 28 48.30	−10 49 42.5	**0.6 ± 0.3**	0.0 ± 0.3	0.6 ± 0.4	1.00	0.0 ± 0.6	0.0 ± 0.7	0.0 ± 0.9	1.00	−0.92	–	
J182849-104344	R5	18 28 49.12	−10 43 44.4	0.1 ± 0.2	0.6 ± 0.3	0.6 ± 0.3	1.00	0.0 ± 0.6	**2.3 ± 0.8**	1.2 ± 1.0	1.00	0.93	–	
J182850-114608	X4	18 28 50.00	−11 46 8.0	0.3 ± 0.3	**1.2 ± 0.4**	**1.5 ± 0.5**	1.00	–	–	–	–	0.54	16.0	U0750_13277273
J182850-104649	R5	18 28 50.77	−10 46 49.5	0.2 ± 0.2	**0.9 ± 0.3**	**0.9 ± 0.4**	1.00	0.5 ± 0.6	**1.7 ± 0.7**	1.9 ± 1.0	1.00	0.58	–	
J182851-101313	X12	18 28 51.04	−10 13 13.4	0.9 ± 0.4	0.0 ± 0.4	0.4 ± 0.6	1.00	**4.4 ± 1.4**	1.8 ± 1.2	**5.6 ± 1.9**	1.00	−0.59	19.7	–
J182851-103535	R5	18 28 51.05	−10 35 35.1	**1.0 ± 0.4**	1.0 ± 0.4	**1.9 ± 0.6**	1.00	0.7 ± 1.0	1.7 ± 1.2	1.8 ± 1.6	1.00	0.12	19.8	–
J182851-105539	R5	18 28 51.15	−10 55 39.6	0.3 ± 0.4	0.1 ± 0.4	0.5 ± 0.5	1.00	0.7 ± 1.0	**5.1 ± 1.4**	**5.5 ± 1.7**	1.00	0.56	–	
J182851-101730	X9	18 28 51.22	−10 17 30.4	0.9 ± 0.5	**2.0 ± 0.7**	**2.9 ± 0.9**	1.00	0.0 ± 0.0	0.0 ± 0.0	0.0 ± 0.0	0.00	0.23	19.7	–
J182851-103047	X9	18 28 51.63	−10 30 47.1	1.0 ± 0.5	0.7 ± 0.6	**1.7 ± 0.8**	1.00	1.1 ± 1.9	2.9 ± 2.2	4.2 ± 2.9	1.00	0.06	16.3	U0750_13278214
J182854-105017	R5	18 28 54.72	−10 50 17.8	0.0 ± 0.2	**1.1 ± 0.4**	**1.0 ± 0.4**	1.00	0.0 ± 0.6	0.0 ± 0.7	0.0 ± 0.9	0.27	0.94	–	
J182854-112656	X6	18 28 54.86	−11 26 56.1	**3.8 ± 0.9**	**5.1 ± 1.0**	**8.8 ± 1.4**	1.00	**9.6 ± 3.3**	**16.1 ± 4.2**	**25.1 ± 5.3**	1.00	0.18	17.6	U0750_13280318 F3R 673 RFS 302
J182855-104003	R5	18 28 55.49	−10 40 3.6	**0.5 ± 0.3**	0.0 ± 0.3	0.5 ± 0.4	1.00	0.0 ± 0.6	0.0 ± 0.7	0.0 ± 1.0	0.27	−0.95	–	
J182855-111148	R4	18 28 55.74	−11 11 48.7	**1.6 ± 0.6**	0.8 ± 0.6	**2.3 ± 0.9**	0.98	1.9 ± 2.1	**3.8 ± 2.4**	**5.8 ± 3.2**	1.00	−0.13	–	
J182856-095413	X12	18 28 56.04	−9 54 13.5	**2.5 ± 0.7**	**42.9 ± 2.6**	**44.6 ± 2.7**	1.00	**7.9 ± 2.0**	**88.3 ± 6.1**	**94.6 ± 6.3**	1.00	0.86	–	
J182856-101702	X12	18 28 56.31	−10 17 2.2	0.1 ± 0.4	**2.4 ± 0.8**	**2.3 ± 0.9**	0.98	0.7 ± 1.4	**8.3 ± 2.3**	**9.3 ± 2.7**	1.00	0.88	–	
J182856-100401	X12	18 28 56.61	−10 4 1.2	0.7 ± 0.3	0.0 ± 0.2	0.5 ± 0.4	1.00	1.0 ± 0.7	1.3 ± 0.8	**2.3 ± 1.1**	1.00	−0.33	–	
J182857-103502	R5	18 28 57.85	−10 35 2.1	0.5 ± 0.4	**1.2 ± 0.5**	**1.6 ± 0.6**	1.00	0.0 ± 0.9	0.9 ± 1.1	0.2 ± 1.5	1.00	0.50	16.9	U0750_13282507
J182858-100002	X12	18 28 58.17	−10 0 2.7	0.0 ± 0.3	0.8 ± 0.4	0.6 ± 0.5	0.71	0.5 ± 0.7	**2.6 ± 1.1**	**3.1 ± 1.3**	1.00	0.81	–	
J182858-113600	X6	18 28 58.36	−11 36 0.2	0.3 ± 0.6	2.1 ± 1.0	**2.2 ± 1.2**	1.00	0.7 ± 2.3	0.0 ± 2.8	0.4 ± 3.4	1.00	0.66	–	
J182858-103908	R5	18 28 58.55	−10 39 8.1	0.3 ± 0.2	**1.3 ± 0.4**	**1.6 ± 0.5**	1.00	0.7 ± 0.7	**2.5 ± 0.9**	**2.8 ± 1.2**	1.00	0.59	–	
J182858-104511	R5	18 28 58.59	−10 45 11.7	0.0 ± 0.2	**0.7 ± 0.3**	0.6 ± 0.3	1.00	0.1 ± 0.5	1.1 ± 0.6	0.9 ± 0.8	1.00	0.86	–	
J182858-095921	X12	18 28 58.70	−9 59 21.6	0.0 ± 0.3	**1.3 ± 0.5**	**1.1 ± 0.5**	1.00	0.7 ± 0.7	1.3 ± 1.0	2.1 ± 1.2	1.00	0.74	–	
J182859-100043	X12	18 28 59.49	−10 0 43.8	0.4 ± 0.3	0.2 ± 0.3	0.5 ± 0.4	1.00	0.8 ± 0.7	2.9 ± 1.1	**3.5 ± 1.3**	1.00	0.31	19.5	–
J182900-111001	X8	18 29 0.38	−11 10 1.9	0.6 ± 0.4	**2.9 ± 0.7**	**3.3 ± 0.8**	1.00	0.0 ± 0.0	0.0 ± 0.0	0.0 ± 0.0	0.00	0.65	–	
J182900-100658	X12	18 29 0.58	−10 6 58.2	0.1 ± 0.2	0.0 ± 0.3	0.0 ± 0.4	1.00	1.1 ± 0.7	**2.5 ± 1.0**	**3.5 ± 1.2**	1.00	0.29	–	
J182901-103925	R5	18 29 1.42	−10 39 25.4	0.3 ± 0.2	0.1 ± 0.3	0.3 ± 0.4	1.00	0.4 ± 0.7	**2.4 ± 0.9**	2.3 ± 1.1	1.00	0.36	–	
J182901-101448	X12	18 29 1.90	−10 14 48.8	0.6 ± 0.4	**1.5 ± 0.6**	**1.9 ± 0.8**	1.00	0.1 ± 1.0	4.3 ± 1.6	**4.1 ± 1.9**	1.00	0.65	–	
J182902-103720	R5	18 29 2.00	−10 37 20.8	0.0 ± 0.3	**1.5 ± 0.4**	**1.5 ± 0.5**	1.00	1.1 ± 0.9	**3.7 ± 1.1**	**4.6 ± 1.4**	1.00	0.72	–	
J182902-115341	X4	18 29 2.65	−11 53 41.8	0.2 ± 0.3	**1.3 ± 0.5**	**1.4 ± 0.6**	1.00	–	–	–	–	0.76	–	
J182903-110230	X8	18 29 3.02	−11 2 30.4	0.4 ± 0.4	**1.2 ± 0.5**	**1.5 ± 0.6**	0.59	0.0 ± 0.0	0.0 ± 0.0	0.0 ± 0.0	0.00	0.52	19.3	–
J182905-104634	R5	18 29 5.70	−10 46 34.7	0.3 ± 0.2	**5.2 ± 0.5**	**5.4 ± 0.5**	1.00	1.4 ± 0.6	**12.4 ± 1.2**	**13.4 ± 1.4**	1.00	0.84	19.8	U0750_13288301
J182907-104432	R5	18 29 7.32	−10 44 32.4	**1.2 ± 0.3**	**2.6 ± 0.4**	**3.7 ± 0.5**	1.00	**2.3 ± 0.7**	**6.6 ± 0.9**	**8.8 ± 1.2**	0.59	0.44	–	
J182907-104604	R5	18 29 7.37	−10 46 4.7	0.2 ± 0.2	**0.7 ± 0.3**	**0.8 ± 0.3**	1.00	1.3 ± 0.6	1.7 ± 0.7	2.7 ± 0.9	1.00	0.26	–	
J182908-102053	X11	18 29 8.29	−10 20 53.4	0.5 ± 0.5	**1.1 ± 0.6**	**1.7 ± 0.8**	1.00	0.1 ± 1.5	2.8 ± 2.0	2.6 ± 2.5	1.00	0.57	–	

Table A1 – *continued*

XGPS-I Designation	Obs	Equinox J2000 RA	DEC	MOS count ks^{-1} s	h	b	q	pn count ks^{-1} s	h	b	q	HR	R	Optical Identification
J182908-104930	R5	18 29 8.71	−10 49 30.6	**0.5 ± 0.3**	**1.4 ± 0.4**	**1.8 ± 0.4**	1.00	1.4 ± 0.7	**2.1 ± 0.8**	**3.5 ± 1.1**	1.00	0.34	17.4	U0750_13290417
J182909-105644	R5	18 29 9.95	−10 56 44.3	0.0 ± 0.4	0.8 ± 0.5	0.2 ± 0.6	1.00	**2.5 ± 1.2**	0.6 ± 1.2	2.0 ± 1.8	1.00	−0.01	–	
J182911-104245	R5	18 29 11.06	−10 42 45.6	0.6 ± 0.2	0.5 ± 0.3	0.9 ± 0.4	1.00	1.4 ± 0.6	**2.0 ± 0.7**	**3.4 ± 0.9**	1.00	0.08	16.4	U0750_13292023
J182911-105544	R5	18 29 11.61	−10 55 44.9	**7.9 ± 0.9**	0.8 ± 0.5	**8.5 ± 1.0**	1.00	**14.7 ± 1.9**	2.7 ± 1.3	**16.6 ± 1.3**	0.98	−0.76	19.1	–
J182913-095729	X12	18 29 13.59	−9 57 29.1	**2.5 ± 0.7**	0.7 ± 0.5	**3.0 ± 0.9**	1.00	**6.2 ± 1.6**	0.5 ± 1.0	**6.7 ± 1.9**	1.00	−0.72	13.1	U0750_13293780
J182914-104629	R5	18 29 14.34	−10 46 29.7	0.6 ± 0.2	0.8 ± 0.3	**1.3 ± 0.4**	1.00	0.2 ± 0.5	0.0 ± 0.6	0.0 ± 0.9	0.41	0.11	–	
J182914-102448	X11	18 29 14.36	−10 24 48.4	**1.4 ± 0.5**	0.2 ± 0.4	**1.6 ± 0.7**	1.00	**14.1 ± 5.5**	0.0 ± 4.7	12.6 ± 7.2	0.27	−0.85	18.5	U0750_13294401
J182914-104419	R5	18 29 14.86	−10 44 19.3	**0.7 ± 0.3**	0.7 ± 0.3	**1.3 ± 0.4**	1.00	0.0 ± 0.5	0.0 ± 0.6	0.0 ± 0.8	0.20	0.03	–	
J182914-105744	X8	18 29 14.94	−10 57 44.5	0.0 ± 0.4	0.0 ± 0.4	0.0 ± 0.6	1.00	0.5 ± 1.0	2.7 ± 1.4	2.7 ± 1.8	1.00	0.69	18.2	–
J182916-104601	R5	18 29 16.15	−10 46 1.4	0.2 ± 0.2	2.7 ± 0.4	2.8 ± 0.5	1.00	0.7 ± 0.6	**6.5 ± 1.0**	6.8 ± 1.1	1.00	0.83	–	
J182916-105444	R5	18 29 16.20	−10 54 44.2	0.0 ± 0.3	**1.3 ± 0.5**	**1.0 ± 0.6**	1.00	0.0 ± 0.9	**4.8 ± 1.3**	**4.4 ± 1.6**	1.00	1.00	–	
J182916-105348	R5	18 29 16.47	−10 53 48.3	0.0 ± 0.3	**0.9 ± 0.5**	0.6 ± 0.6	1.00	0.9 ± 0.9	2.3 ± 1.1	2.8 ± 1.4	0.73	0.65	–	
J182917-094723	X15	18 29 17.37	−9 47 23.2	0.8 ± 1.1	0.0 ± 1.1	0.4 ± 1.6	1.00	**15.5 ± 5.0**	0.9 ± 4.5	13.4 ± 6.8	1.00	−0.90	–	
J182918-103240	R5	18 29 18.37	−10 32 40.4	**2.8 ± 0.7**	0.2 ± 0.5	**3.0 ± 0.9**	1.00	**10.4 ± 1.9**	0.0 ± 1.2	**9.9 ± 2.3**	1.00	−0.94	15.9	U0750_13297244
J182918-112951	X6	18 29 18.67	−11 29 51.4	0.6 ± 0.5	1.1 ± 0.6	**1.6 ± 0.8**	1.00	0.0 ± 1.6	0.0 ± 1.5	0.0 ± 1.5	0.9	0.33	–	
J182918-104451	R5	18 29 18.80	−10 44 51.7	0.2 ± 0.2	**1.0 ± 0.3**	1.2 ± 0.4	1.00	0.3 ± 0.5	0.2 ± 0.6	0.1 ± 0.8	1.00	0.48	–	
J182919-110708	X8	18 29 19.12	−11 7 8.1	0.2 ± 0.3	**1.0 ± 0.4**	1.2 ± 0.5	1.00	0.4 ± 0.8	1.3 ± 0.9	1.6 ± 1.2	0.88	0.62	–	
J182919-104433	R5	18 29 19.35	−10 44 33.4	0.2 ± 0.2	**0.8 ± 0.3**	0.9 ± 0.4	1.00	0.0 ± 0.5	0.0 ± 0.6	0.0 ± 0.9	0.59	0.66	–	
J182920-104237	R5	18 29 20.39	−10 42 37.3	0.3 ± 0.2	0.2 ± 0.3	0.4 ± 0.4	1.00	**1.9 ± 0.7**	0.0 ± 0.7	1.1 ± 0.9	1.00	−0.77	–	
J182920-105042	R5	18 29 20.83	−10 50 42.2	0.8 ± 1.2	0.8 ± 1.5	1.2 ± 1.9	0.39	1.3 ± 0.8	**3.1 ± 0.9**	**4.4 ± 1.2**	1.00	0.34	–	
J182921-100304	X12	18 29 21.80	−10 3 4.6	0.1 ± 0.3	**2.0 ± 0.6**	**2.1 ± 0.6**	1.00	0.0 ± 0.0	0.0 ± 0.0	0.0 ± 0.0	0.00	0.91	–	
J182922-103239	R5	18 29 22.16	−10 32 39.5	0.3 ± 0.5	**2.2 ± 0.7**	**2.3 ± 0.9**	1.00	1.0 ± 1.3	3.0 ± 1.6	3.6 ± 2.1	1.00	0.67	–	
J182923-101211	X12	18 29 23.68	−10 12 11.3	0.3 ± 0.4	**3.0 ± 0.8**	**3.0 ± 0.9**	1.00	0.3 ± 0.9	**3.6 ± 1.5**	**3.7 ± 1.8**	0.7	0.83	–	
J182924-100456	X12	18 29 24.24	−10 4 56.7	0.0 ± 0.3	0.6 ± 0.4	0.4 ± 0.5	1.00	1.8 ± 1.0	2.5 ± 1.2	**4.5 ± 1.6**	1.00	0.34	–	
J182924-102957	X11	18 29 24.41	−10 29 57.6	**3.0 ± 0.6**	1.1 ± 0.5	**4.2 ± 0.8**	1.00	**11.0 ± 2.1**	**6.5 ± 1.8**	**16.9 ± 2.8**	1.00	−0.35	16.1	U0750_13301346
J182924-111634	X8	18 29 24.51	−11 16 34.3	**1.0 ± 0.4**	**4.4 ± 0.7**	**5.4 ± 0.8**	1.00	2.1 ± 1.1	**11.9 ± 1.9**	**13.6 ± 2.2**	1.00	0.66	–	
J182924-094624	X15	18 29 24.76	−9 46 24.6	1.1 ± 0.9	0.2 ± 1.0	1.2 ± 1.3	1.00	**10.2 ± 4.3**	3.7 ± 4.2	9.8 ± 6.1	1.00	−0.51	–	
J182924-105114	R5	18 29 24.93	−10 51 14.5	**1.1 ± 0.4**	**2.6 ± 0.5**	**3.6 ± 0.7**	1.00	**3.7 ± 1.0**	**4.5 ± 1.1**	**8.1 ± 1.5**	1.00	0.25	16.0	U0750_13301735
J182926-095147	X15	18 29 26.99	−9 51 47.1	**2.8 ± 1.3**	0.0 ± 1.3	1.6 ± 1.8	1.00	8.7 ± 5.7	0.7 ± 5.4	7.5 ± 7.9	1.00	−0.92	18.3	U0750_13303273
J182927-095218	X15	18 29 27.26	−9 52 18.9	1.1 ± 1.2	0.0 ± 1.3	0.0 ± 1.7	1.00	**18.5 ± 6.3**	6.1 ± 5.9	23.1 ± 8.7	1.00	−0.56	–	
J182927-102919	X11	18 29 27.34	−10 29 19.1	**0.9 ± 0.4**	0.2 ± 0.4	1.1 ± 0.6	1.00	0.1 ± 1.0	0.3 ± 1.2	0.1 ± 1.5	1.00	−0.58	–	
J182928-105257	R5	18 29 28.43	−10 52 57.9	0.0 ± 0.3	0.0 ± 0.3	0.0 ± 0.5	0.43	2.7 ± 1.1	2.2 ± 1.1	**4.5 ± 1.6**	1.00	−0.10	–	
J182929-094224	X15	18 29 29.82	−9 42 24.4	1.1 ± 0.8	0.0 ± 0.9	0.3 ± 1.2	1.00	3.8 ± 3.7	**10.8 ± 3.7**	11.6 ± 5.3	1.00	0.26	–	
J182930-105926	X8	18 29 30.87	−10 59 26.3	1.3 ± 0.6	**6.2 ± 1.1**	**7.3 ± 1.3**	1.00	1.4 ± 1.0	**7.0 ± 1.4**	**8.5 ± 1.7**	0.96	0.65	–	
J182930-113013	X6	18 29 30.94	−11 30 13.9	0.4 ± 0.5	1.4 ± 0.7	**1.8 ± 0.8**	0.86	4.5 ± 2.8	7.4 ± 3.3	11.6 ± 4.4	1.00	0.38	–	
J182931-110418	X8	18 29 31.22	−11 4 18.6	0.1 ± 0.3	0.2 ± 0.4	0.4 ± 0.5	1.00	**1.5 ± 0.8**	0.2 ± 0.7	1.5 ± 1.0	1.00	−0.54	–	
J182933-103150	X11	18 29 33.11	−10 31 50.3	0.1 ± 0.3	**1.7 ± 0.6**	**1.8 ± 0.7**	1.00	0.7 ± 1.1	**6.1 ± 1.7**	**6.1 ± 2.1**	1.00	0.85	–	
J182934-105142	R5	18 29 34.13	−10 51 42.7	0.6 ± 0.4	**1.6 ± 0.5**	**2.0 ± 0.7**	1.00	0.2 ± 0.9	2.9 ± 1.2	2.7 ± 1.5	1.00	0.65	–	
J182935-111552	X8	18 29 35.23	−11 15 52.5	0.5 ± 0.3	0.7 ± 0.4	1.3 ± 0.5	1.00	2.2 ± 1.0	**4.4 ± 1.2**	**6.6 ± 1.5**	1.00	0.27	–	
J182936-100726	X12	18 29 36.14	−10 7 26.9	0.4 ± 0.4	2.1 ± 0.8	**2.4 ± 0.9**	1.00	1.5 ± 1.2	**9.0 ± 2.1**	**10.6 ± 2.3**	1.00	0.70	–	
J182937-104503	R5	18 29 37.07	−10 45 3.2	0.0 ± 0.3	1.0 ± 0.4	0.9 ± 0.5	1.00	0.0 ± 0.8	**3.3 ± 1.0**	2.8 ± 1.2	1.00	0.99	–	

© 2004 RAS, MNRAS **351,** 31–56

Table A1 – *continued*

XGPS-I Designation	Obs	Equinox J2000 RA	DEC	MOS count ks^{-1} s	h	b	q	pn count ks^{-1} s	h	b	q	HR	*R*	Optical Identification
J182937-093750	X15	18 29 37.59	−9 37 50.9	2.0 ± 1.0	2.6 ± 1.1	**4.6 ± 1.5**	1.00	0.0 ± 4.6	0.0 ± 4.5	0.0 ± 6.6	1.00	0.11	–	
J182938-094900	X15	18 29 38.87	−9 49 0.8	2.4 ± 0.9	2.6 ± 1.0	**4.9 ± 1.4**	1.00	16.0 ± 4.6	9.8 ± 4.4	**22.5 ± 6.4**	1.00	−0.15	–	
J182938-094818	X15	18 29 38.90	−9 48 18.8	0.9 ± 0.8	**6.3 ± 1.2**	**7.1 ± 1.4**	1.00	4.7 ± 4.1	11.4 ± 4.3	13.3 ± 6.0	1.00	0.60	–	
J182939-105834	X8	18 29 39.73	−10 58 34.1	**2.8 ± 0.5**	0.2 ± 0.4	**2.9 ± 0.6**	1.00	**5.7 ± 1.3**	1.46 ± 0.9	**7.1 ± 1.6**	1.00	−0.72	14.9	U0750_13311799
J182940-113225	X6	18 29 40.30	−11 32 25.1	0.9 ± 0.6	1.4 ± 0.8	**2.3 ± 1.0**	1.00	0.8 ± 2.2	4.0 ± 3.7	3.9 ± 4.4	0.98	0.32	–	
J182942-110050	X8	18 29 42.30	−11 0 50.6	0.1 ± 0.3	0.8 ± 0.3	0.9 ± 0.4	1.00	0.7 ± 0.8	**1.4 ± 0.8**	1.8 ± 1.1	0.59	0.56	17.9	–
J182943-105801	X8	18 29 43.98	−10 58 1.4	0.4 ± 0.4	**4.5 ± 0.7**	**4.8 ± 0.7**	1.00	0.2 ± 0.9	**7.4 ± 1.4**	**7.2 ± 1.6**	0.73	0.87	–	
J182944-095122	X15	18 29 44.17	−9 51 22.7	0.0 ± 0.9	**2.2 ± 1.2**	1.1 ± 1.5	1.00	0.0 ± 4.9	0.0 ± 4.9	0.0 ± 7.0	1.00	1.00	18.9	GAL 021.7+00.3
J182946-104357	X10	18 29 46.62	−10 43 57.0	**1.5 ± 0.7**	0.0 ± 0.6	1.3 ± 0.9	1.00	0.0 ± 0.0	0.0 ± 0.0	0.0 ± 0.0	0.00	−0.99	–	
J182947-110945	X8	18 29 47.69	−11 9 45.1	0.0 ± 0.2	0.1 ± 0.2	0.1 ± 0.3	1.00	1.2 ± 0.6	1.4 ± 0.6	**2.6 ± 0.9**	1.00	0.10	–	
J182948-110604	X8	18 29 48.80	−11 6 4.3	**0.8 ± 0.3**	**3.4 ± 0.4**	**4.3 ± 0.5**	1.00	**3.9 ± 0.7**	**10.4 ± 1.1**	**14.2 ± 1.3**	0.88	0.52	–	
J182949-110319	X8	18 29 49.21	−11 3 19.4	0.0 ± 0.2	0.0 ± 0.2	0.0 ± 0.3	1.00	1.2 ± 0.6	1.0 ± 0.6	**2.1 ± 0.9**	1.00	−0.05	–	
J182949-103611	X11	18 29 49.78	−10 36 11.1	0.5 ± 0.5	**2.1 ± 0.8**	2.4 ± 1.0	0.73	2.0 ± 1.7	2.9 ± 1.9	4.7 ± 2.6	1.00	0.41	–	
J182950-110159	X8	18 29 50.27	−11 1 59.8	0.0 ± 0.2	0.3 ± 0.2	0.2 ± 0.3	1.00	0.6 ± 0.6	**1.5 ± 0.7**	2.0 ± 0.9	1.00	0.51	–	
J182950-110942	X8	18 29 50.77	−11 9 42.1	0.0 ± 0.2	0.5 ± 0.2	0.4 ± 0.3	1.00	0.8 ± 0.6	**2.2 ± 0.7**	2.9 ± 0.9	1.00	0.61	–	
J182950-111634	X8	18 29 50.87	−11 16 34.2	0.0 ± 0.3	**1.8 ± 0.5**	**1.8 ± 0.6**	1.00	0.0 ± 0.8	**5.8 ± 1.3**	**5.6 ± 1.5**	1.00	0.99	–	
J182951-100441	X14	18 29 51.57	−10 4 41.0	**12.6 ± 3.0**	0.0 ± 3.4	10.9 ± 4.6	1.00	0.0 ± 8.8	0.0 ± 11.4	0.0 ± 14.3	0.14	−1.00	–	
J182952-110700	X8	18 29 52.94	−11 7 0.0	0.0 ± 0.2	0.3 ± 0.2	0.4 ± 0.3	1.00	1.4 ± 0.6	**1.6 ± 0.6**	**2.9 ± 0.8**	1.00	0.27	16.4	U0750_13321102
J182954-102852	X11	18 29 54.79	−10 28 52.3	0.1 ± 0.3	**1.0 ± 0.5**	**1.0 ± 0.5**	1.00	0.7 ± 1.0	0.7 ± 1.0	1.1 ± 1.5	0.59	0.56	19.0	–
J182955-110533	X8	18 29 55.97	−11 5 33.8	0.1 ± 0.2	0.4 ± 0.3	0.6 ± 0.3	1.00	0.5 ± 0.5	1.6 ± 0.6	**1.9 ± 0.8**	1.00	0.60	17.8	U0750_13323591
J182956-111313	X8	18 29 56.52	−11 13 13.5	**0.8 ± 0.3**	**2.2 ± 0.4**	**3.0 ± 0.5**	1.00	2.0 ± 0.8	**5.5 ± 1.0**	**7.5 ± 1.3**	1.00	0.45	–	
J182956-110458	X8	18 29 56.85	−11 4 58.8	**0.7 ± 0.3**	**0.6 ± 0.3**	**1.3 ± 0.4**	1.00	0.6 ± 0.5	1.1 ± 0.6	1.6 ± 0.7	1.00	0.05	–	
J182957-110235	X8	18 29 57.14	−11 2 35.8	**0.6 ± 0.3**	0.5 ± 0.3	**1.1 ± 0.4**	1.00	0.7 ± 0.6	0.0 ± 0.5	0.6 ± 0.8	1.00	−0.32	–	
J182958-103054	X11	18 29 58.20	−10 30 54.0	**1.7 ± 0.5**	**2.5 ± 0.6**	**4.2 ± 0.8**	0.88	**8.2 ± 1.7**	**6.3 ± 1.7**	**14.3 ± 2.4**	1.00	0.01	16.3	U0750_13325431
J183000-110720	X8	18 30 0.38	−11 7 20.3	0.2 ± 0.2	**1.7 ± 0.3**	**2.0 ± 0.4**	1.00	1.2 ± 0.6	**5.0 ± 0.8**	**6.0 ± 1.0**	1.00	0.71	–	
J183000-094118	X15	18 30 0.85	−9 41 18.9	1.4 ± 0.8	1.0 ± 0.9	2.4 ± 1.2	1.00	5.9 ± 4.2	**14.1 ± 4.5**	17.7 ± 6.3	1.00	0.27	–	
J183002-094953	X15	18 30 2.04	−9 49 53.8	**2.6 ± 1.1**	1.6 ± 1.1	3.8 ± 1.6	1.00	0.0 ± 4.9	0.0 ± 4.9	0.0 ± 6.9	1.00	−0.25	–	
J183002-110735	X8	18 30 2.31	−11 7 35.6	0.1 ± 0.2	**1.4 ± 0.3**	**1.6 ± 0.4**	1.00	0.0 ± 0.0	0.0 ± 0.0	0.0 ± 0.0	0.27	0.67	–	
J183005-104205	X10	18 30 5.60	−10 42 5.5	**1.3 ± 0.5**	0.4 ± 0.5	1.6 ± 0.8	1.00	0.0 ± 1.5	1.0 ± 2.0	0.0 ± 2.3	1.00	−0.29	13.9	U0750_13332059
J183006-102221	X11	18 30 6.89	−10 22 21.1	0.5 ± 0.4	0.0 ± 0.4	0.4 ± 0.6	1.00	0.0 ± 1.1	**2.9 ± 1.4**	2.4 ± 1.7	0.86	0.37	19.9	–
J183012-110759	X8	18 30 12.70	−11 7 59.4	**0.5 ± 0.3**	0.3 ± 0.3	**0.9 ± 0.4**	1.00	**2.0 ± 0.7**	**1.2 ± 0.6**	**3.4 ± 0.9**	1.00	−0.27	–	
J183013-102759	X11	18 30 13.43	−10 27 59.7	0.1 ± 0.3	**3.2 ± 0.7**	**3.2 ± 0.8**	1.00	8.2 ± 15.7	24.3 ± 19.1	30.0 ± 24.8	0.27	0.84	19.2	–
J183013-110450	X8	18 30 13.72	−11 4 50.2	0.1 ± 0.2	0.0 ± 0.2	0.0 ± 0.3	1.00	0.1 ± 0.6	**1.9 ± 0.7**	1.7 ± 0.9	1.00	0.77	–	
J183015-104538	X10	18 30 15.94	−10 45 38.5	0.5 ± 0.4	**6.2 ± 0.7**	**6.6 ± 0.8**	1.00	0.0 ± 1.3	**4.8 ± 1.8**	**4.3 ± 2.2**	0.49	0.89	13.2	U0750_13340834
J183015-102458	X11	18 30 15.98	−10 24 58.0	**1.3 ± 0.5**	**1.5 ± 0.6**	**2.9 ± 0.8**	1.00	2.5 ± 1.3	0.5 ± 1.3	2.5 ± 1.8	0.41	−0.16	13.3	–
J183017-103143	X11	18 30 17.03	−10 31 43.5	0.0 ± 0.5	**1.7 ± 0.8**	1.5 ± 0.9	1.00	0.0 ± 1.5	1.0 ± 1.5	0.3 ± 2.0	1.00	1.00	–	
J183017-095326	X14	18 30 17.12	−9 53 26.3	**9.7 ± 2.9**	0.2 ± 3.4	9.4 ± 4.5	1.00	19.4 ± 8.8	18.0 ± 11.3	37.2 ± 14.3	1.00	−0.44	15.6	U0750_13341855
J183017-110215	X8	18 30 17.34	−11 2 15.6	0.0 ± 0.3	**0.8 ± 0.4**	0.8 ± 0.5	0.73	1.1 ± 0.8	**1.8 ± 0.9**	**2.9 ± 1.1**	1.00	0.50	19.7	–
J183017-102730	X11	18 30 17.99	−10 27 30.5	**1.8 ± 0.6**	0.7 ± 0.6	**2.4 ± 0.8**	1.00	**7.5 ± 1.9**	0.0 ± 1.5	**7.1 ± 2.3**	1.00	−0.74	12.0	U0750_13342616
J183018-100340	X14	18 30 18.43	−10 3 40.7	0.0 ± 1.4	1.0 ± 2.0	0.0 ± 2.5	1.00	2.8 ± 4.7	**20.5 ± 6.4**	24.1 ± 7.9	1.00	0.79	–	
J183021-105040	X10	18 30 21.31	−10 50 40.1	0.7 ± 0.4	0.0 ± 0.4	0.4 ± 0.6	1.00	**4.4 ± 1.6**	1.7 ± 1.6	5.9 ± 2.3	1.00	−0.60	13.9	U0750_13345799
J183029-111110	X8	18 30 29.38	−11 11 10.9	0.3 ± 0.4	0.0 ± 0.4	0.1 ± 0.5	1.00	1.1 ± 0.9	**2.2 ± 0.9**	3.2 ± 1.3	1.00	0.11	19.7	–

Table A1 – *continued*

XGPS-I		Equinox J2000		MOS count ks^{-1}				pn count ks^{-1}						Optical
Designation	Obs	RA	DEC	s	h	b	q	s	h	b	q	HR	R	Identification
J183031-105152	X10	18 30 31.90	−10 51 52.1	**1.6 ± 0.5**	0.0 ± 0.4	1.7 ± 0.6	0.63	**2.6 ± 1.4**	0.0 ± 1.4	1.7 ± 2.0	0.37	−1.00	8.3	U0750_13355585 HD 170566
J183031-094030	X17	18 30 31.99	−9 40 30.5	0.0 ± 0.8	**11.0 ± 1.8**	**10.0 ± 1.9**	1.00	0.0 ± 3.0	**17.9 ± 3.9**	**17.9 ± 4.5**	0.73	1.00	19.6	–
J183032-094726	X17	18 30 32.64	−9 47 26.4	0.3 ± 0.9	**2.6 ± 1.3**	2.8 ± 1.5	1.00	1.3 ± 2.5	**4.6 ± 3.3**	5.3 ± 4.2	1.00	0.70	14.1	U0750_13355870
J183035-102105	X11	18 30 35.91	−10 21 5.9	13.2 ± 1.9	0.8 ± 0.9	**14.2 ± 2.0**	1.00	**36.4 ± 4.5**	1.0 ± 2.1	**38.2 ± 5.0**	1.00	−0.92	13.9	U0750_13358796
J183037-110831	X8	18 30 37.74	−11 8 31.2	**1.0 ± 0.5**	0.0 ± 0.4	0.9 ± 0.6	1.00	2.1 ± 1.0	1.1 ± 0.9	3.1 ± 1.3	0.98	−0.57	17.0	U0750_13360556
J183038-100248	X14	18 30 38.11	−10 2 48.6	3.4 ± 1.3	**24.5 ± 2.2**	**26.7 ± 2.5**	1.00	11.7 ± 4.6	**42.5 ± 6.3**	**55.6 ± 7.7**	1.00	0.68	–	
J183040-100155	X14	18 30 40.92	−10 1 55.9	0.4 ± 1.3	3.0 ± 1.8	2.4 ± 2.3	1.00	6.4 ± 4.3	26.7 ± 5.9	**34.2 ± 7.3**	1.00	0.65	–	
J183041-103320	X10	18 30 41.11	−10 33 20.5	0.2 ± 0.6	0.0 ± 0.7	0.0 ± 0.9	1.00	2.7 ± 2.3	**5.7 ± 2.9**	**8.2 ± 3.7**	1.00	0.27	19.4	–
J183041-104121	X10	18 30 41.19	−10 41 21.4	0.4 ± 0.4	**1.2 ± 0.4**	1.6 ± 0.6	1.00	0.4 ± 1.2	3.5 ± 1.5	3.7 ± 1.9	1.00	0.62	19.6	–
J183041-103939	X10	18 30 41.46	−10 39 39.2	0.3 ± 0.4	**3.5 ± 0.7**	**3.7 ± 0.8**	1.00	0.0 ± 1.4	**9.3 ± 2.0**	**9.5 ± 2.4**	1.00	0.92	–	
J183045-104414	X10	18 30 45.50	−10 44 14.2	0.1 ± 0.3	**0.8 ± 0.4**	**1.0 ± 0.5**	1.00	**2.8 ± 1.2**	1.6 ± 1.2	**4.2 ± 1.7**	1.00	0.08	–	
J183046-104623	X10	18 30 46.63	−10 46 23.8	0.1 ± 0.3	**1.5 ± 0.5**	**1.6 ± 0.5**	1.00	1.4 ± 1.1	1.2 ± 1.2	2.5 ± 1.6	0.88	0.52	–	
J183047-103853	X10	18 30 47.15	−10 38 53.9	0.0 ± 0.4	**2.1 ± 0.7**	2.0 ± 0.7	1.00	0.0 ± 1.4	0.0 ± 1.5	0.0 ± 2.1	0.53	1.00	–	
J183047-093925	X17	18 30 47.85	−9 39 25.0	0.3 ± 0.7	0.2 ± 0.7	0.5 ± 1.0	1.00	**5.0 ± 2.3**	0.0 ± 2.0	4.2 ± 2.9	1.00	−0.79	–	
J183048-095941	X14	18 30 48.02	−9 59 41.6	0.4 ± 1.4	2.3 ± 2.0	1.3 ± 2.5	1.00	12.8 ± 5.0	**31.5 ± 6.7**	**44.8 ± 8.3**	1.00	0.46	–	
J183048-100036	X14	18 30 48.26	−10 0 36.3	1.1 ± 1.4	2.4 ± 2.0	2.1 ± 2.5	1.00	5.3 ± 4.8	**20.1 ± 6.4**	**26.5 ± 8.0**	1.00	0.51	–	
J183049-102428	X13	18 30 49.98	−10 24 28.0	1.1 ± 0.7	0.0 ± 0.8	0.8 ± 1.1	1.00	3.1 ± 2.5	**7.2 ± 2.9**	**9.2 ± 3.9**	1.00	0.11	–	
J183050-103817	X10	18 30 50.02	−10 38 17.3	0.2 ± 0.4	**2.9 ± 0.7**	**3.1 ± 0.8**	1.00	0.0 ± 1.5	**5.5 ± 2.0**	**4.6 ± 2.4**	1.00	0.94	–	
J183050-104735	X10	18 30 50.08	−10 47 35.4	0.1 ± 0.3	**0.9 ± 0.4**	0.9 ± 0.5	1.00	0.0 ± 1.1	**3.1 ± 1.4**	2.7 ± 1.7	0.9	0.95	–	
J183050-102955	X13	18 30 50.31	−10 29 55.5	**4.0 ± 1.2**	0.3 ± 1.0	**4.1 ± 1.6**	1.00	6.8 ± 3.2	0.0 ± 3.4	4.8 ± 4.3	1.00	−0.92	14.8	U0750_13371710
J183051-104809	X10	18 30 51.54	−10 48 9.3	0.3 ± 0.4	0.8 ± 0.4	1.1 ± 0.6	1.00	2.3 ± 1.2	**3.7 ± 1.4**	**5.3 ± 1.9**	1.00	0.30	16.8	U0750_13373184
J183052-095053	X17	18 30 52.78	−9 50 53.1	1.0 ± 0.8	**5.4 ± 1.3**	**6.3 ± 1.5**	1.00	0.0 ± 2.5	0.0 ± 2.5	0.0 ± 3.6	0.12	0.68	–	
J183053-101936	X13	18 30 53.32	−10 19 36.3	3.4 ± 1.2	1.5 ± 1.2	4.5 ± 1.7	0.37	6.3 ± 2.9	**8.5 ± 3.3**	**14.0 ± 4.4**	1.00	−0.08	15.3	U0750_13374636
J183053-111255	X8	18 30 53.53	−11 12 55.2	0.0 ± 0.0	0.0 ± 0.0	0.0 ± 0.0	0.00	**4.1 ± 1.6**	**2.6 ± 1.5**	**6.7 ± 2.2**	1.00	−0.18	–	
J183057-103452	X13	18 30 57.96	−10 34 52.3	1.9 ± 1.1	**5.2 ± 1.7**	**6.7 ± 2.0**	1.00	4.8 ± 3.6	8.6 ± 4.3	11.9 ± 5.7	1.00	0.37	18.2	U0750_13379212
J183058-104157	X10	18 30 58.20	−10 41 57.4	**1.2 ± 0.5**	0.6 ± 0.5	**1.9 ± 0.7**	1.00	2.7 ± 1.4	1.2 ± 1.5	3.4 ± 2.1	1.00	−0.35	19.3	–
J183059-105719	X10	18 30 59.12	−10 57 19.4	0.0 ± 0.6	**4.0 ± 1.1**	**3.6 ± 1.2**	1.00	0.5 ± 2.0	**9.8 ± 3.1**	**9.5 ± 3.7**	1.00	0.95	–	
J183101-093619	X17	18 31 1.65	−9 36 19.8	1.6 ± 0.7	0.0 ± 0.6	1.0 ± 0.9	1.00	**4.8 ± 2.2**	0.6 ± 1.7	**5.5 ± 2.8**	1.00	−0.89	13.4	U0750_13382260
J183102-094607	X17	18 31 2.57	−9 46 7.7	**0.6 ± 0.5**	0.5 ± 0.6	1.1 ± 0.8	1.00	0.0 ± 1.6	2.8 ± 1.8	0.6 ± 2.2	0.86	0.36	–	
J183103-095813	X14	18 31 3.69	−9 58 13.5	**7.2 ± 2.2**	3.7 ± 2.7	**10.2 ± 3.5**	1.00	8.6 ± 7.1	0.0 ± 7.9	0.0 ± 10.1	0.88	−0.47	18.0	G 155-20
J183104-094433	X17	18 31 5.55	−9 44 33.7	0.2 ± 0.5	0.0 ± 0.5	0.0 ± 0.6	1.00	4.8 ± 1.7	**3.7 ± 1.7**	**8.3 ± 2.5**	1.00	−0.17	–	
J183109-105113	X10	18 31 9.98	−10 51 13.9	1.8 ± 0.7	0.0 ± 0.6	1.3 ± 0.9	0.71	**10.5 ± 2.2**	1.6 ± 2.0	**12.1 ± 3.0**	1.00	−0.81	12.5	U0750_13390292
J183113-094924	X17	18 31 13.12	−9 49 24.5	**3.6 ± 0.8**	**5.5 ± 1.0**	**9.2 ± 1.3**	1.00	**5.4 ± 2.1**	**8.4 ± 2.5**	**13.2 ± 3.3**	0.73	0.20	18.6	U0750_13393881
J183113-102941	X13	18 31 13.74	−10 29 41.8	0.8 ± 0.5	**2.1 ± 0.8**	**2.9 ± 1.0**	1.00	1.9 ± 1.9	3.2 ± 2.3	4.8 ± 3.0	1.00	0.36	17.0	U0750_13394553
J183113-094745	X17	18 31 13.83	−9 47 45.5	0.0 ± 0.5	0.4 ± 0.6	0.5 ± 0.7	1.00	0.0 ± 1.6	**5.8 ± 2.0**	**5.2 ± 2.5**	1.00	0.99	14.1	U0750_13394829
J183115-102757	X13	18 31 15.01	−10 27 57.8	1.2 ± 0.5	1.4 ± 0.7	2.3 ± 0.9	1.00	3.6 ± 1.8	3.5 ± 2.0	**6.3 ± 2.8**	0.63	0.01	–	
J183116-100517	X16	18 31 16.22	−10 5 17.3	1.4 ± 1.0	0.9 ± 1.1	2.3 ± 1.4	1.00	**6.6 ± 3.2**	0.0 ± 3.6	4.0 ± 4.2	1.00	−0.65	–	
J183116-105242	X10	18 31 16.43	−10 52 42.4	**2.2 ± 0.8**	0.1 ± 0.7	2.2 ± 1.1	1.00	0.8 ± 2.0	1.6 ± 2.4	2.1 ± 3.2	1.00	−0.58	14.6	U0750_13397375
J183116-100921	X16	18 31 16.51	−10 9 21.2	0.0 ± 0.0	0.0 ± 0.0	0.0 ± 0.0	0.00	5.8 ± 3.4	**42.3 ± 5.8**	**46.6 ± 6.7**	1.00	0.69	13.2	U0750_13397443

© 2004 RAS, MNRAS **351,** 31–56

Table A1 – *continued*

XGPS-I Designation	Obs	Equinox J2000 RA	DEC	MOS count ks^{-1} s	h	b	q	pn count ks^{-1} s	h	b	q	HR	*R*	Optical Identification
J183119-103230	X13	18 31 19.79	−10 32 30.9	0.3 ± 0.6	**3.0 ± 1.0**	**3.1 ± 1.1**	1.00	0.0 ± 2.1	0.0 ± 2.6	0.0 ± 3.4	0.63	0.83	–	
J183119-102546	X13	18 31 19.98	−10 25 46.5	0.0 ± 0.3	0.7 ± 0.5	0.3 ± 0.6	1.00	**4.3 ± 1.7**	0.8 ± 1.6	**5.0 ± 2.4**	0.88	−0.22	19.9	–
J183122-101912	X13	18 31 22.84	−10 19 12.4	0.1 ± 0.4	**1.9 ± 0.7**	**1.8 ± 0.8**	0.82	0.1 ± 1.7	3.4 ± 2.3	2.7 ± 2.9	1.00	0.91	–	
J183123-094005	X17	18 31 23.78	−9 40 5.8	**0.8 ± 0.5**	0.0 ± 0.5	0.2 ± 0.6	1.00	1.5 ± 1.6	0.8 ± 1.4	1.7 ± 2.1	1.00	−0.69	–	
J183124-104751	X10	18 31 24.77	−10 47 51.5	**5.6 ± 1.0**	0.0 ± 2.5	**5.6 ± 1.3**	1.00	17.2 ± 9.4	0.0 ± 8.6	9.3 ± 12.6	0.27	−1.00	–	
J183129-103435	X13	18 31 29.34	−10 34 35.0	0.7 ± 0.8	1.5 ± 1.0	2.1 ± 1.2	0.86	1.2 ± 2.6	**6.5 ± 3.5**	6.6 ± 4.4	1.00	0.52	–	
J183131-102957	X13	18 31 31.52	−10 29 57.0	0.0 ± 0.4	0.0 ± 0.6	0.0 ± 0.7	0.73	1.9 ± 1.8	4.6 ± 2.4	**7.2 ± 3.0**	1.00	0.42	–	
J183133-102208	X13	18 31 33.08	−10 22 8.7	0.4 ± 0.4	0.2 ± 0.4	0.5 ± 0.6	1.00	**4.3 ± 1.8**	3.2 ± 1.9	7.5 ± 2.7	0.98	−0.19	19.0	–
J183134-095155	X17	18 31 34.29	−9 51 55.2	0.3 ± 0.6	1.5 ± 0.9	1.7 ± 1.1	1.00	1.7 ± 2.4	4.3 ± 2.6	**5.7 ± 3.5**	1.00	0.58	16.9	U0750_13416775
J183134-100945	X16	18 31 34.47	−10 9 45.1	0.0 ± 0.6	**2.5 ± 1.0**	2.1 ± 1.2	1.00	0.3 ± 2.1	0.0 ± 2.9	0.0 ± 3.8	1.00	0.91	17.4	U0750_13416951
J183135-102452	X13	18 31 35.20	−10 24 52.5	0.9 ± 0.5	0.9 ± 0.5	**1.6 ± 0.7**	1.00	0.0 ± 1.3	0.0 ± 1.6	0.0 ± 2.0	0.16	0.03	–	
J183135-100142	X16	18 31 35.64	−10 1 42.6	1.4 ± 0.6	**2.6 ± 0.8**	**3.9 ± 1.0**	1.00	**3.8 ± 2.1**	**6.6 ± 2.4**	**9.9 ± 3.2**	1.00	0.27	–	
J183135-102855	X13	18 31 35.72	−10 28 55.4	0.0 ± 0.4	0.7 ± 0.6	0.6 ± 0.7	1.00	1.8 ± 1.8	**5.2 ± 2.3**	6.4 ± 3.0	1.00	0.60	–	
J183140-093550	X17	18 31 40.77	−9 35 50.4	**1.2 ± 0.6**	0.5 ± 0.7	1.6 ± 0.9	1.00	0.0 ± 1.7	0.6 ± 2.0	0.0 ± 2.5	1.00	−0.30	15.6	U0750_13423792
J183142-100525	X16	18 31 42.00	−10 5 25.5	0.3 ± 0.5	**1.0 ± 0.6**	1.3 ± 0.8	1.00	0.0 ± 1.8	0.0 ± 2.0	0.0 ± 2.8	0.98	0.48	–	
J183144-103328	X13	18 31 44.90	−10 33 28.7	1.6 ± 0.8	0.3 ± 0.8	2.0 ± 1.1	1.00	**8.7 ± 3.4**	1.0 ± 3.1	**9.6 ± 4.6**	1.00	−0.77	17.4	U0750_13428311
J183153-102449	X13	18 31 53.26	−10 24 49.3	**1.5 ± 0.6**	0.8 ± 0.6	**2.4 ± 0.9**	1.00	3.9 ± 2.3	0.0 ± 2.1	2.5 ± 3.2	0.41	0.42	–	
J183155-094706	X17	18 31 55.46	−9 47 6.3	0.2 ± 0.6	**1.9 ± 0.8**	2.1 ± 1.0	1.00	2.7 ± 2.4	**10.8 ± 3.3**	**13.4 ± 4.1**	1.00	0.66	–	
J183156-102447	X13	18 31 56.36	−10 24 47.8	1.5 ± 0.7	**3.2 ± 0.9**	**4.8 ± 1.1**	1.00	3.0 ± 2.2	**7.5 ± 2.9**	**8.9 ± 3.8**	0.88	0.37	–	
J183157-100033	X16	18 31 57.46	−10 0 33.3	0.0 ± 0.3	**3.7 ± 0.7**	**3.6 ± 0.8**	1.00	0.1 ± 1.3	1.0 ± 1.5	0.7 ± 2.0	1.00	0.99	–	
J183157-101123	X16	18 31 57.91	−10 11 23.8	0.0 ± 0.4	**3.2 ± 0.8**	**2.7 ± 0.9**	1.00	0.0 ± 1.8	5.1 ± 2.3	4.0 ± 2.9	1.00	1.00	–	
J183201-095342	X16	18 32 1.94	−9 53 42.6	1.3 ± 0.7	2.0 ± 0.8	**3.3 ± 1.0**	1.00	0.0 ± 2.0	0.0 ± 2.2	0.0 ± 2.9	0.41	0.21	16.1	–
J183204-100035	X16	18 32 4.18	−10 0 35.9	0.8 ± 0.4	**1.3 ± 0.5**	**2.1 ± 0.6**	1.00	0.0 ± 1.3	1.8 ± 1.5	0.5 ± 1.9	0.98	0.40	–	
J183204-100601	X16	18 32 4.76	−10 6 1.3	0.3 ± 0.4	0.0 ± 0.4	0.4 ± 0.5	1.00	**3.9 ± 1.5**	1.6 ± 1.4	**5.6 ± 2.1**	1.00	−0.49	17.6	U0750_13450456
J183208-093906	X17	18 32 8.93	−9 39 6.2	**7.1 ± 1.3**	**62.9 ± 3.4**	**68.8 ± 3.6**	1.00	0.0 ± 0.0	0.0 ± 0.0	0.0 ± 0.0	0.00	0.79	17.8	GPSR 22.154-0.154
J183209-100648	X16	18 32 9.14	−10 6 48.4	0.0 ± 0.3	**0.5 ± 0.4**	0.2 ± 0.5	1.00	0.7 ± 1.3	0.1 ± 1.3	0.7 ± 1.9	1.00	0.37	–	
J183210-100031	X16	18 32 10.80	−10 0 31.1	0.9 ± 0.4	**2.3 ± 0.5**	**3.2 ± 0.7**	1.00	1.9 ± 1.4	**4.5 ± 1.6**	**6.4 ± 2.1**	1.00	0.42	–	
J183213-100633	X16	18 32 13.12	−10 6 33.3	**4.1 ± 0.6**	0.0 ± 0.4	**4.1 ± 0.7**	1.00	**8.3 ± 1.9**	0.0 ± 1.3	**7.8 ± 2.3**	1.00	−1.00	13.6	U0750_13460167
J183213-095648	X16	18 32 13.88	−9 56 48.6	0.2 ± 0.4	**1.4 ± 0.6**	1.6 ± 0.7	1.00	0.0 ± 1.6	1.7 ± 1.7	1.2 ± 2.3	1.00	0.78	–	
J183216-102303	X13	18 32 16.38	−10 23 3.1	**14.0 ± 2.3**	**44.6 ± 4.0**	**57.5 ± 4.6**	1.00	0.0 ± 0.0	0.0 ± 0.0	0.0 ± 0.0	0.00	0.51	12.2	U0750_13463736
J183222-095546	X16	18 32 22.54	−9 55 46.8	0.0 ± 0.4	**2.1 ± 0.7**	**2.0 ± 0.8**	1.00	0.0 ± 1.6	3.1 ± 2.0	0.0 ± 2.2	0.88	1.00	17.8	U0750_13471175
J183225-100158	X16	18 32 25.19	−10 1 58.7	0.7 ± 0.4	**0.9 ± 0.4**	**1.5 ± 0.6**	1.00	0.2 ± 1.2	1.4 ± 1.5	1.3 ± 1.9	1.00	0.28	–	
J183228-100946	X16	18 32 28.44	−10 9 46.8	**1.5 ± 0.5**	3.2 ± 0.6	**4.8 ± 0.8**	1.00	3.0 ± 1.7	7.5 ± 2.0	8.9 ± 2.6	0.88	0.15	–	
J183228-100133	X16	18 32 28.59	−10 1 33.8	0.0 ± 0.3	**1.1 ± 0.5**	1.0 ± 0.6	1.00	0.5 ± 1.4	3.2 ± 1.7	3.5 ± 2.2	1.00	0.83	–	
J183234-100437	X16	18 32 34.32	−10 4 37.7	0.0 ± 0.3	**3.0 ± 0.6**	**3.1 ± 0.7**	1.00	0.0 ± 1.5	**8.8 ± 2.2**	**8.1 ± 2.6**	1.00	1.00	–	
J183236-101144	X16	18 32 36.64	−10 11 44.8	1.6 ± 0.7	**5.3 ± 1.0**	**6.9 ± 1.2**	1.00	0.0 ± 2.4	**19.3 ± 3.8**	**19.1 ± 4.4**	1.00	0.75	–	
J183246-100530	X16	18 32 46.78	−10 5 30.6	**1.8 ± 0.6**	0.0 ± 0.5	1.9 ± 0.8	1.00	1.4 ± 2.1	0.0 ± 1.8	0.0 ± 2.6	1.00	−1.00	15.4	U0750_13500933
J183251-100106	X16	18 32 51.65	−10 1 6.7	**8.8 ± 1.1**	**16.4 ± 1.5**	**25.2 ± 1.8**	1.00	**14.6 ± 3.2**	**24.3 ± 3.8**	**38.8 ± 5.0**	0.51	0.27	–	
J183256-100729	X16	18 32 56.28	−10 7 29.4	0.6 ± 0.6	1.4 ± 0.8	**2.1 ± 1.0**	1.00	0.0 ± 2.8	4.8 ± 3.3	4.3 ± 4.2	0.59	0.67	17.7	U0750_13512064